AD-A042 187 SYSTEMS RESEARCH LABS INC DAYTON OHIO F/G 20/4
FLOW CALIBRATION OF THE LASER TEST SHELTER AIRFLOW DUCT.(U)
DEC 76 C N EASTLAKE, E E DITMER F33615-76-C-2095
UNCLASSIFIED AFAPL-TR-76-103 NL

1 OF 2
ADA042187

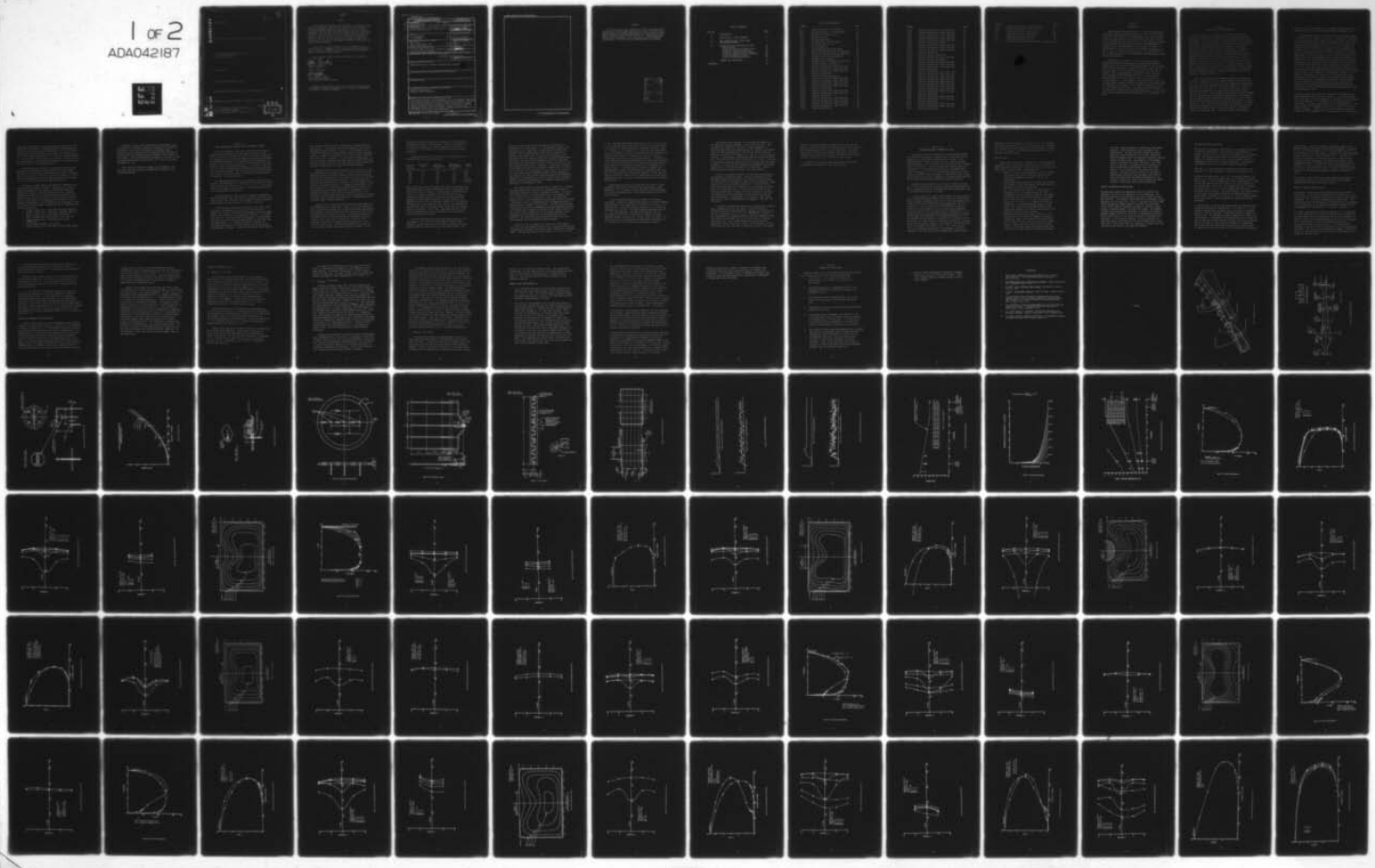

AFAPL-TR-76-103

FLOW CALIBRATION OF THE LASER TEST SHELTER AIRFLOW DUCT

SYSTEMS RESEARCH LABORATORIES, INC.
2800 Indian Ripple Road
Dayton, Ohio 45440

December 1976

Technical Report AFAPL-TR-76-103

Final Report for Period April 1976 - September 1976.

Air Force Aero Propulsion Laboratory
Air Force Wright Aeronautical Laboratories
Air Force Systems Command
Wright-Patterson Air Force Base, Ohio 45433

NOTICE

When Government drawings, specifications, or other data are used for any purpose other than in connection with a definitely related Government procurement operation, the United States Government thereby incurs no responsibility nor any obligation whatsoever; and the fact that the Government may have formulated, furnished, or in any way supplied the said drawings, specifications, or other data, is not to be regarded by implication or otherwise as in any manner licensing the holder or any other person or corporation, or conveying any rights or permission to manufacture, use, or sell any patented invention that may in any way be related thereto.

This report has been reviewed by the Information Office (ASD/OIP) and is releasable to the National Technical Information Service (NTIS). At NTIS, it will be available to the general public, including foreign nations.

This technical report has been reviewed and is approved for publication.

Allan Ferrenberg

Allan J. Ferrenberg
Project Engineer

FOR THE COMMANDER

B. P. Botteri

B. P. Botteri, Chief
Fire Protection Branch
Fuels and Lubrication Division

Copies of this report should not be returned unless return is required by security considerations, contractual obligations, or notice on a specific document.

UNCLASSIFIED

SECURITY CLASSIFICATION OF THIS PAGE (When Data Entered)

REPORT DOCUMENTATION PAGE	READ INSTRUCTIONS BEFORE COMPLETING FORM
1. REPORT NUMBER: AFAPL-TR-76-103	2. GOVT ACCESSION NO.
3. RECIPIENT'S CATALOG NUMBER	
4. TITLE (and Subtitle): Flow Calibration of the Laser Test Shelter Airflow Duct	5. TYPE OF REPORT & PERIOD COVERED: Technical Report, Apr 76 — Sept 76
6. PERFORMING ORG. REPORT NUMBER	
7. AUTHOR(s): C. N. Eastlake, E. E. Ditmer	8. CONTRACT OR GRANT NUMBER(s): F33615-76-C-2095
9. PERFORMING ORGANIZATION NAME AND ADDRESS: SRL, Inc., 2800 Indian Ripple Road, Dayton, Ohio 45440	10. PROGRAM ELEMENT, PROJECT, TASK AREA & WORK UNIT NUMBERS: 30480774 07
11. CONTROLLING OFFICE NAME AND ADDRESS: Air Force Aero Propulsion Laboratory (SFH), Air Force Systems Command, Wright-Patterson AFB, Ohio 45433	12. REPORT DATE: Dec 1976
	13. NUMBER OF PAGES: 102
14. MONITORING AGENCY NAME & ADDRESS (if different from Controlling Office): 110 p.	15. SECURITY CLASS. (of this report): Unclassified
	15a. DECLASSIFICATION/DOWNGRADING SCHEDULE

16. DISTRIBUTION STATEMENT (of this Report)

Approved for public release; distribution unlimited

17. DISTRIBUTION STATEMENT (of the abstract entered in Block 20, if different from Report)

62203F

18. SUPPLEMENTARY NOTES

19. KEY WORDS (Continue on reverse side if necessary and identify by block number)

Velocity Distribution
Boundary Layer Simulation

20. ABSTRACT (Continue on reverse side if necessary and identify by block number)

This report documents an experimental flow field mapping conducted in the airflow duct of the laser/fuels/airflow facility. Velocity distributions throughout the test section and in wall boundary layers were measured and correlated with flight data on typical aircraft boundary layer conditions. Flight conditions are reasonably simulated by the observed airflow, both with and without artificial boundary layer thickening.

DD FORM 1 JAN 73 1473 EDITION OF 1 NOV 65 IS OBSOLETE

UNCLASSIFIED

SECURITY CLASSIFICATION OF THIS PAGE (When Data Entered)

$40 400

PREFACE

This final report was submitted by Systems Research Laboratories, Inc., under Contract F33615-76-C-2095. The effort was sponsored by the Air Force Aero Propulsion Laboratory; Air Force Systems Command, Wright-Patterson AFB, Ohio under Project 3048, Task 304807, Work Unit 30480774 with Allan J. Ferrenberg/AFAPL/SFH as Project Engineer. C. N. Eastlake of Systems Research Laboratories, Inc. was technically responsible for the work.

TABLE OF CONTENTS

LIST OF ILLUSTRATIONS

Section 1

INTRODUCTION

Systems Research Laboratories, Inc. (SRL) is developing a Laser Test Shelter adjoining Building 71B at the Air Force Aero Propulsion Laboratory and is integrating it with the air supply system and laser system currently operational at that facility. For the intended use of this facility, it is necessary to provide an airflow over the tank exterior surface which approximates boundary layer flow experienced on an aircraft in flight. To accomplish this end, an airflow duct has been incorporated into the facility, as depicted in the isometric view of Figure I-1. This airflow duct and its instrumentation are described in detail in the next section.

Substantiation of the fact that the duct airflow does reasonably simulate airflow over an aircraft tank surface in flight must be provided by detailed measurement of the velocities and pressures in the duct. Briefly, the airflow over the test article location in the duct must present a fully turbulent boundary layer at approximately atmospheric static pressure. Data provided by AFAPL/SFH indicate that a typical boundary layer thickness on a wing tank is 1/2 to 1-1/2 inches on a fuselage tank is 4 - 6-1/2 inches. A preliminary test plan for an experimental program to gather and analyze the necessary data is documented in Reference 1. This report describes in detail the test procedure carried out, data acquired, and analysis of the data which stemmed from that preliminary plan. A total of 183 test runs were made during the period April 27 to September 30, 1976.

Section II
DESCRIPTION OF TEST APPARATUS

The airflow duct is a subsonic, blowdown wind tunnel of rectangular cross section supplied by two high pressure bottles with a total volume of 14.2 cubic feet and capable of storing up to 2000 psi. It is constructed of welded 1/8-inch thick stainless steel sheet. The bottom wall is flat, parallel to the ground, and has a 6-inch diameter hole which will serve as the mounting position for the fuel tank surface in later tests. Directly opposite (in the top wall) the test fuel tank location is a 3-inch diameter hole through which the laser beam will be aimed to impinge on the test article surface. The entire duct can be rotated 90 degrees to facilitate aiming of the laser, which is located in the adjoining test cell. The center of the test tank surface is defined to be the origin of the XYZ-coordinate system used in acquisition and reduction of the airflow calibration data. The cross section of the duct is 5.6 inches high by 9 inches wide at this streamwise position. A side view schematic of the duct geometry is shown in Figure II-1.

Flow is controlled by two pressure regulators in series on the outlet from each of the air supply bottles. These two pipes tie into a single 4-inch pipe in which a pneumatically controlled ball valve 84 inches upstream of the test article is installed to provide total flow shut-off. A 45 degree half-angle, 10-inch diameter perforated cone is installed 19 inches downstream of the ball valve (X = -65) to damp turbulence and to restore uniformity to flow which was not attached to the walls of the 4-inch to 10-inch expansion cone immediately downstream of the ball valve. The duct continues through the wall of the Test Shelter at 10-inch diameter, then a conical nozzle reduces the diameter to 7 inches. Rectangular openings in the sides of the conical nozzle serve as inlets to the bypass ducts, each of which has an area equal to half of the main duct area. A butterfly valve with pneumatic

control in the 7-inch diameter duct provides for blockage of the main flow so that all flow is routed through the bypass ducts.

This provides a means of cutting off the air (oxygen) supply in the main duct in later tests should a fire develop. The butterfly valve was always fully open in these calibration tests, except when the bypass ducts were blocked off by means of a flat plate installed in the flanged joint at X = -30. This increased the maximum velocity attainable in the test section, and when this was done the butterfly valve was removed. A transition section from 7-inch diameter to 4-inch × 9-inch rectangular is installed downstream of the butterfly valve, and a constant cross section approach duct of these dimensions and 18 inches long leads to the test section. A reference velocity is provided by the permanent calibration probe installed on the centerline of the top wall of the constant area section 16 inches upstream of the test article (X = -16). This probe incorporates a wall static pressure tap, a pitot probe at the geometric center of the 4-inch × 9-inch cross section, and a total temperature thermocouple. Figure II-2 is a sketch of this probe, and Figure II-3 is a compressible flow calculation curve used to correlate calibration probe readings with flow velocity. Readings from this probe are not primary data for these airflow calibration tests, but correlation of calibration probe readings with readings obtained in the test section will provide a reference reading for use during the later fire propagation tests.

Primary test data were taken with pitot-static instrumentation installed temporarily in the test section. It will be removed when calibration tests are completed. Two styles of pitot pressure rakes were employed. A five-probe vertical rake was used for measurement of boundary layer velocities on the bottom wall. This rake (Figure II-4) employed 0.032-inch O.D. tubing at 0.10-inch height intervals. It mounted on a 6-inch diameter plate which filled the hole intended for later installation of a test article.

Flush wall static taps in the mounting plate (Figure II-5) provided static pressures at streamwise stations corresponding to the tips of the boundary layer rake probes. This rake could be installed at nominal positions of the center of the test article (X = 0), two inches upstream (X = -2), and two inches downstream (X = 1-3/4, moved forward 1/4-inch from nominal to avoid mechanical interference). It could also be mounted 1-1/2 inches to the left and right of the centerline at X = 0.

The second style of rake is a five-probe horizontal rake which employs 1/8-inch O.D. tubes spaced 1-1/2 inches apart laterally. The rigid tubes are brought out through a clearance hole in the top wall of the duct and the rake mounts on a vertical knife-edge strut so that the vertical position of the rake can be set at any desired height (see Figure II-6).

Data taken on these probes and rakes were recorded on an eight-track oscillograph recorder. Temperature was read on a type-T thermocouple at the permanent calibration probe and assumed to be valid at the test article location. Pressure readings were taken on differential pressure transducers calibrated to 2 psi full scale on six of the oscillograph channels and 5 psi full scale on the permanent probe channel. Scale doublers incorporated in the preamplifiers were employed in some of the higher velocity runs. A detailed list of instrumentation used is as follows:

1	Beckman (Offner Div.), Type 504D, Dynograph Recorder
2	Beckman (Offner Div.), Type 428A, Dynograph Amplifier
8	Beckman (Offner Div.), Type 481B, Preamplifier
1	Type-T Thermocouple, Bare Junction, 0.10-inch wire
1	Beckman (Offner Div.), Type 9827 Cold Junction Compensator
7	CEC 4-321MA Transducer, ±7-1/2 psid
7	Beckman (Offner Div.), Type 9803, Strain Gauge Coupler

Finally, a row of vortex generators was provided as shown in Figure II-7 to create an additional momentum loss along the bottom wall, artificially thickening the boundary layer. Following initial tests the vortex generators were narrowed 50 percent making two staggered rows of blades as shown shaded in the figures. This row was mounted transverse in the duct, either 14 inches upstream of the test article (X = -14) or 27 inches upstream (X = -27).

Data taken with these instruments, test procedure, and results of the data analysis are described in detail in the following sections.

Section III
TEST PROCEDURE AND INITIAL FLOW IMPROVEMENT EFFORTS

The first procedural task to be undertaken was to define an axis system consistent with the amount and type of data required to define the duct flow field. Figure III-1 shows the axis system and the locations at which data points were measured. As mentioned previously, the streamwise axis is defined as the X-axis, and X = 0 being the center of the test article hole and positive values progressing downstream. The Y-axis is vertical with the origin corresponding to the surface of the bottom duct wall and positive upward. The Z-axis is lateral with the origin at the left-to-right centerline and positive to the right when the observer is looking upstream.

The downstream projection of the geometric center of the constant area approach duct is arbitrarily defined as the nominal center of the test section (X = 0, Y = 2, Z = 0). This was the velocity measurement position used in initial checkout of the flow characteristics of the duct.

The first series of test runs was intended to determine whether sufficient test time would be available for steady flow establishment and to determine what pressure regulator settings would produce the desired velocity in the test section.

At the nominal test section velocity of 250 ft/sec, which was used for approximately 50 percent of the test runs, a usable test time of 3-4 seconds was experienced when the supply bottles were filled to half capacity or 1000 psi. This agrees well with the initial estimates of Reference 1, which assumed the total flow to be evenly divided between the main duct and the bypass ducts. At a supply pressure of 1200 psi, the available test time at a nominal velocity of 350 ft/sec was approximately 3 seconds. Blockage of the bypass ducts doubled

both of these velocities while maintaining the same test times, respectively. In all cases this is very adequate test time for calibration data acquisition. Should it be desirable to have longer test times for fire propagation tests, filling the supply bottles to capacity will nearly double the test time. Since the flow velocity is low enough to be essentially incompressible, it can be concluded in general that test times will vary from those stated in direct proportion to supply bottle initial pressure and inversely proportional to nominal test section velocity.

Steadiness of the mean flow velocity as a function of time had proven to be fairly sensitive to relative values of the two pressure regulator settings in another test facility employing this same air supply system. This does not appear to be the case for the Laser Test Shelter Airflow Duct. Some time-dependent variation of the mean flow is visible on the oscillograph traces of total and dynamic pressure. It appears simultaneously at all probe locations and is most likely attributable to minute self-adjustments by the pressure regulators to compensate for the continuous decrease of pressure in the supply bottles. The variation is small enough (typically only a few percent of dynamic pressure) that a representative mean value of dynamic pressure on any given probe is easily selected.

Supply bottle pressure and dome pressure for each regulator were recorded for all test runs. Once a set of dome pressures which produced the desired test section velocity was experimentally determined, these settings were very stable and could be left untouched for a full day of testing. A statistical analysis of the measured duct velocities was made to determine the repeatability of the data, given a fixed set of regulator dome pressures, and the results were quite acceptable for a flow facility of this type. Fifty-nine consecutive runs conducted over a period of eight days produced velocity readings at the

permanent calibration probe which exhibited a root-mean-square (standard) deviation of 2.24 percent. That is, 95 percent of the velocity readings would then be expected to fall with a $\pm 2\sigma$ band, or ± 4.5 percent, for a given set of regulator dome pressures.

Regulator settings which were used are summarized in the following table for future reference.

$V_{nominal}$ (ft/sec)	Perforated Cone	Upstream Dome Pressure (psi)	Downstream Dome Pressure (psi)	Bypass Ducts
250	out	100	90	open
250	in	160	130	open
350	in	220	200	open
500	in	160	130	blocked
700	in	220	200	blocked

Once it was established that sufficient test time and mean flow steadiness were available, examination of the flow distribution in the duct began in earnest. Installation of the horizontal rake at Y = 2 made it immediately clear that the flow was drastically offset toward the right wall (looking upstream). Subsequent investigation showed that internal stops in the pneumatic actuator for the butterfly valve at X = -43 had been improperly set. The result was that the full open position of the valve was about 30 degrees offset rather than the intended position of parallel to the flow. Minor modification of the internal mechanism and careful alignment of the reinstalled valve alleviated this problem.

The flow distribution over the duct cross section at X = 0 and $V_{nominal}$ = 250 ft/sec was then mapped to ensure that a reasonably uniform distribution had been attained and that the boundary layer thickness was within the desired range. This

proved to be true, and the plotted data are presented and discussed in the next section. It was apparent, however, that an unrealistically high level of turbulent fluctuations was present. The fluctuations were large enough to make data reduction very tedious and left uncertain confidence in the accuracy of the mean velocity read from the oscillograph traces. Electrical filtering of the transducer output was considered but finally rejected because of the difficulty in ensuring that false readings would not be introduced. "Mechanical filtering" of the probe pressures was successfully accomplished by installing 0.020-inch I.D. tubing about 1/2-inch long in the 1/8-inch I.D. flex tubing used to plumb the probes to the transducers. This solution was also rejected after discussion with AFAPL/SFH personnel on the possibility of unrealistically high turbulence levels introducing unrepresentative transport properties into subsequent fire propagation tests.

The course chosen at this point was to fabricate a 45 degree half-angle cone with a 10-inch base diameter from 0.060-inch thick perforated steel sheet of 35 percent porosity. This cone was installed with its vertex downstream in an existing flange joint in the 10-inch I.D. pipe at X = -65. The 0.080-inch diameter holes in the perforated cone provided a striking decrease in turbulence level, as demonstrated by the comparison oscillograph traces in Figures III-2 and III-3. The price paid was the increased pressure drop, evidenced by pressure regulator settings in the above table required to maintain a 250 ft/sec velocity in the test section. Examination of the dynamic pressure traces subsequent to installation of the perforated cone led the authors to the conclusion that satisfactory flow quality had been achieved and the calibration should proceed.

Referring back to Figure III-1, data were first taken at X= 0 with the laser penetration hole open, as this represents the configuration intended to be employed most frequently in follow-up tests. The boundary layer rake was used at Z = -1 1/2, 0, and

+1 1/2. The horizontal rake was set at Y = 1/2, 1, 2, 3, 4, and 5. This provides sufficient data to map the velocity distribution through the cross section with reasonable accuracy. Since it is possible, yet undesirable, to close the laser penetration hole with a window, a number of rake positions were repeated with a plate clamped over the flanged top of the laser hole to investigate the effect on the flow distribution. In addition, a few rake positions were repeated with the laser hole taped over on the inside of the top wall of the duct, thus eliminating the cavity left in the wall when the laser hole is blocked at the outside flange. A viewing window 4 inches in diameter and approximately 6 inches (center-to-center) upstream of the laser hole in the top wall was found to be indented 1/8-inch from the surface rather than flush, so this indentation was filled flush temporarily to see if it had a noticeable effect on the velocity distribution.

Essentially the same set of data was then taken 2 inches upstream of the center of the test plate and again 2 inches downstream. This provided a rather detailed three-dimensional map of the flow distribution in the region around the center of the test plate.

A set of vortex generators (see Figure II-7) had been fabricated in order to attempt simulation of the thicker boundary layer typical of that experienced in flight on the surface of a fuselage tank. This was installed initially at X = -14 on the bottom wall of the duct. The data sequence described above for X = 0 was then repeated. The effect was dramatic and, as discussed in detail in the next section, showed too large a momentum removal, so data at X = +2 and -2 were not taken. The vortex generators were modified and reinstalled alternately at X = -14 and X = -27 with much more satisfactory results.

The velocity was increased to the maximum obtainable with the regulator settings currently in use in the facility. The test section velocity was 350 ft/sec. Since capability to produce higher velocities seemed potentially valuable, the bypass ducts were blocked temporarily, and the test section velocity doubled as compared to the bypass ducts open for a given regulator setting. In this manner, calibrations were run at 500 and 700 ft/sec. Data were taken at these velocities at $Y = 0$ only. The effect of the laser penetration hole being open or closed and the vortex generator in or out was investigated with substantially the same results found at the nominal velocity of 250 ft/sec. Again, these data are discussed in detail in the next section.

In all of the above test runs, the velocity was recorded at the permanent calibration probe. The ratio of velocity at the permanent probe to maximum velocity at the test section center was calculated and is plotted in Figure III-4 as V_{cal}/V_{max}. V_{max} occurs at Y = 2 with the VG out and at Y = 3 with the VG in. Since this probe does not interfere with fire propagation equipment to be installed later, it will be left in place and the velocity correlation in Figure III-4 will provide an indication that velocities being experienced at the test article are the desired magnitude. Data plotted is for $V_{nominal}$ = 250 ft/sec only, but is equally representative of $V_{nominal}$ = 350, 500, and 700 ft/sec.

In making the above correlation and in reducing all velocity data, incompressible flow was shown to provide acceptable calculation accuracy and pitot-static readings were converted to velocity accordingly, i.e., using $V = \sqrt{2(P_T-P_S)/\rho}$. Density ($\rho$) was calculated for atmospheric pressure and the temperature reading taken 2 seconds after the initial flow start-up transient had settled out. This 2-second delay was used because the temperature reading exhibited a nearly linear decrease with time over the entire test time due to expansion cooling in the supply

bottles. A 2-second interval between initial start-up and taking of data was judged to be representative of the manner in which fire propagation tests will be conducted. Since the thermocouple is 0.010-inch diameter, bare wire, Reference 2 indicates a time constant of 0.3-0.4 seconds and the initial transient should thus have no effect on this reading.

Plots of all the above data and a discussion of their significance are presented in the next section.

Section IV
PRESENTATION AND DISCUSSION OF DATA

The principal goal of these tests is to determine whether the airflow duct produces a boundary layer on the test article surface which simulates that experienced in flight. For a representative Air Force aircraft, the F-4, typical boundary layer thickness, δ, on a wing tank is one inch and for a fuselage tank is five inches. Using the traditional seventh power law (Reference 3) for velocity distribution in a boundary layer, $V_{local}/V_{freestream} = (Y/\delta)^{1/7}$, the boundary layer velocity profiles for boundary layer thicknesses of one through eight inches are plotted in Figure IV-1. These are the velocity distributions on the bottom wall of the airflow duct which are desired.

A second simulation goal is to provide a surface pressure on the test article which is near but slightly below atmospheric. This is representative of the prevailing surface pressure on most of the exterior tank skins in flight.

It also results in a small inflow through the laser penetration hole which may help contain a fire within the airflow duct. Static pressures measured on the wall of the duct throughout the series of tests are plotted versus streamwise position, X, in Figure IV-2. In all cases, the static pressure in the test section is within roughly 1/4 to 1-1/2 psi below atmospheric Since the upper wall of the test section is diverging at a 7.35 degree angle, the static pressure becomes slightly more negative as the probe moves upstream. The divergence begins at X = -12 and upstream of that point, as indicated by the dashed lines on the figure, the cross section is constant and the static pressure should also be nearly constant. The permanent calibration probe is in the constant area section at X = -16. Since the duct flow is low subsonic and exhausts to atmosphere, the static pressure in the test section is correspondingly farther below

atmosphere at higher nominal velocities. It is also apparent from this figure that the open laser penetration hole provides some relaxation of static pressure, for the pressure in almost all cases is slightly farther below atmosphere with the hole blocked than with it open.

BASELINE DATA

Figures IV-3 through IV-7 summarize the velocity profiles measured at 250 ft/sec nominal velocity and at X = 0 with the laser penetration hole open. This is the basic set of data for these tests. The key points to be noted are:

1. There is an area of approximately 2 inches in height in the vertical center of the duct over which the velocity is reasonably constant. This is the "freestream."
2. The boundary layer thickness is roughly one inch and the velocity distribution agrees quite well with the theorectical profile in Figure IV-1.
3. The left-to-right distribution of flow velocity is reasonably good in the lower half of the duct. Interference with the inflow through the open laser hole retards the velocity distribution in the upper half of the duct near Z = 0. This is especially evident at Y = 4 and Y = 5 in Figure IV-5, and in Figure IV-7. The slightly higher velocity to the left of the centerline within the boundary layer, Figure IV-6, appears consistently though there is no apparent reason for such a pattern.
4. Referring to Figure IV-7, cross plotting of V vs Y profiles and V vs Z profiles produces the velocity contour map shown. The contours circumscribe that part of the duct cross section in which the velocity is at or higher than the velocity identifying the contour. This figure shows that slightly more than a third of the cross section is within the contour,

240 ft/sec, which represents 96 percent of the nominal velocity. This indicates a quite acceptable flow distribution. The fact that the contours are nearly parallel to the bottom wall is a further indication that the boundary layer is essentially constant laterally across the test plate. The asymmetry in the higher velocity contours, which does not occur in the lower velocity contours, is probably due to the manner in which curves were faired through V-vs-Y and V-vs-Z data and is not significant in analyzing the flow quality. The high velocity sections of the velocity profiles are relatively flat and small variations in curve fairing produce noticeable differences in the physical location of a given velocity magnitude, which is used to cross-plot the velocity contour map.

EFFECT OF TURBULENCE DAMPING CONE

The data taken before the perforated cone was installed are presented in Figures IV-8 through IV-10 for comparison. The velocity profiles are qualitatively the same as after the cone was installed. The boundary layers appear to be somewhat thinner, especially on the upper wall. This is consistent with the higher effective Reynolds number caused by the very high turbulence level, since turbulent boundary thickness is inversely proportional to Reynolds number to the one-fifth power. For example, following the discussion of Reference 4, doubling the effective Reynolds number from 10×10^6 to 20×10^6 by increasing turbulence factor would result in a 13 percent decrease in boundary layer thickness. In all fairness, however, it must be pointed out that this earlier data required a bit more subjectivity in data reduction as can be seen from the comparison in Figure III-2 and that may be the source of any small differences.

STREAMWISE VELOCITY VARIATION

The next set of comparison data examines the streamwise variation in velocity distribution. Two sources for differences are present. First is that the upper wall diverges at a 7.35 degree angle. The diffusion should reduce the maximum velocity and thicken the boundary layer due to adverse pressure gradient as measurement location moves further downstream. The second is interference with flow in through the open laser hole.

Data for X = -2 are presented in Figures IV-11 through IV-13. Data for X = +2 are presented in Figures IV-14 through IV-16.

Referring to Figure IV-11, at X = -2, the boundary layer is the same as X = 0 on the bottom wall but is significantly thinner on the top wall. This is probably due to less interference with flow through the laser hole as this station is 1/2 inch upstream of the forward edge of the hole. The maximum velocity is slightly higher than at X = 0, as one would expect since the cross-sectional area is smaller. More significantly, the higher velocity is felt over a much larger portion of the cross section as is shown clearly by Figure IV-12 and IV-13. And the retarding effect of the laser hole is less pronounced, but certainly not gone altogether.

In Figure IV-14, it can be seen clearly that the velocity distribution near the wall is identical for X = +2 and X = 0. It is severely retarded near the upper wall to the point of complete separation and flow reversal. This shows even more clearly in Figure IV-15. The explanation becomes apparent when Figure IV-16 is considered. A separated or reversed flow region is formed on the top wall where inflow through the laser hole cannot negotiate the 97.35 degree turn required for boundary layer attachment. This region not only causes the duct velocity to fall to zero at some point away from the wall, but also presents an effective

area blockage. The area blockage is essentially equal to the geometric area increase due to upper wall divergence. The result is that the effective area at X = +2 nearly equals that at X = 0, and no centerline velocity decrease is noted. The major difference between the constant velocity contours at X = +2 and X = 0 is that the high velocity contours are squeezed in the vertical direction by the blockage and they expand horizontally. This compensating effect is simply that dictated by conservation of momentum. It has been observed in other three-dimensional flow fields which are artifically forced to deviate from their normal shape and is described and analyzed in detail in References 5 and 6.

The important final result from these comparisons is that for experimental purposes the boundary layer can be considered constant over the entire test plate surface.

EFFECT OF LASER PENETRATION HOLE

The effect of closing the laser penetration hole on velocity distribution can be seen by referring back to Figure IV-3. The distribution at and below the center of the duct is substaintially unchanged. This is further demonstrated by Figure IV-17. The distribution above the centerline is less affected by the presence of the laser hole, but as Figure IV-18 confirms, there is still some degradation of velocity at Y = 4 and Y = 5 near Z = 0.

To further investigate the velocity decrease at Z = 0, the laser hole was taped over on the inside of the duct wall eliminating the open cavity left by blocking the hole at the top flange. In addition, the recessed viewing window was filled flush and taped over. Figures IV-19 and IV-20 show the resulting data. A noticeable increase in velocity at Z = 0 is observed, but a decrement still exists even with everything on the inside surface made flush. The cause of the decrement is unknown. Fortunately, it does not adversely affect the velocity distribution on the surface of the test plate.

A velocity contour map with the laser hole closed, Figure IV-21, reaffirms the conclusion that closing the hole has no significant effect except that of lessening the interference near the top center of the duct.

Referring back to Figure IV-11, at two inches upstream of the test plate center (X = -2) there is no significant effect of closing the laser hole, as would be expected since this is 1/2 inch upstream of the edge of the hole. Figures IV-22 and IV-23 confirm this.

A X = +2, Figure IV-14 shows that closing the laser hole eliminates the separated region on the upper wall caused by inflow through the hole. It also shows that the expected centerline velocity decrease relative to X = 0 is now present (see Figure IV-24 also) though the boundary layer thickness is unchanged. Figure IV-25 shows that the left-to-right distribution now shows no center decrement up to Y = 4. Figure IV-26 indicates that making the interior surface of the upper wall flush has a noticeable but not really significant effect at Y = 5, as was the case at X = 0.

ARTIFICIAL BOUNDARY LAYER THICKENING

Initial installation of the vortex generators had a dramatic effect on the velocity distribution. The heart of the comparison is shown in Figure IV-27. It is immediately clear that the drag of the vortex generators causes too large a momentum loss in the boundary layer. The resulting flow blockage on the bottom wall of the duct shifts the entire velocity distribution upward, leaving a velocity profile in the boundary layer which is too slow. The result is consistent with calculations made using a modification of the format of Reference 7, which relates desired momentum loss in a boundary layer to drag characteristics of circular cyclinders used to artificially thicken boundary layers.

The drag (frontal area) of the vortex generator set was subsequently reduced by approximately one-half, and the mounting location was moved 13 inches upstream (X = -27) to allow more mixing length ahead of the test plate. As the plotted profile shows, this VG produces a velocity distributuion characteristic of a turbulent boundary layer of about 2-inch thickness, or double that which naturally exists.

Figures IV-28 through IV-30 show that the left-to-right distribution with the original vortex generator is qualitatively the same as without the vortex generator. In fact, Figure IV-30 shows such close correspondence that it is somewhat misleading. It is merely coincidence that at Y = 2 the magnitudes of the two V vs Y profiles are nearly identical, in spite of the fact that the profiles are drastically different. The dramatic upward shift of the entire flow distribution is clearly pointed out by comparing Figure IV-31 with Figure IV-7. The distribution throughout the cross section with the modified VG is completely analogous to that produced by the original VG, except that the upward shift of the high velocity contour is less pronounced. The effect of closing the laser hole on the artificially thickened boundary layer using the original VG is shown in Figures IV-32 through IV-34. The difference is somewhat more pronounced than observed with the natural boundary layer. This is due to the profiles being skewed toward the upper wall so that the interference with inflow through the laser hole (or lack thereof) is felt more strongly by the boundary layer on the bottom wall.

INCREASED NOMINAL VELOCITY

A. $V_{nominal}$ = 350 ft/sec

At the highest settings available on the flow control regulators with the bypass ducts open, the test section centerline velocity (see Figure IV-35) is just below 350 ft/sec. The distribution is nearly identical to that measured at the lower nominal velocity as can be seen by comparing Figure IV-3. The consequence is that the boundary layer thickness is not changed. Comparison of Figure IV-36 with Figure IV-5 and Figure IV-37 with Figure IV-6 shows that the left to right distribution of essentially unchanged. This fact is also demonstrated in Figure V-1 in the summary. Figure IV-38 indicates that the distribution over the duct cross section at X = 0 has not changed significantly at higher nominal velocity.

Closing the laser hole has basically the same effect as it had at the lower velocity. Figures IV-35 and IV-39 indicate that lessening of interference with inflow at the top wall thins the boundary layer on the top wall while not changing the distribution markedly on the bottom wall. The V vs Z profile at Y = 2 is unchanged and that at Y = 5 exhibits significantly reduced velocity retardation at Z = 0.

Figures IV-40 through IV-42 show the effect of reinstalling the original vortex generator. Once again, the change is striking and the velocity decrement near the lower wall is larger than desired. The left-to-right uniformity is comparable to that observed at the lower velocity, with a significant velocity profile interference at Y = 4 and Y = 5 from flow through the laser hole.

The effect of closing the laser hole, Figure IV-43 and IV-44, is also directly comparable to that observed at the lower velocity. The entire flow pattern is lifted slightly toward the upper wall, the lower boundary layer is slowed even further, and there is less interference at Y = 4 and Y = 5.

B. $V_{nominal}$ = 500 ft/sec

In order to produce higher test section velocities the bypass ducts were blocked, diverting the total flow through the center section of the duct. This was accomplished by clamping a flat plate into the flanged joint at X = -30. Using the same flow control regulator settings that orignally produced 250 and 350 ft/sec, the test section velocities which result are 500 and 700 ft/sec, respectively. Figures IV-45 and IV-46 show the profiles measured along the Y-axis at $V_{nominal}$ = 500 ft/sec with the laser hole open. This distribution is once again comparable to that measured at the other velocities (see also Figure V-1). The boundary layer thickness is approximately one inch. Figure IV-47 shows the profiles across the Z-axis. It is apparent that the retarding influence of the laser penetration hole is even more pronounced in the upper half of the duct at the higher velocity, although the character of the flow in the bottom half of the duct is not significantly altered. Constant velocity contours across the cross-section at X = 0 are plotted in Figure IV-48. The flow distribution is of very adequate uniformity.

Figures IV-49 through IV-51 show the effect of closing the laser penetration hole. The result is analogous to that found at lower velocities, but is a bit more pronounced. Closing the hole produces a sufficiently fuller profile in the Y direction to cause a noticeable reduction in the maximum velocity, as dictated by conservation of momentum. This is also evident in the Z-profiles and the constant velocity contours.

The boundary layer thickening effect of the row of vortex generators is defined in Figure IV-52. At this higher velocity, provision was made to mount the original vortex generator configuration as far upstream of the test plate (X = -27) as was mechanically practical. This provided more streamwise length for the wake of the protuberances to mix into a boundary layer type profile. The outcome was that the original configuration still produces a profile with a slight S-curve, which is not representative of a natural boundary layer. The modified vortex generator produces a profile of the desired shape when mounted at X = -27, but the S-curve reappears when it is moved to X = -14. This demonstrates that mixing distance is also of paramount importance. The profile resulting from the modified vortex generator installed at X = -27 appears to provide an adequate representation of a very thick boundary layer, at least in the region extending up to approximately one inch above the test plate. It is impossible to simulate the entirety of a thick profile, since the duct is only 5.6 inches high and a boundary layer exists on the upper wall also. However, the layer closest to the wall dominates the shear stress and mixing properties of the boundary layer. Thus, it is the author's conclusion that this last profile is representative of a boundary layer with a thickness of approximately 10 inches. Figures IV-52 and IV-53 show the left-to-right distribution of velocity and the constant velocity contours at X = 0 for this configuration.

C. $V_{nominal}$ = 700 ft/sec

Setting the flow control regulators wide open with the bypass ducts blocked produced a maximum velocity of slightly over 700 ft/sec. Calibration data at this maximum velocity was taken only with the laser hole open and the vortex generator removed. Figures IV-55 and V-1 show that in this open tunnel configuration the boundary layer velocity distribution is again

typical of a one inch thick boundary layer. As expected from trends shown in lower velocity data, the inflow through the laser hole has its greatest retarding effect at maximum nominal velocity. The flow over the test surface, however, is not adversely affected.

GENERAL FLOW CHARACTERISTICS

1. It is estimated that mean values of dynamic pressure were read from the oscillograph traces within an accuracy band of ±.02 psi or less. At the magnitudes of dynamic pressure and temperature typically observed, the resulting estimated accuracy is approximately ±4 ft/sec.

2. The flow split was assumed in the original duct design to be 50 percent through the main duct and 50 percent through these bypass ducts. An attempt was made to experimentally verify this assumption. Ten runs were analyzed. Total flow rate was estimated by calculating total mass stored in the 14.2 cubic foot bottles at the known initial pressure, and dividing by the observed run time. Mass flow through the main duct was calculated from the product of cross-sectional area, local density, and an estimated average velocity. This method is admittedly crude, and the resulting calculations varied from about 35 percent to 65 percent of the total flow going through the main duct. In the absence of more detailed instrumentation, it seems reasonable to maintain the assumption of a 50 percent flow split. This hypothesis is further borne out by the fact that blocking the bypass duct did in fact nearly double the flow velocity through the main duct.

3. The time-dependent fluctuations in the pressure traces display a sufficiently consistent pattern to warrant some speculation that their source is not random turbulence. Referring to Figures II-2 and II-3, the prominent fluctuations before the damping cone was installed are typically 60 - 70 cycles per second. This frequency is observed in nearly all runs and is considered to be freestream turbulence. After the perforated cone was installed, the fluctuations at this frequency are still noticeable but at an insignificant magnitude. Reduction of the magnitude of the rapid fluctuations gives visibility to a slower fluctuation, generally 6 - 8 cycles per second. The striking pattern in the slower fluctuations are of opposite sign on opposite sides of the duct. That is, at any instant when a positive fluctuation occurs left of center a negative fluctuation occurs right of center. And the magnitude is slightly greater closer to the side than in the center.

Initially the 7-inch diameter butterfly valve was suspected as the source, especially when careful measurement showed that the valve shaft could oscillate just over one degree due to mechanical tolerance in the shaft-to-actuator coupling. However, a level arm clamped to the shaft and wired down to eliminate the shaft motion did not affect the fluctuations at all. Finally, the butterfly valve was removed entirely, and the fluctuations persisted.

Investigation of unsteady flow in ejector nozzles (Reference 8) led to the discovery that nozzle flow could be made to oscillate at a characteristic frequency by providing externally interconnected cavities on opposite sides of the nozzle inside surface. The bypass duct inlets bear a certain similarity to this cavity arrangement. And they are interconnected in the sense that they dump into a common chamber downstream of the test section. It seemed plausible that this "fluidic switch" could be source of the slower

frequency oscillations. However, blockage of the bypass ducts to achieve higher test section velocity did not eliminate the fluctuation. At this point, efforts to determine the source were terminated since the magnitude of the fluctuations is manageable in reading data from the traces.

Section V
SUMMARY AND CONCLUSIONS

Extensive study of the reduced data presented here and also of the raw data has led to the following conclusions.

1. Sufficient run time exists for steady flow establishment. Run times of 6-8 seconds can be attained.

2. The flow distribution, reasonably uniform, is of acceptable uniformity to conduct the planned fire propagation tests.

3. The turbulence level is modestly high, but is well within the limits which allow accurate reading of data.

4. Repeatability of data is within the reading/reduction accuracy of the data.

5. The boundary layer thickness on the surface of the test plate over the entire velocity range calibrated is representative of a wing tank ($\delta \approx 1$ inch) and is uniform over the 6-inch diameter of the test plate. This is clearly shown in Figures V-1, V-2, and V-5.

6. The thicker boundary layer representative of a fuselage tank surface is attainable with the modified vortex generator as shown in Figures V-3 through V-5 for intermediate velocities in the calibrated range. The effect of the vortex generator is velocity dependent. Thus, several different sets would be required to simulate the same artificially thickened boundary layer at different velocities.

7. The open laser penetration hole does not adversely affect the flow on the test plate surface. There is no apparent reason to require closing it with a laser "window."

REFERENCES

1. C.W. Ingram, "Analysis and Experimental Plan for Laser Test-Flow Duct," SRL Aerosystems Research Division Note 75-16-15.

2. The Omega Temperature Measurement Handbook, Omega Engineering Inc., Stamford, Conn., 1975.

3. H. Schlicting, Boundary Layer Theory, McGraw-Hill, Second Edition, 1960.

4. A. Pope, Wind-Tunnel Testing, Wiley and Sons, Second Edition, 1958.

5. C.N. Eastlake, "The Macroscopic Characteristics of Some Subsonic Nozzles and the Three-Dimensional Turbulent Jets They Produce," AF Aerospace Research Laboratories Report ARL 71-0058, March 1971.

6. C.N. Eastlake, "Velocity Measurements in Partially Confined Rectangular Jets," AF Aerospace Research Laboratories Report ARL-72-0121, September 1972.

7. L.J. Otten and J.T. VanKuren, "Artificial Thickening of Transonic Boundary Layers," AIAA Paper 76-51, January 1976.

8. H. Viets, "Thrust Augmenting Ejectors," AF Aerospace Research Laboratories Report ARL 75-0224, June 1975.

FIGURES

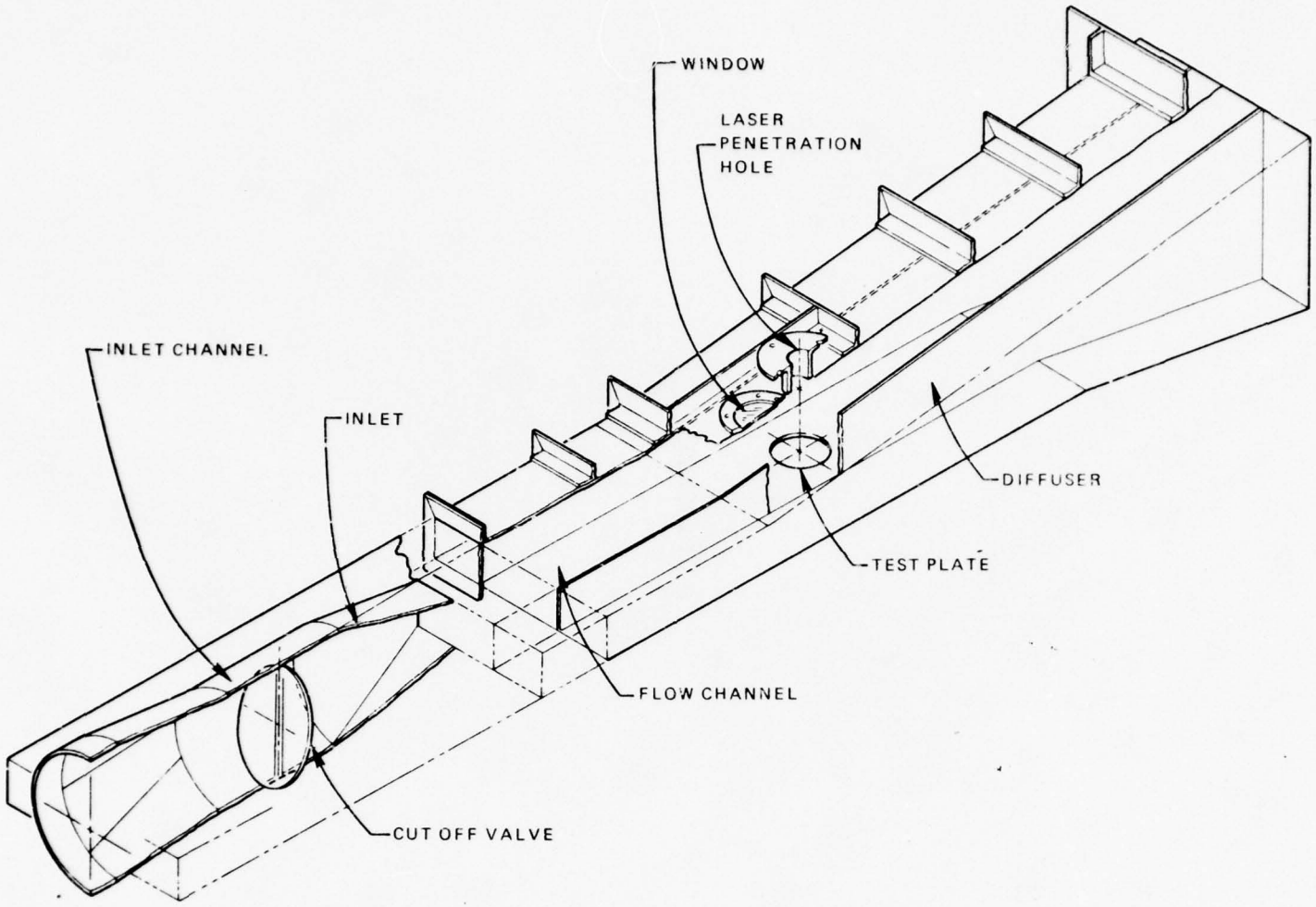

Figure I-1. Laser Test Shelter - Airflow Duct.

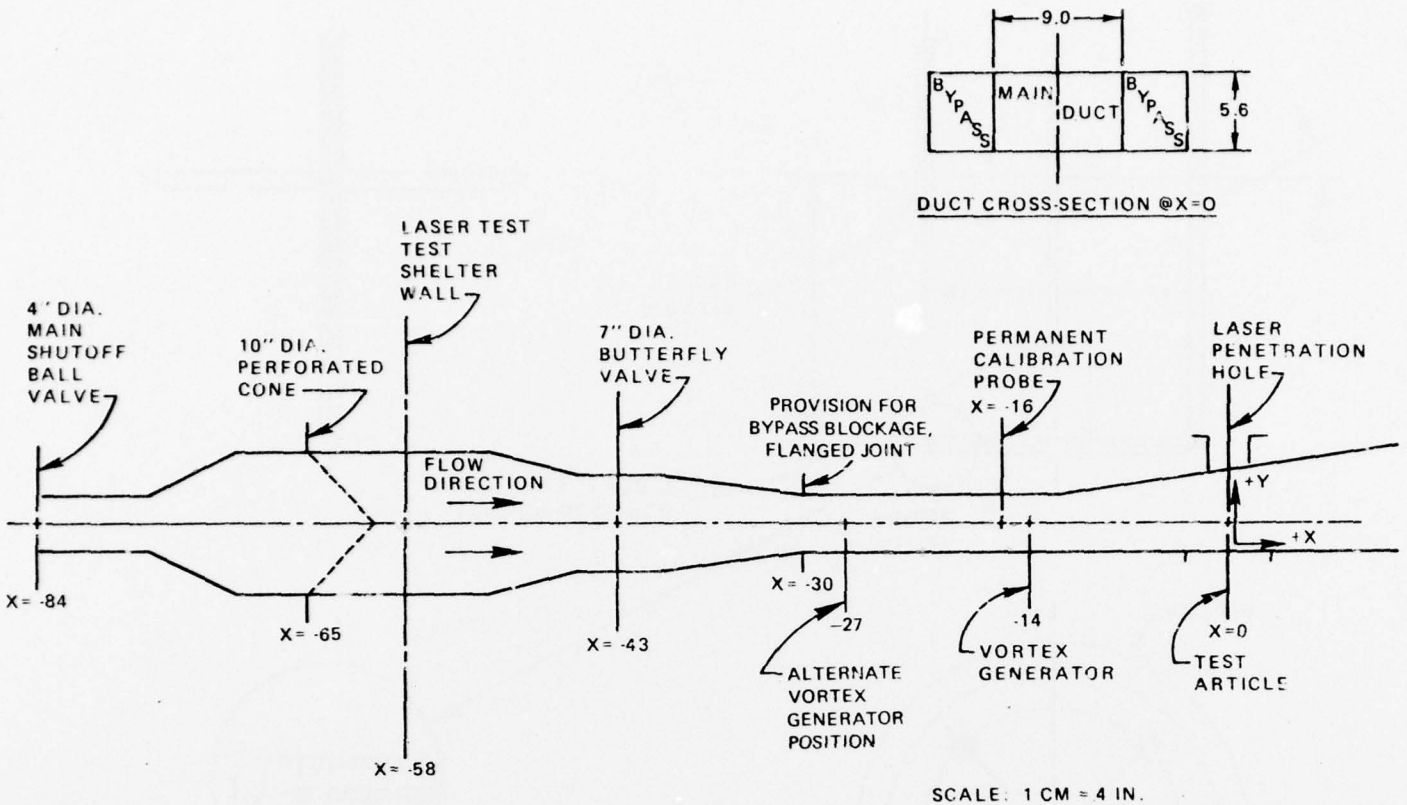

Figure II-1. Sideview Schematic of Airflow Duct.

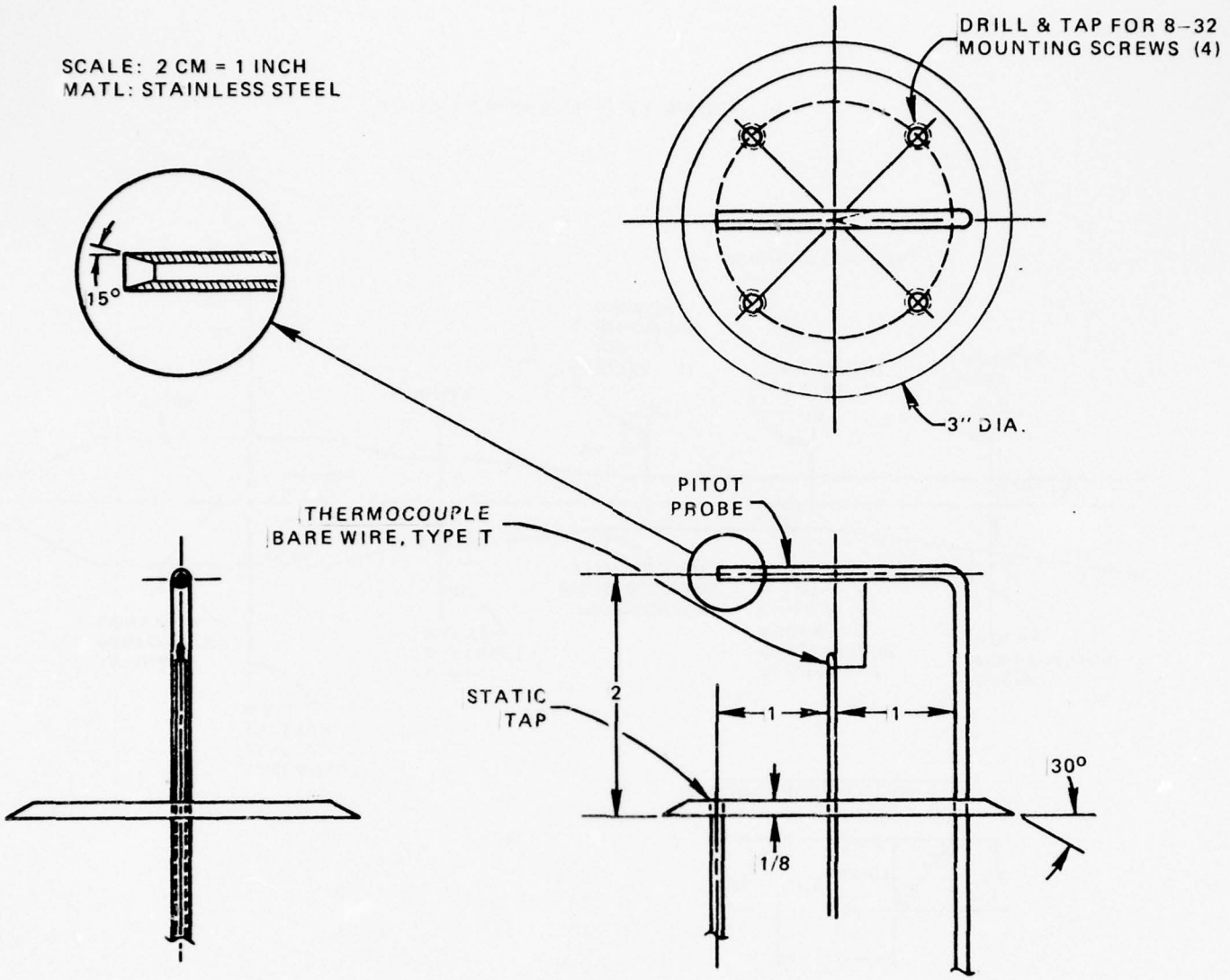

Figure II-2. Permanent Calibration Probe.

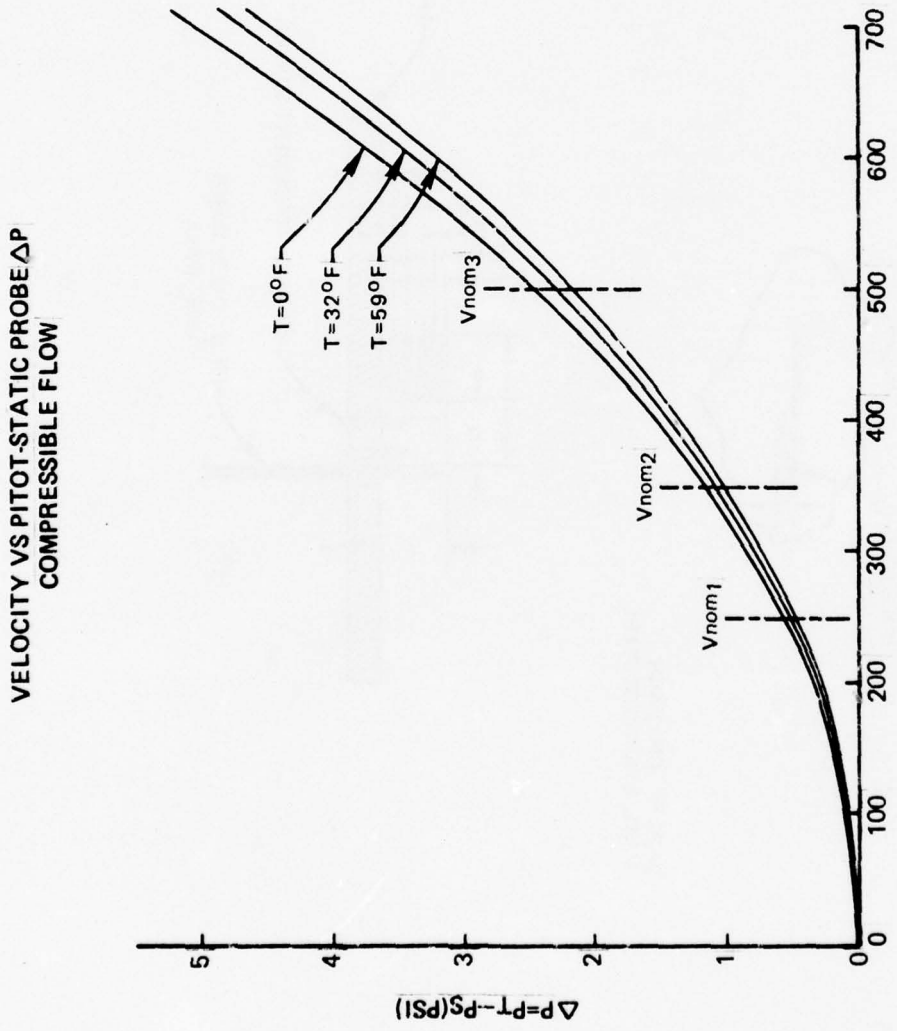

Figure II-3. Calibration Curve.

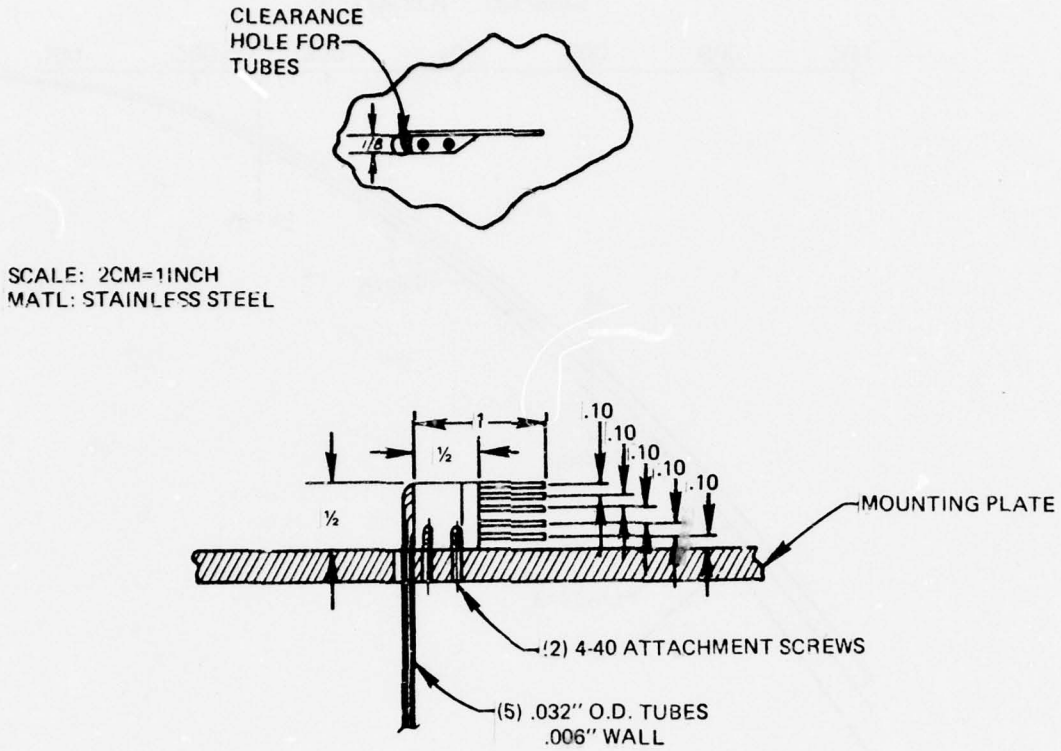

Figure II-4. Boundary Layer Rake.

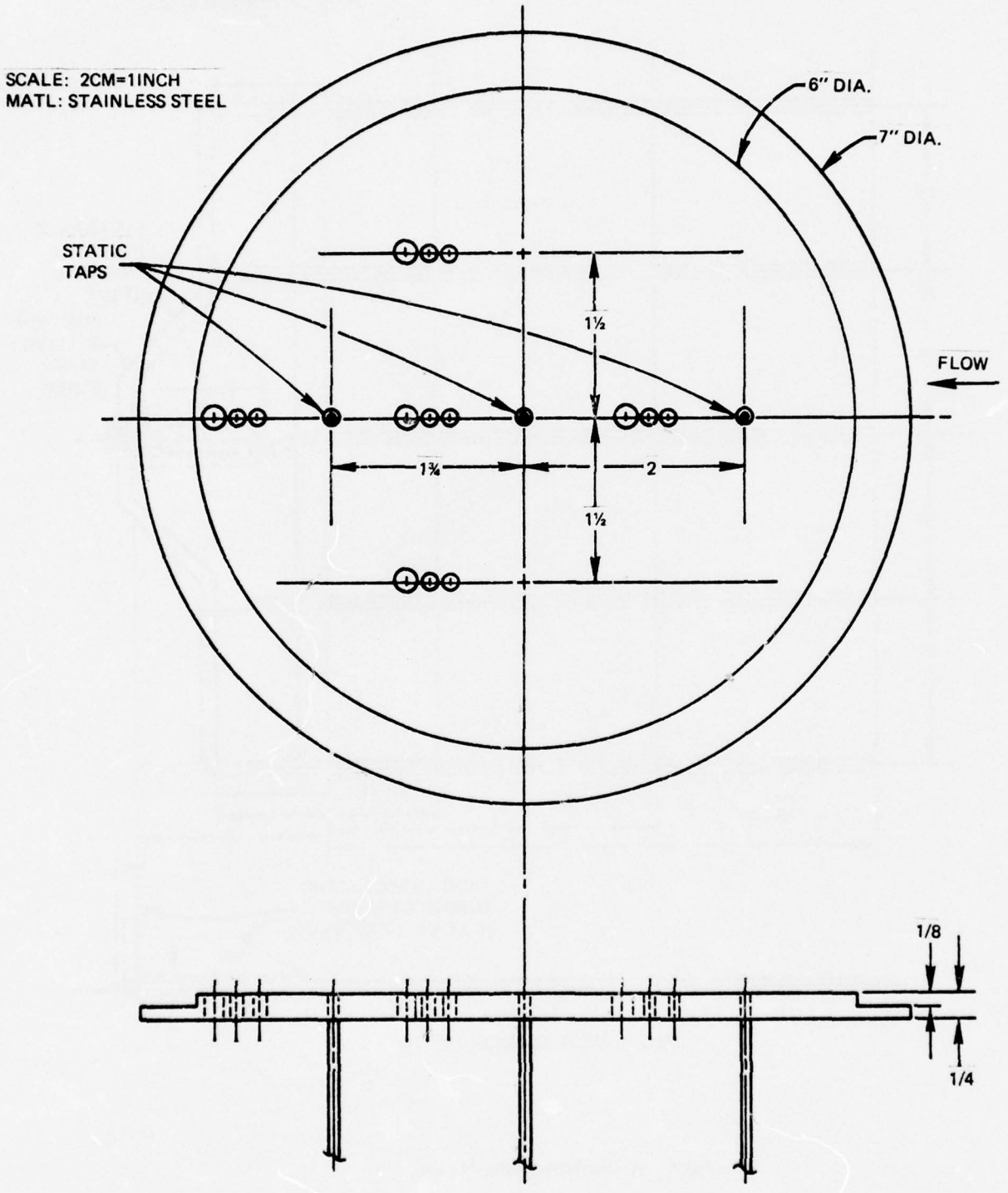

Figure II-5. Instrumentation Mounting Plate.

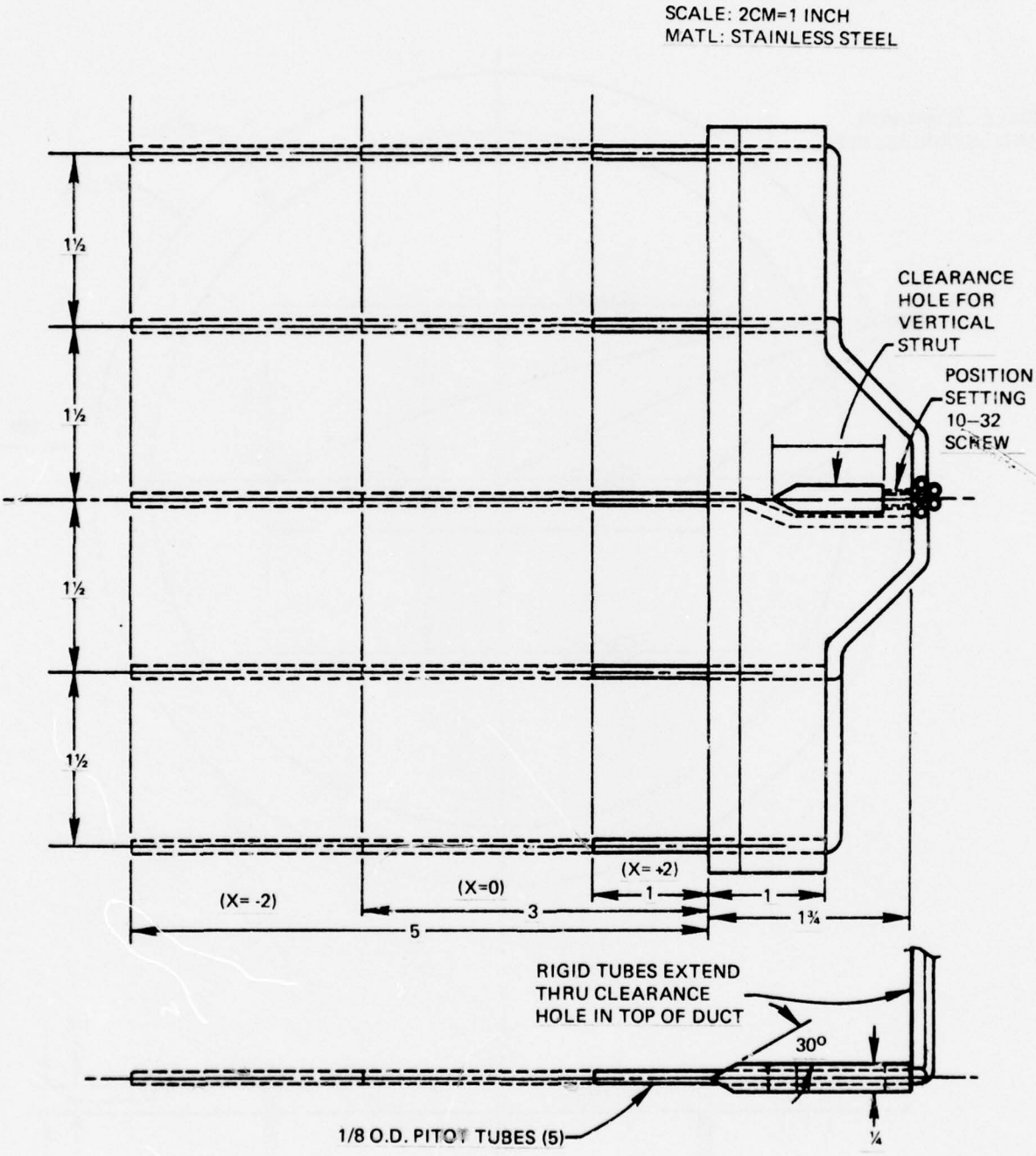

Figure II-6. Horizontal Rake (3 each).

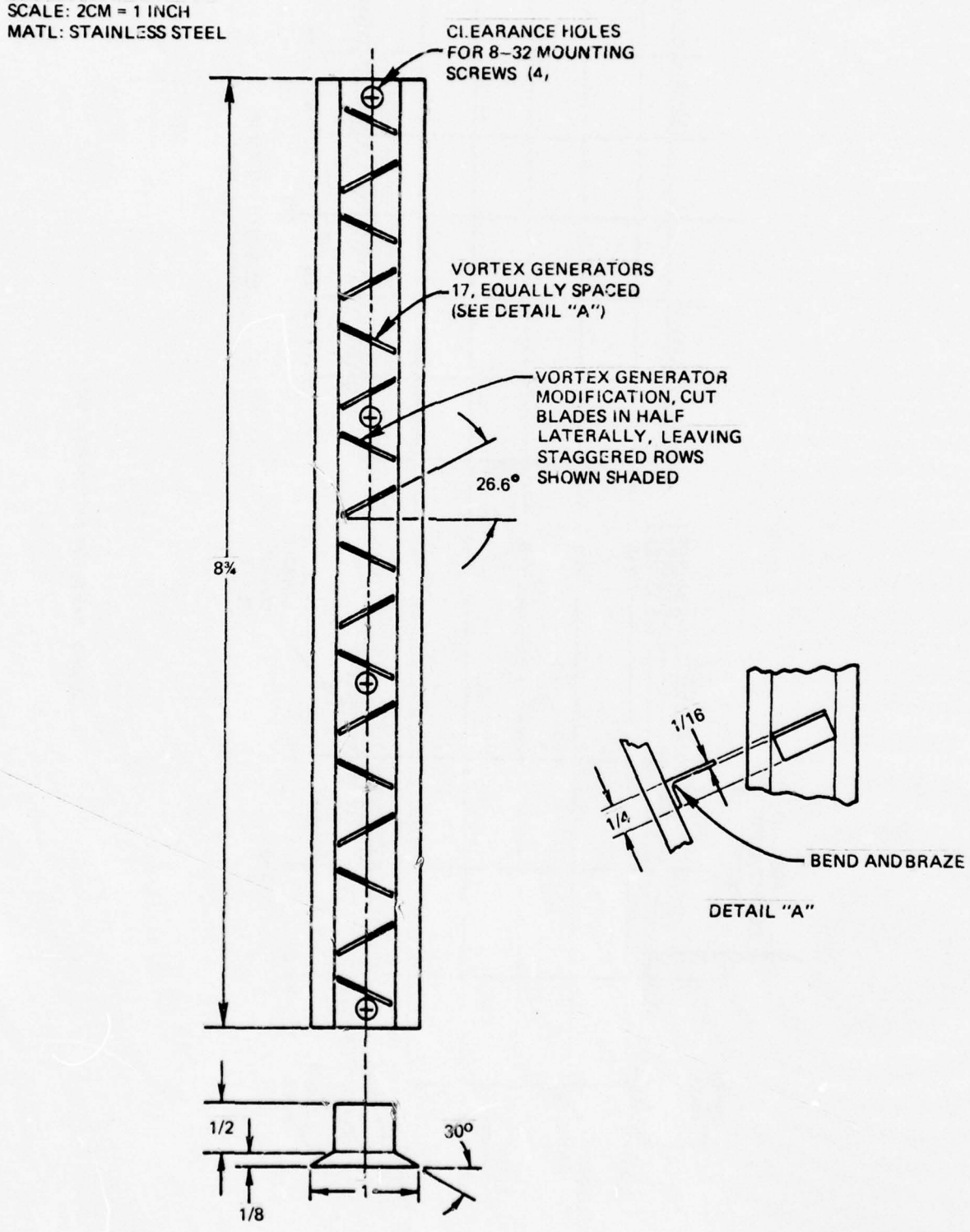

Figure II-7. Vortex Generator.

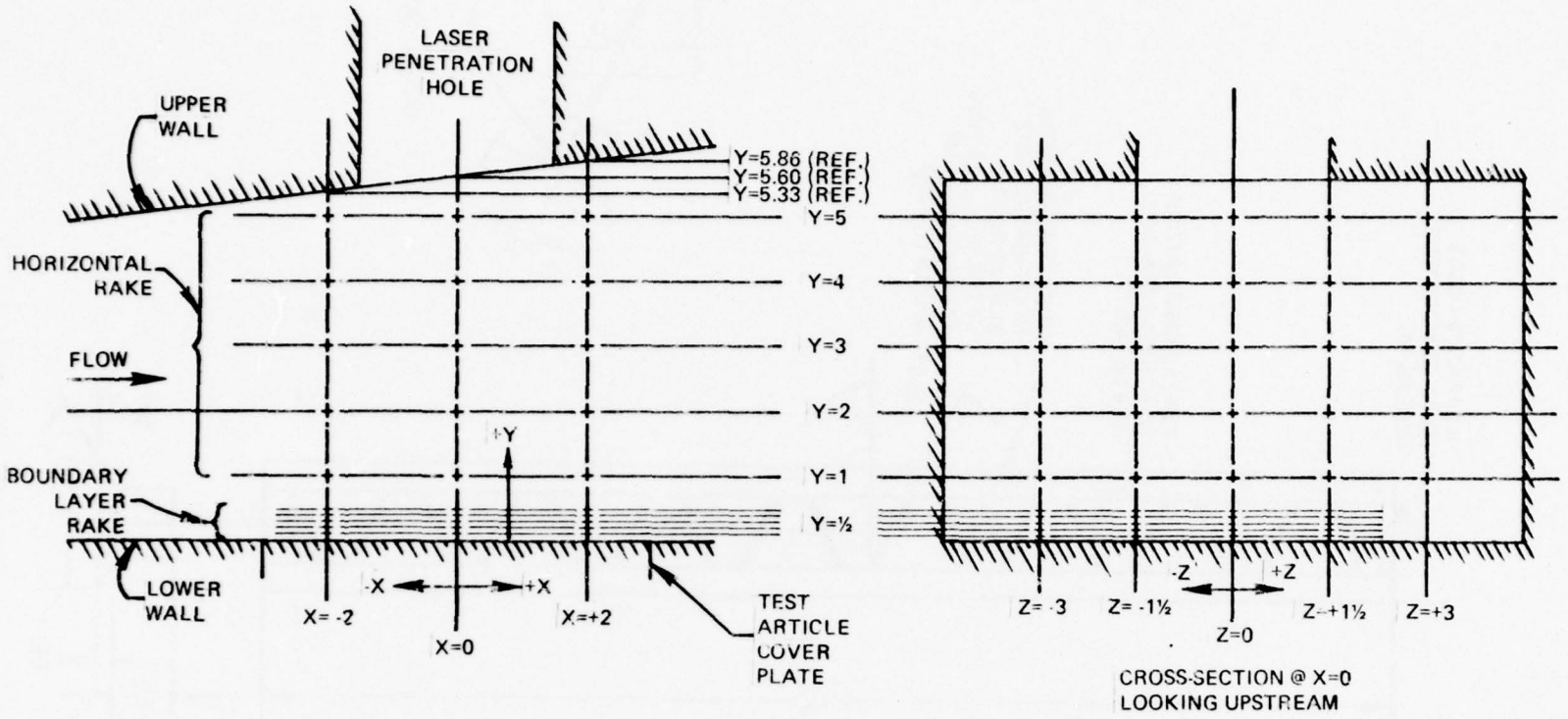

Figure III-1. Axis System and Test Point Grid.

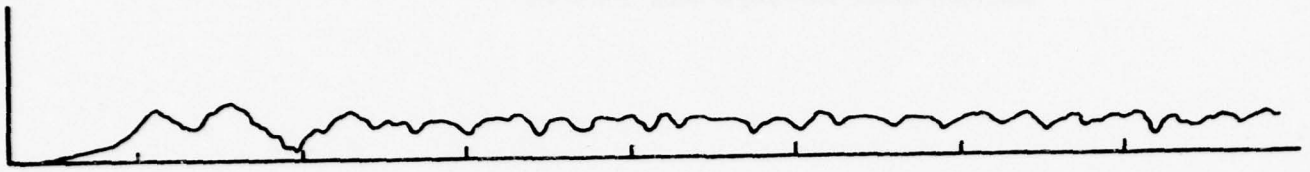

P TOTAL, X=0, Y=2, Z= -3, PERFORATED CONE IN

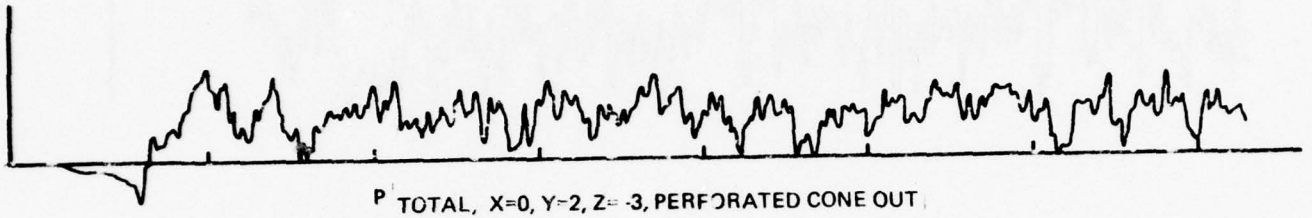

P TOTAL, X=0, Y=-2, Z= -3, PERFORATED CONE OUT

Figure III-2. Effect of Perforated Cone on Turbulence.

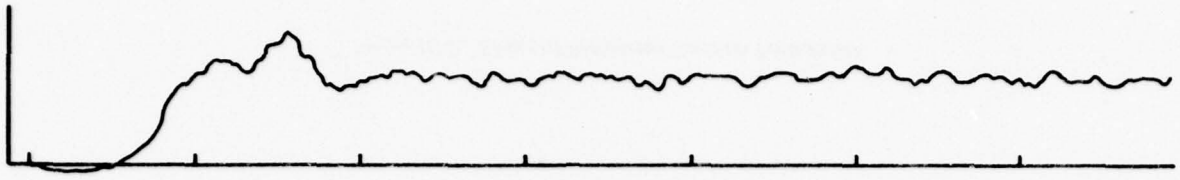

P_S, X= -16, Y=4, Z=0, PERFORATED CONE IN

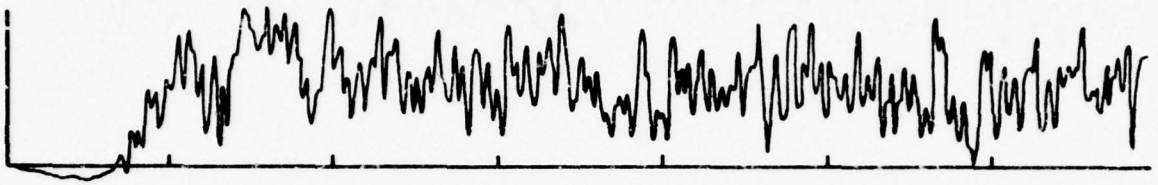

P_S, X= -16, Y=4, Z=0, PERFORATED CONE OUT

Figure III-3. Effect of Perforated Cone on Turbulence.

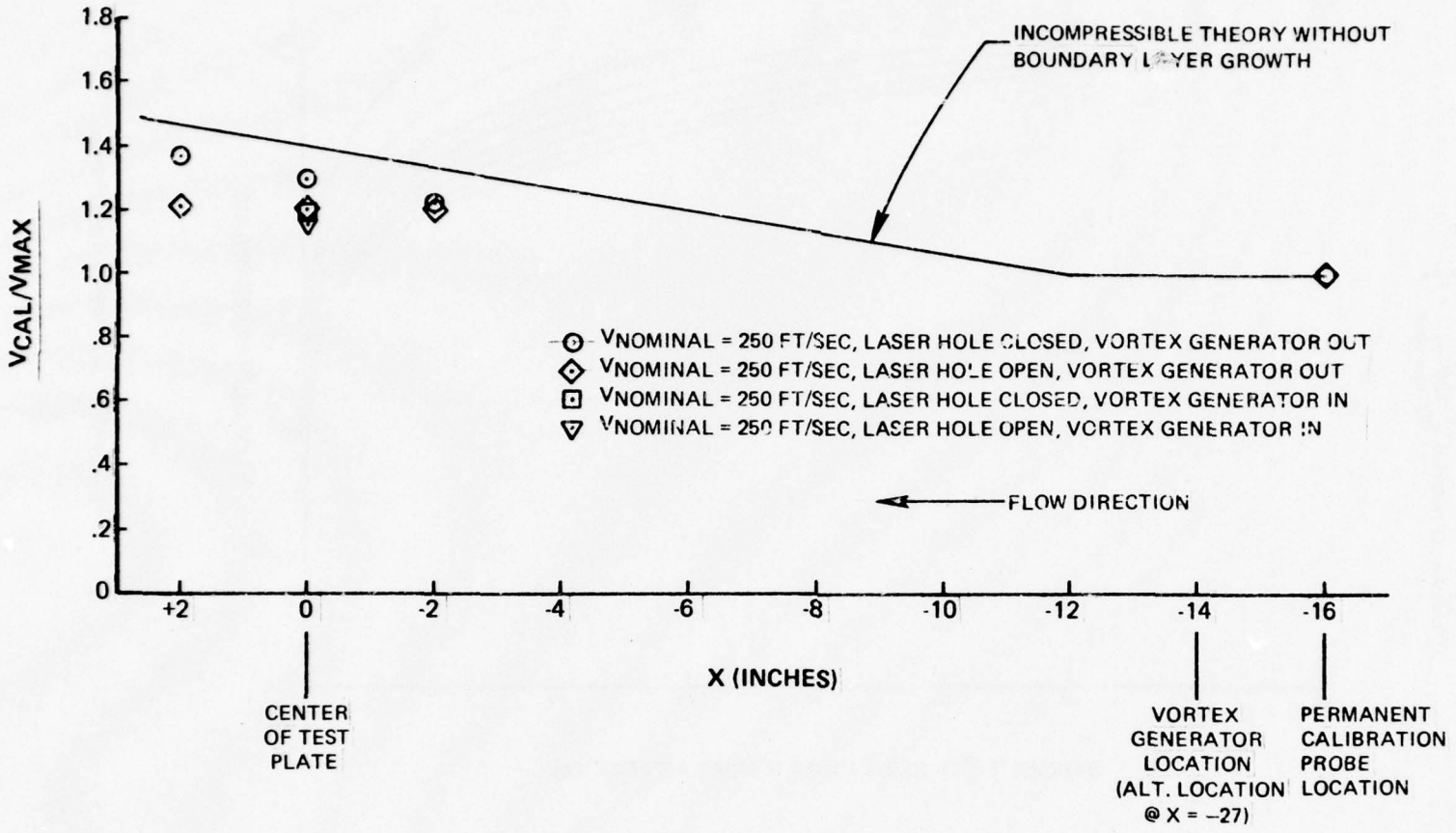

Figure III-4. Streamwise Velocity Distribution.

Turbulent Correlation, $\frac{V_{Local}}{V_{Freestream}} = \left(\frac{Y}{\delta}\right)^{1/7}$

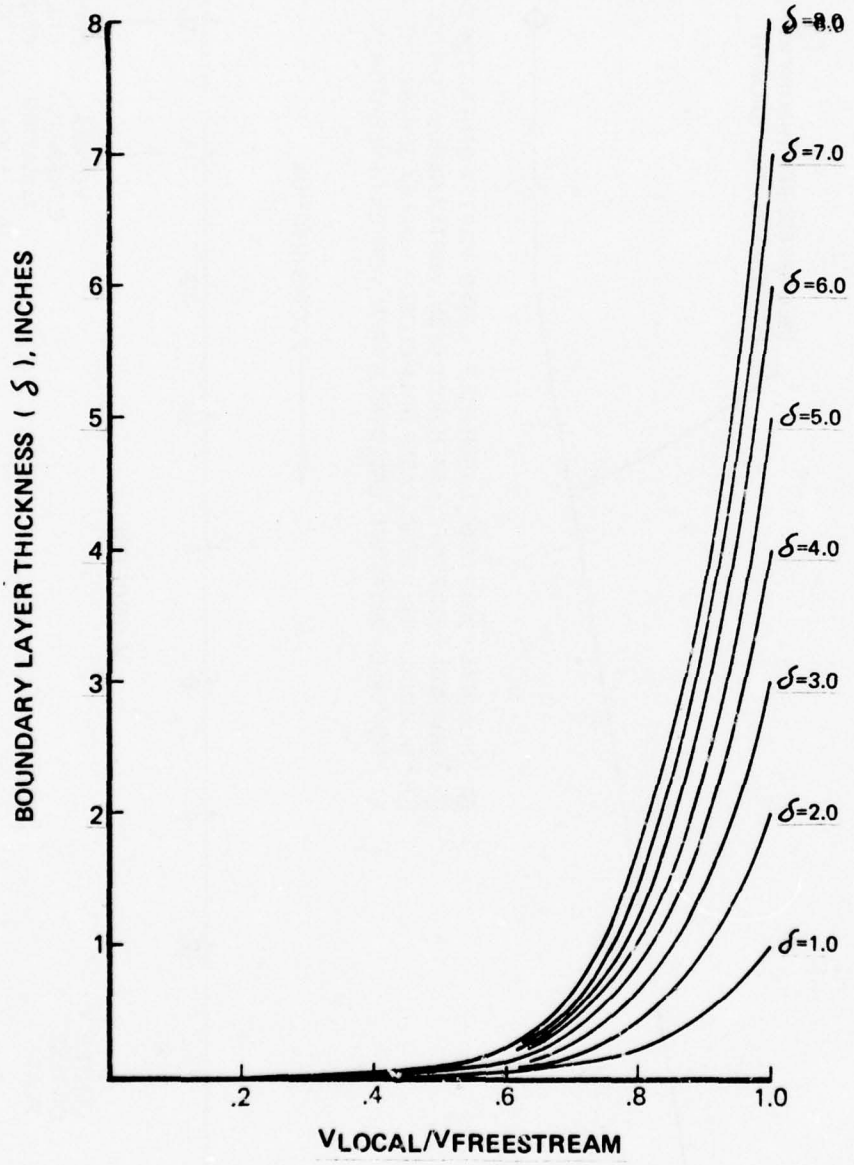

Figure IV-1. Boundary Layer Profiles.

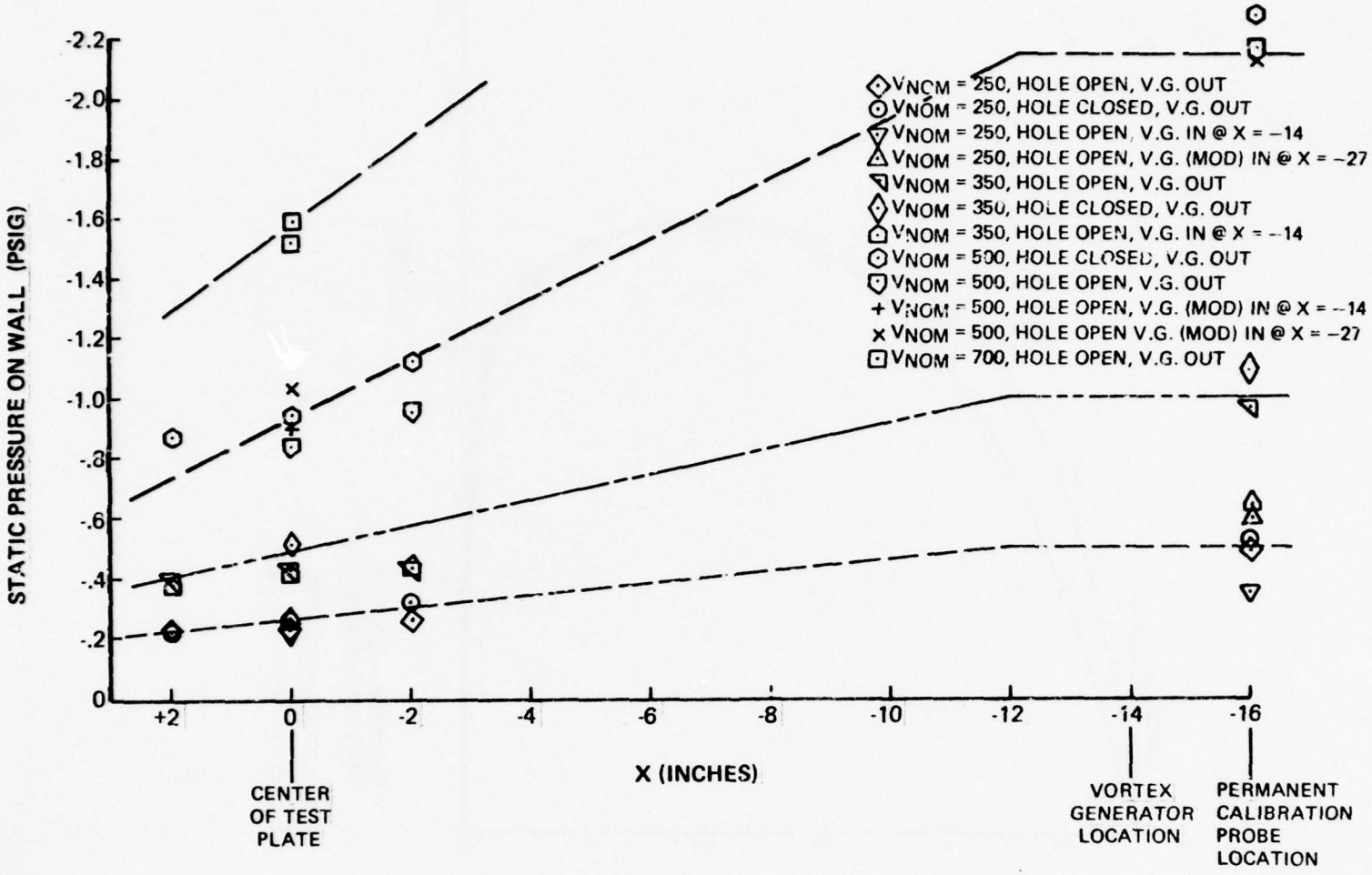

Figure IV-2. Streamwise Static Pressure Distribution.

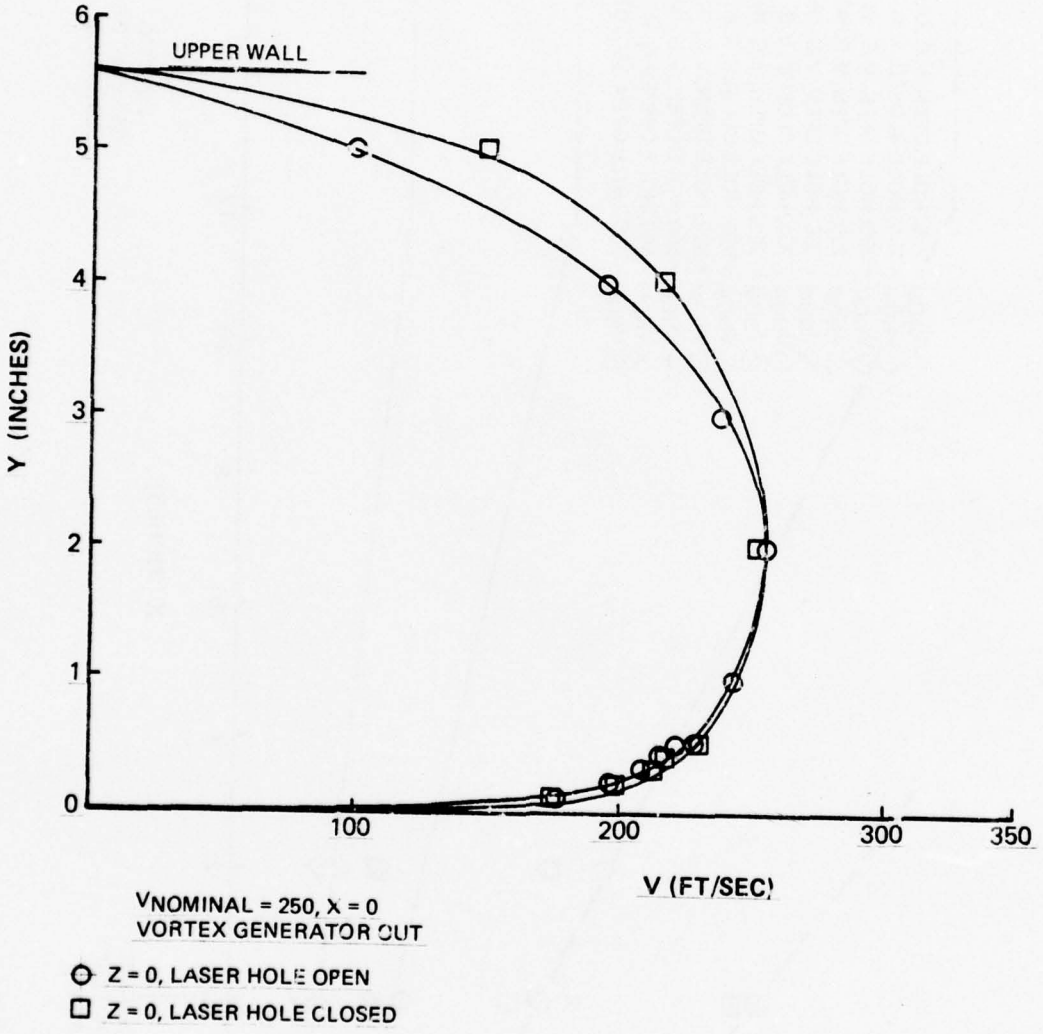

Figure IV-3. Velocity Profile Calibration.

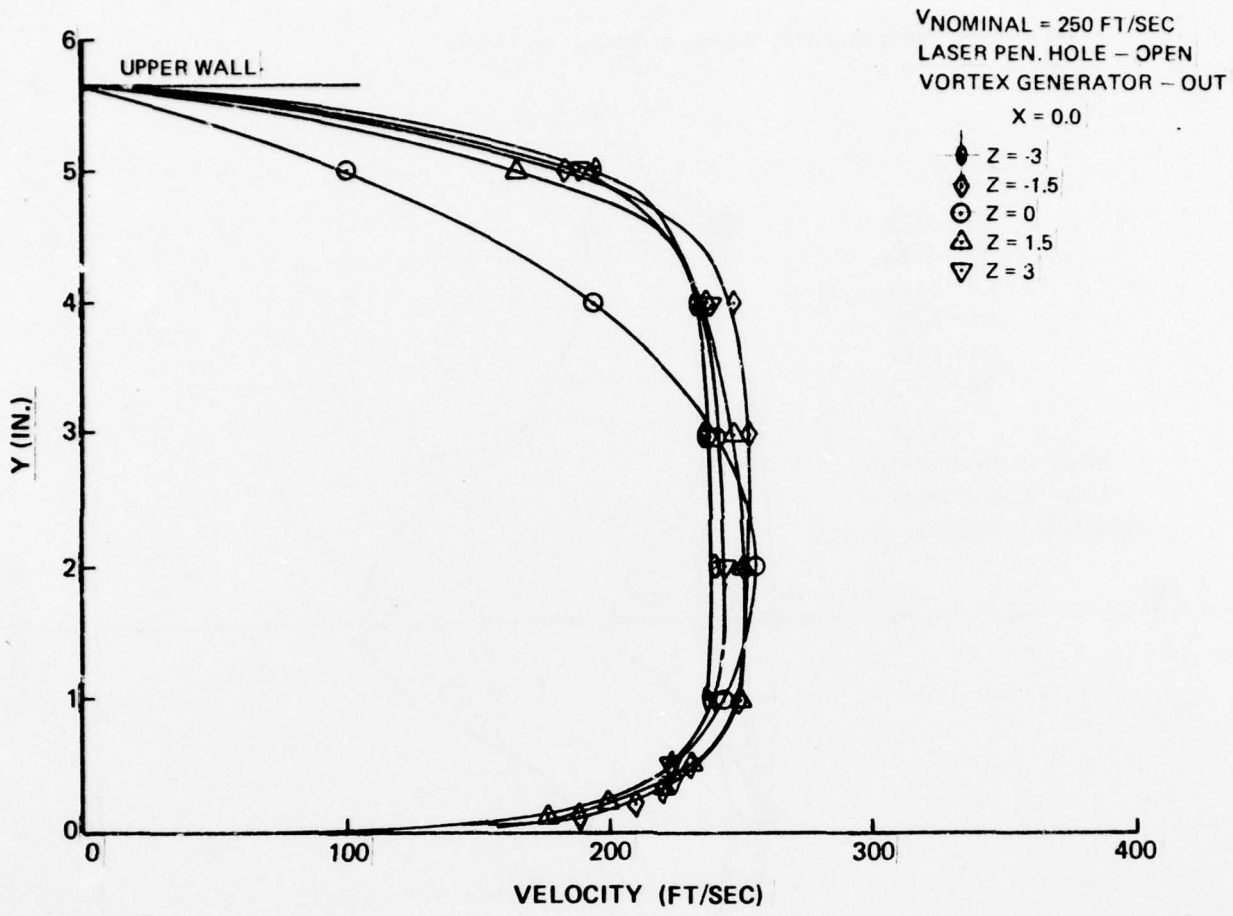

Figure IV-4. Velocity Calibration, Laser Flow Duct.

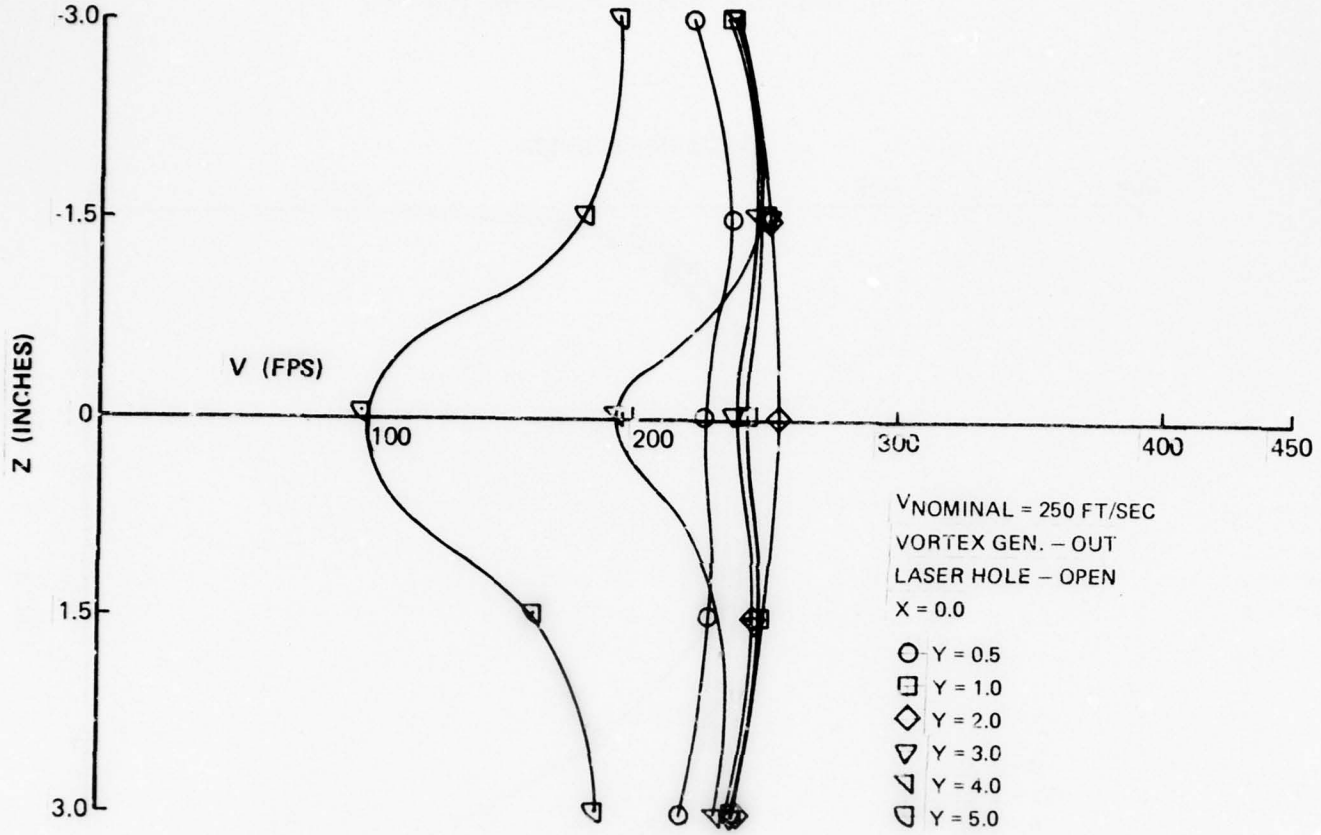

Figure IV-5. Velocity Calibration, Laser Flow Duct.

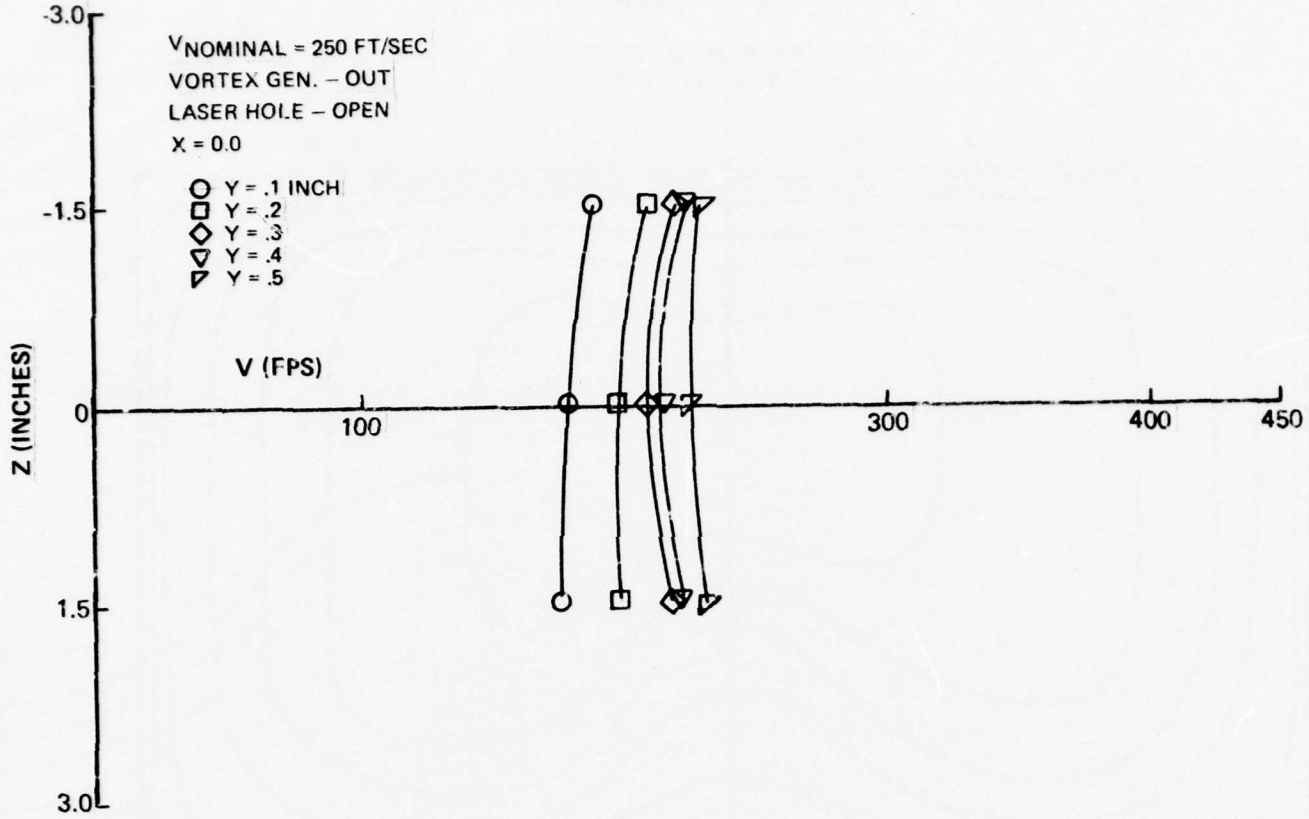

Figure IV-6. Velocity Calibration, Laser Flow Duct.

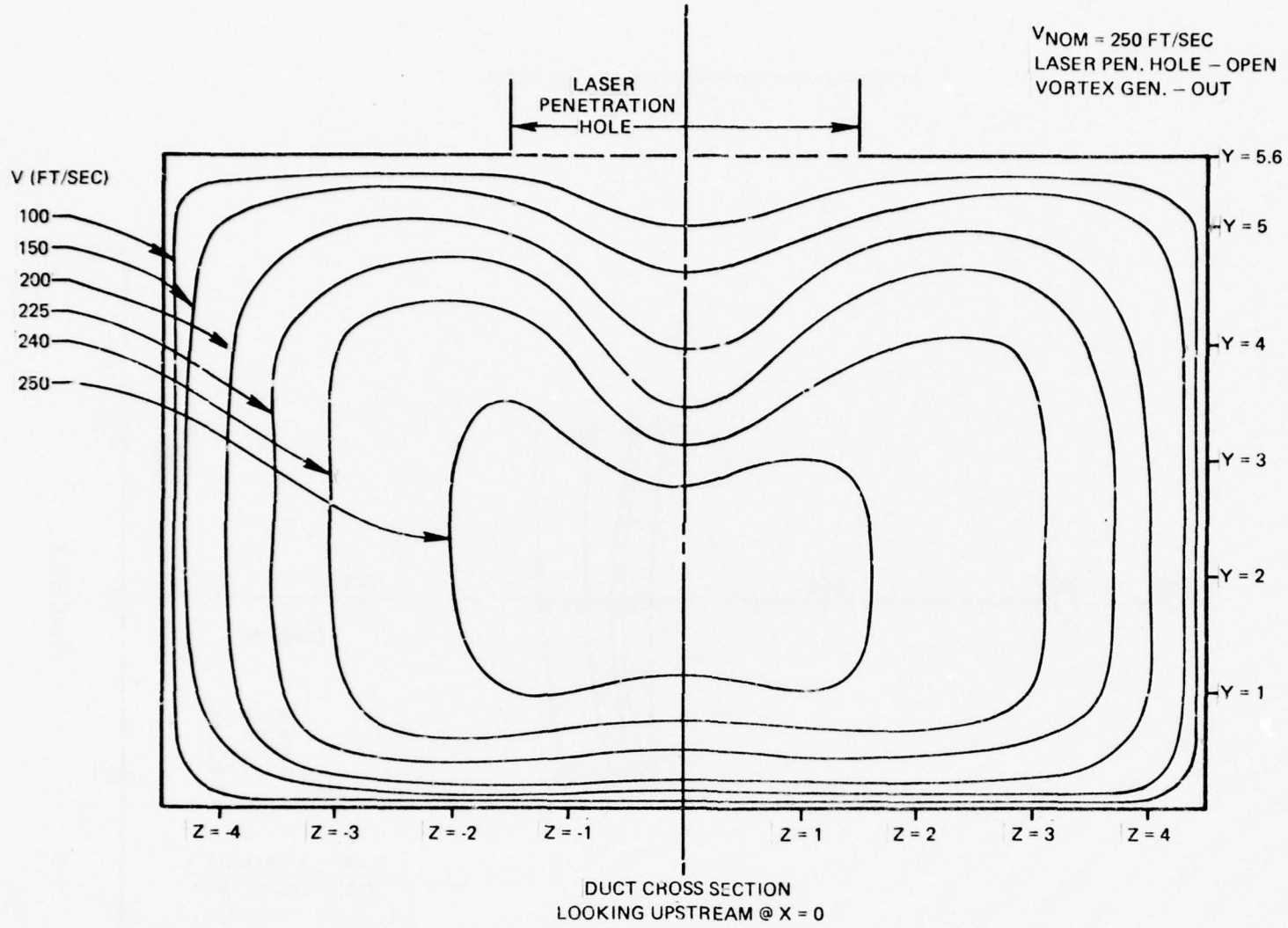

Figure IV-7. Velocity Contour Map.

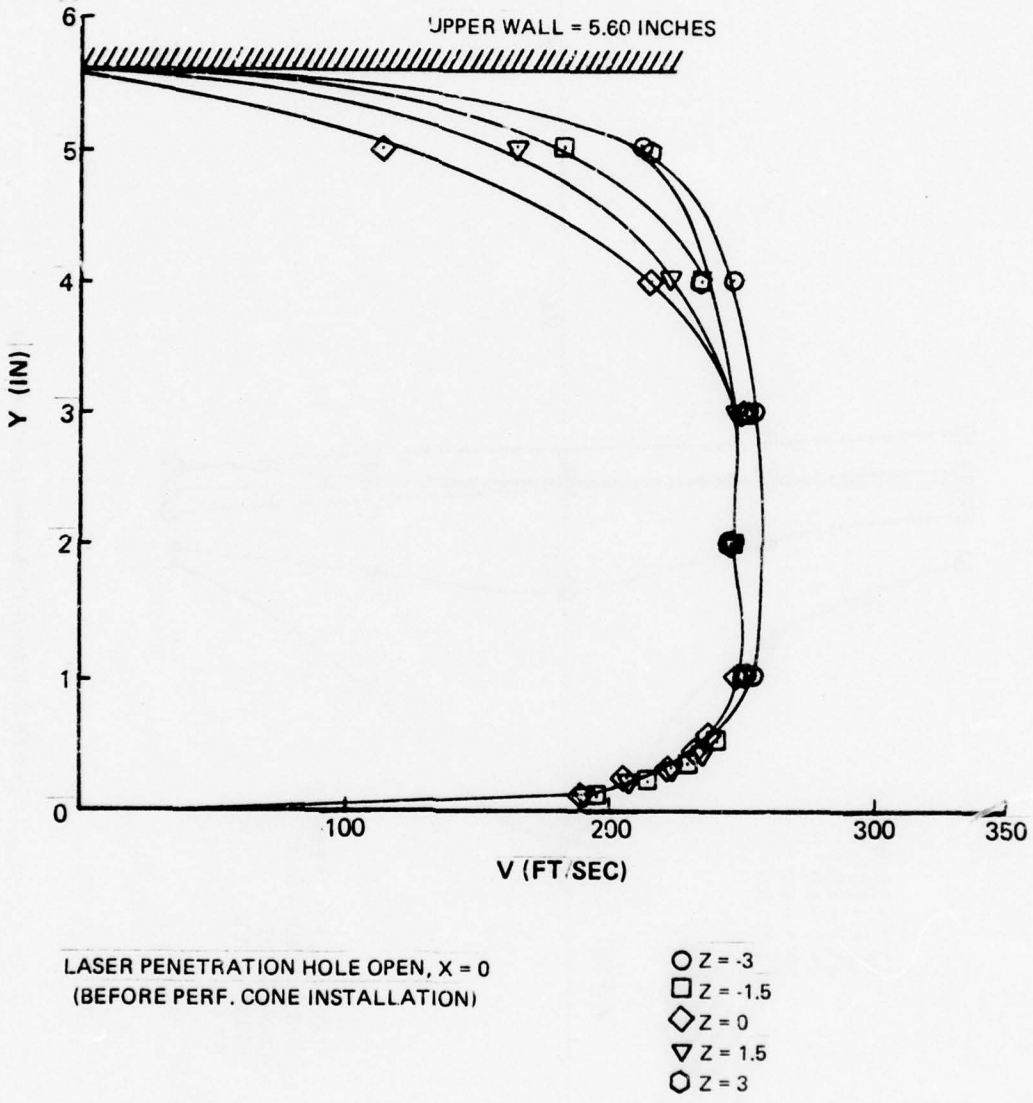

Figure IV-8. Velocity Profile Calibration.

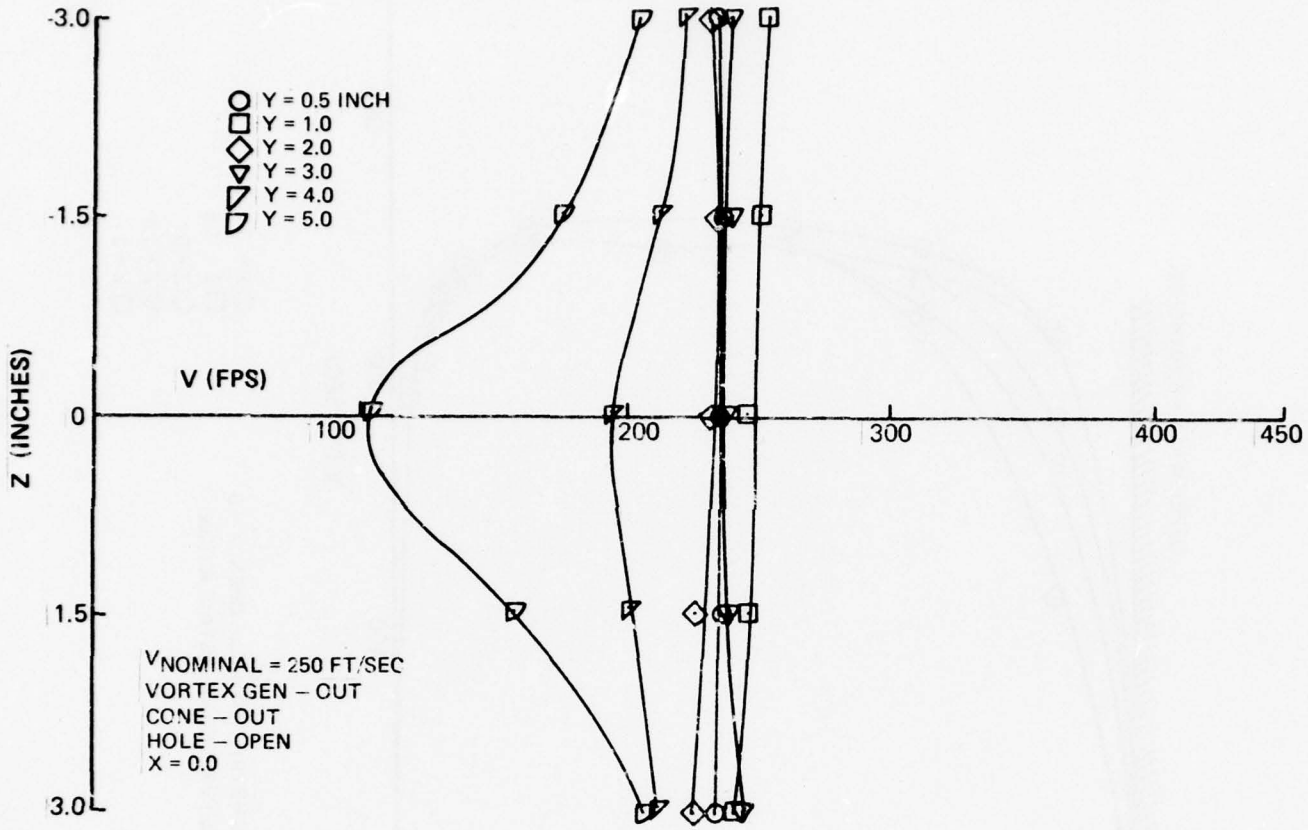

Figure IV-9. Velocity Calibration, Laser Flow Duct.

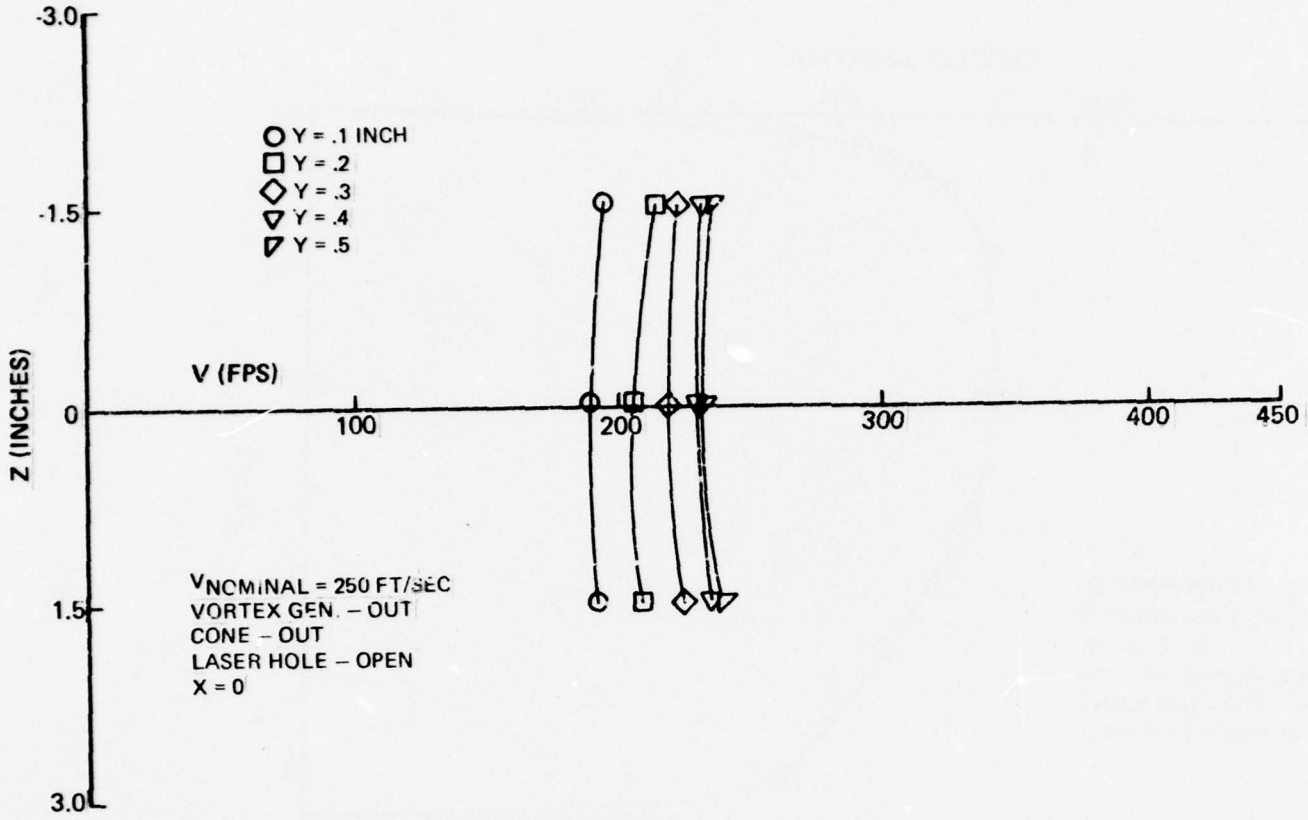

Figure IV-10. Velocity Calibration, Laser Flow Duct.

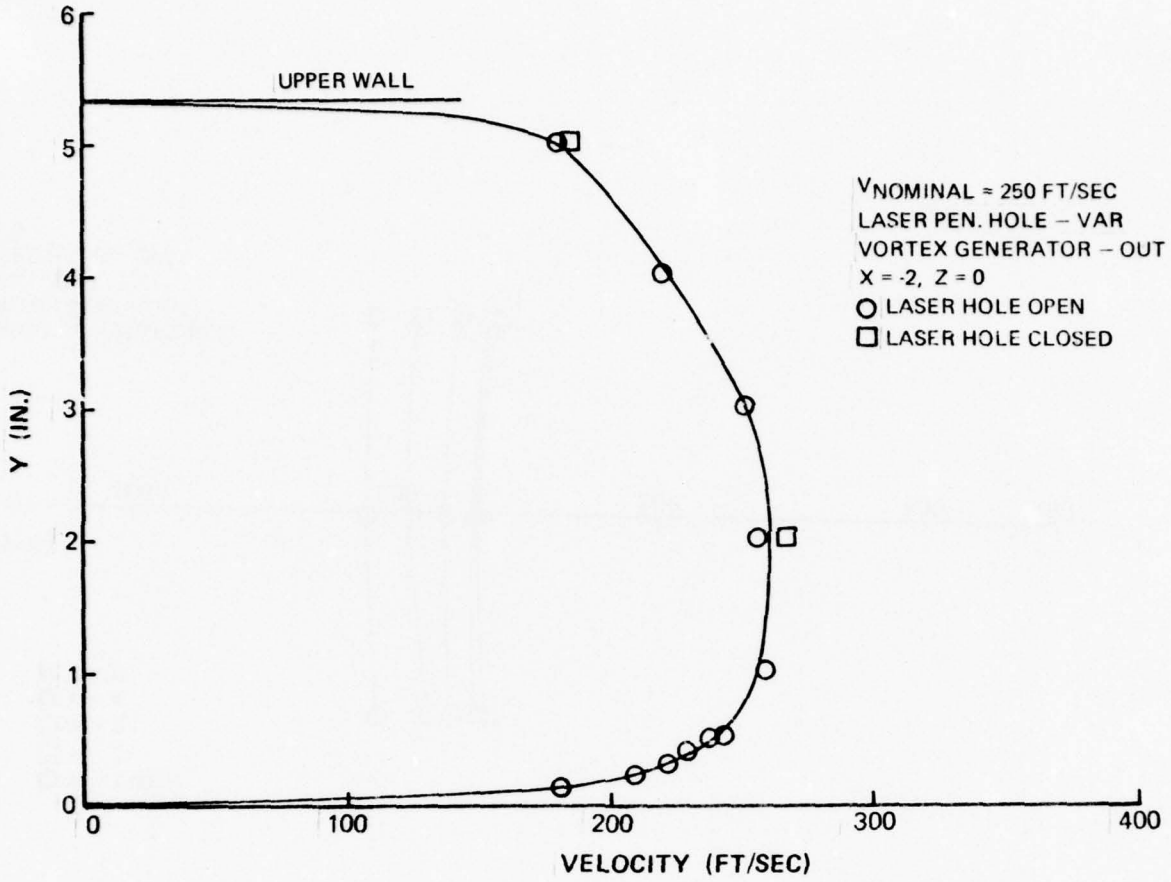

Figure IV-11. Velocity Calibration, Laser Flow Duct.

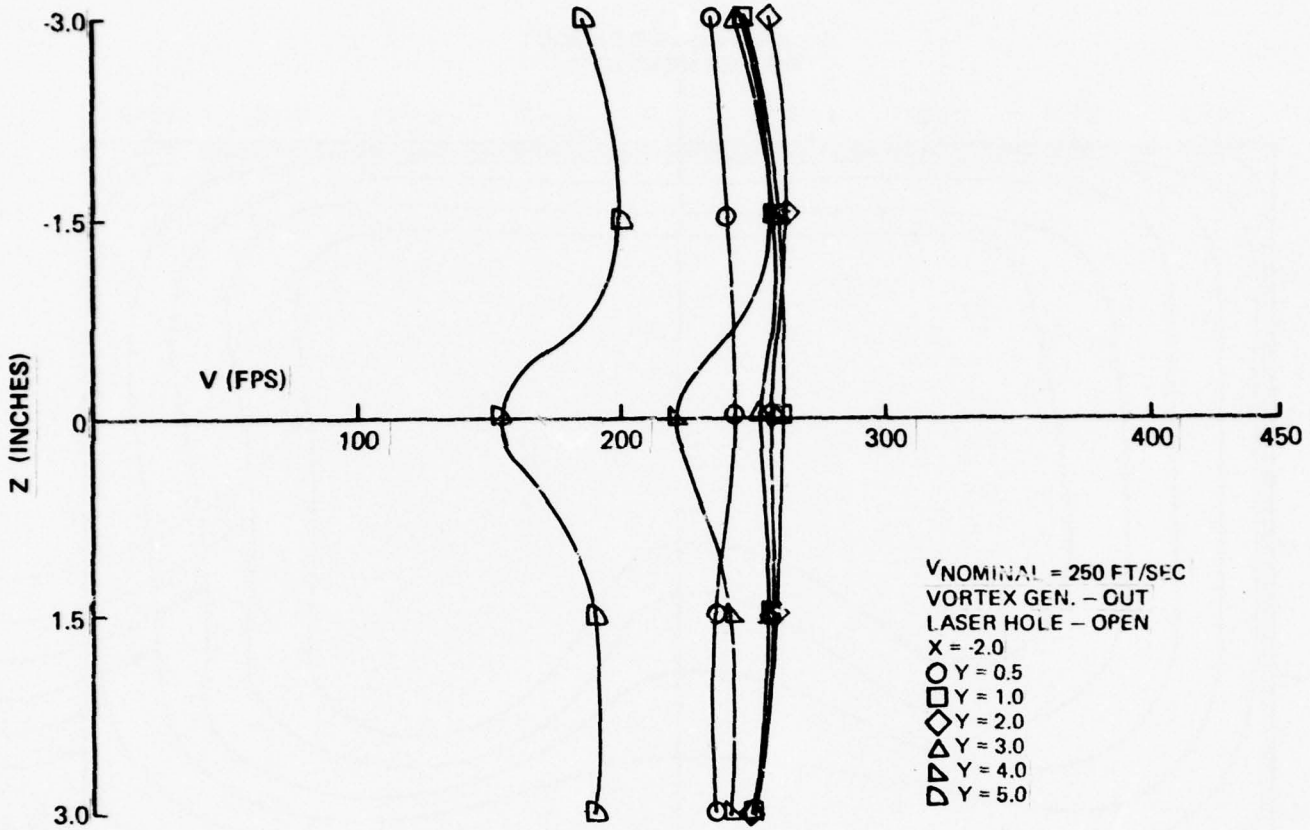

Figure IV-12. Velocity Calibration, Laser Flow Duct.

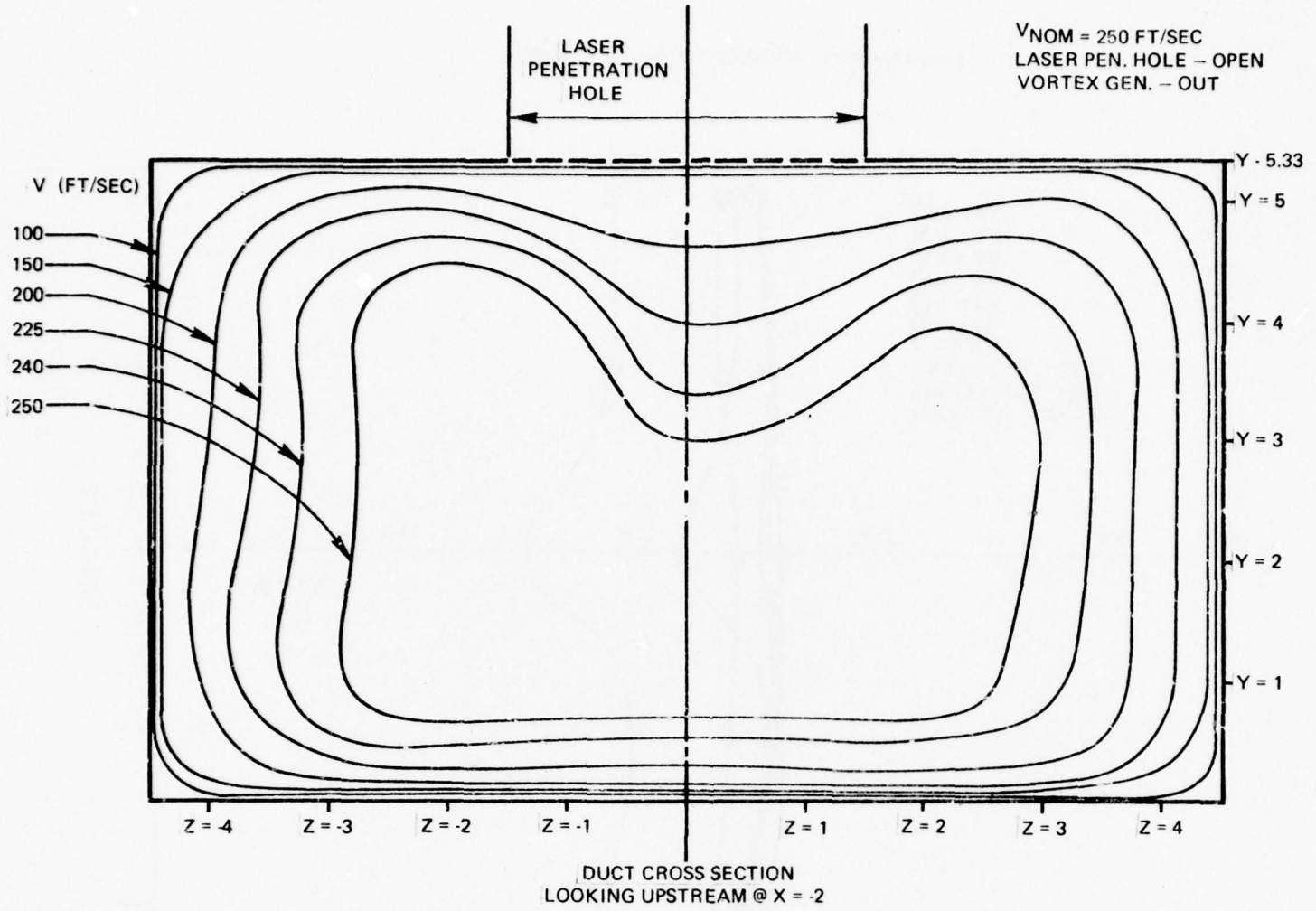

Figure IV-13. Velocity Contour Map.

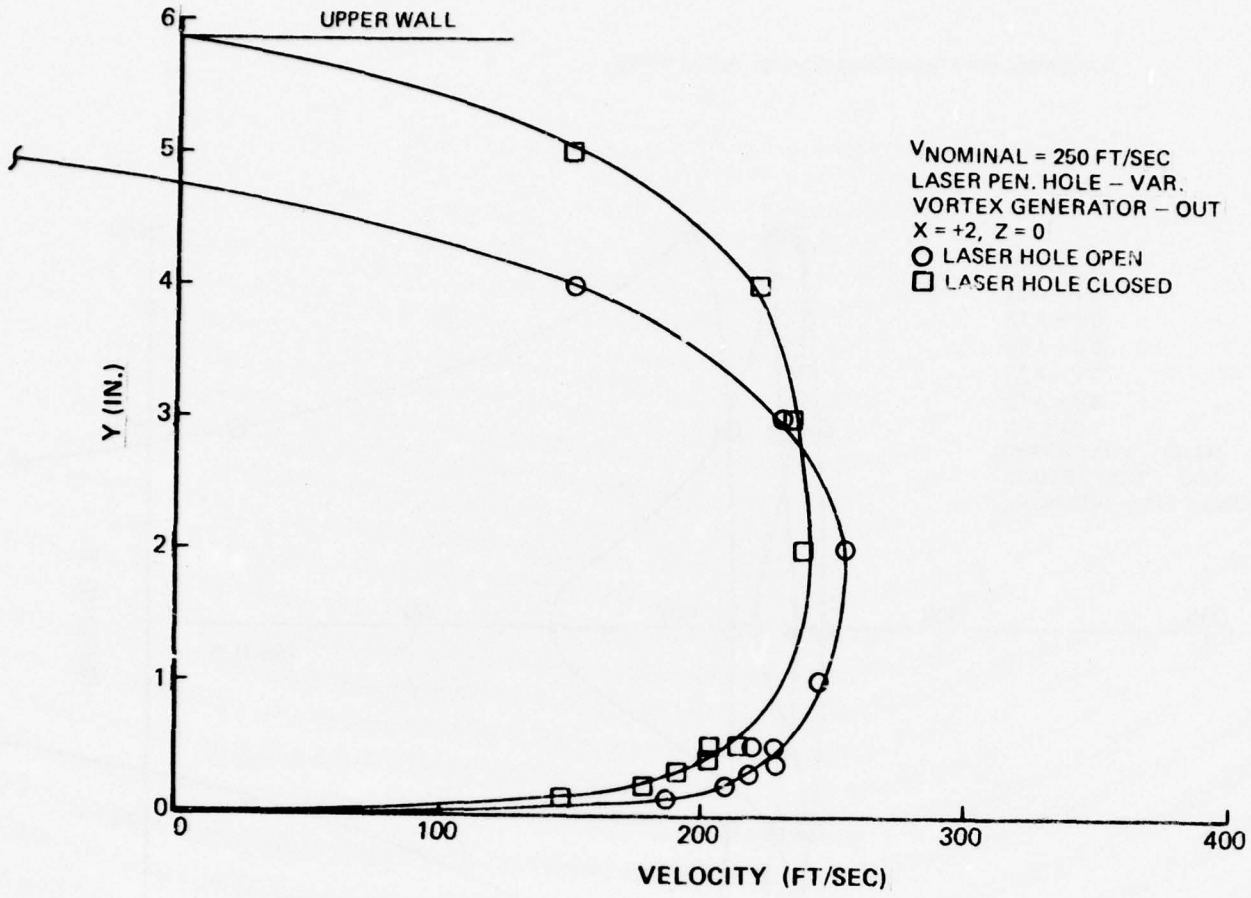

Figure IV-14. Velocity Calibration, Laser Flow Duct.

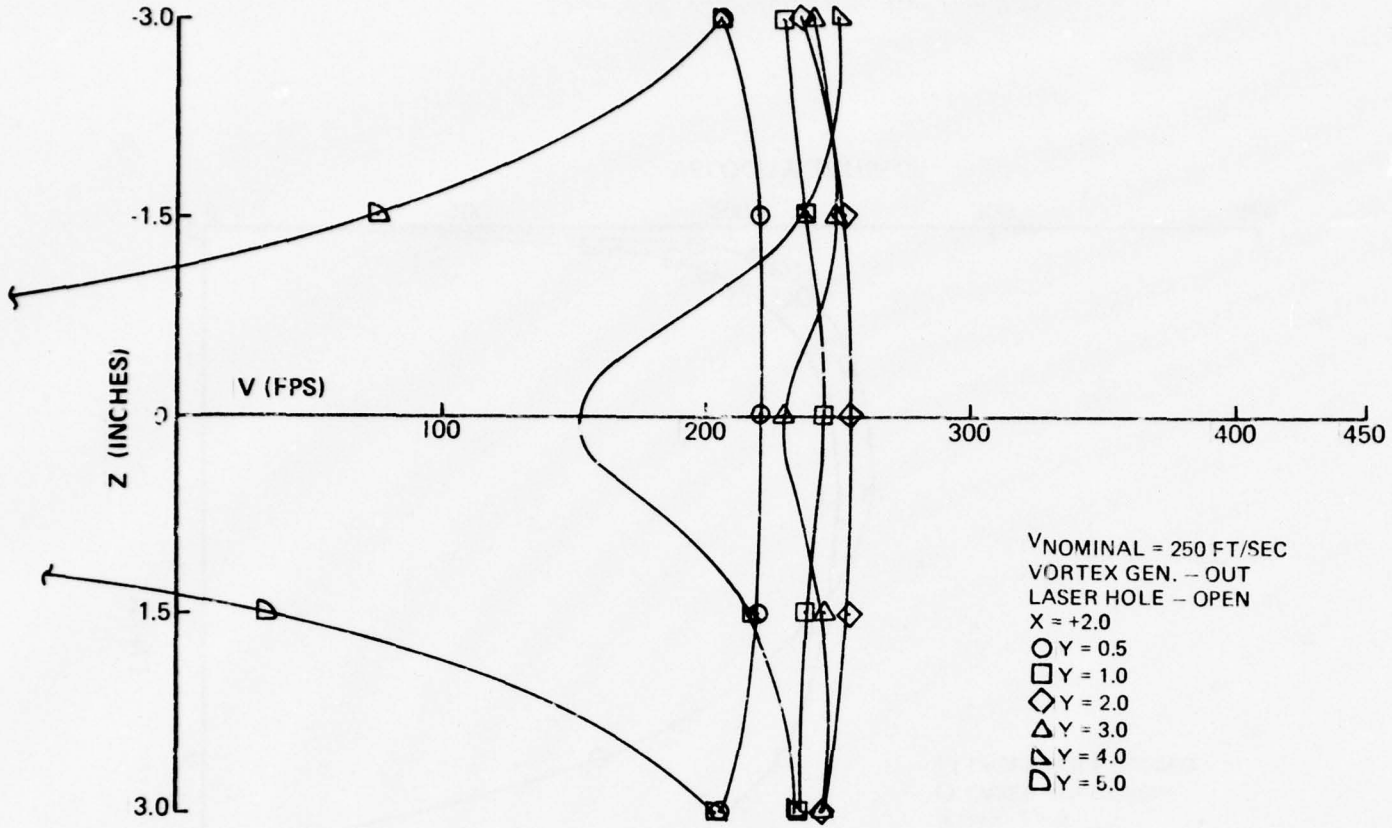

Figure IV-15. Velocity Calibration, Laser Flow Duct.

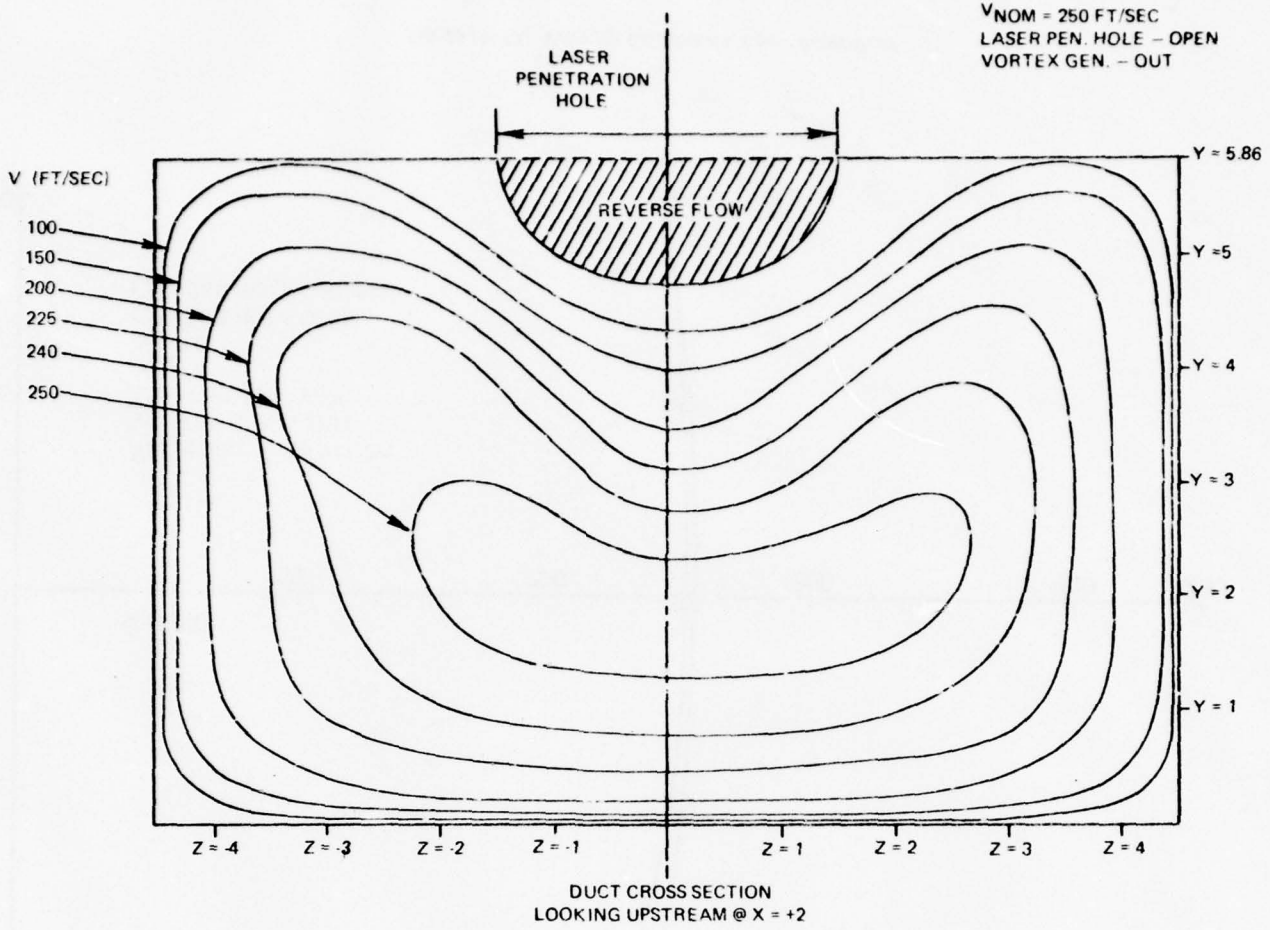

Figure IV-16. Velocity Contour Map.

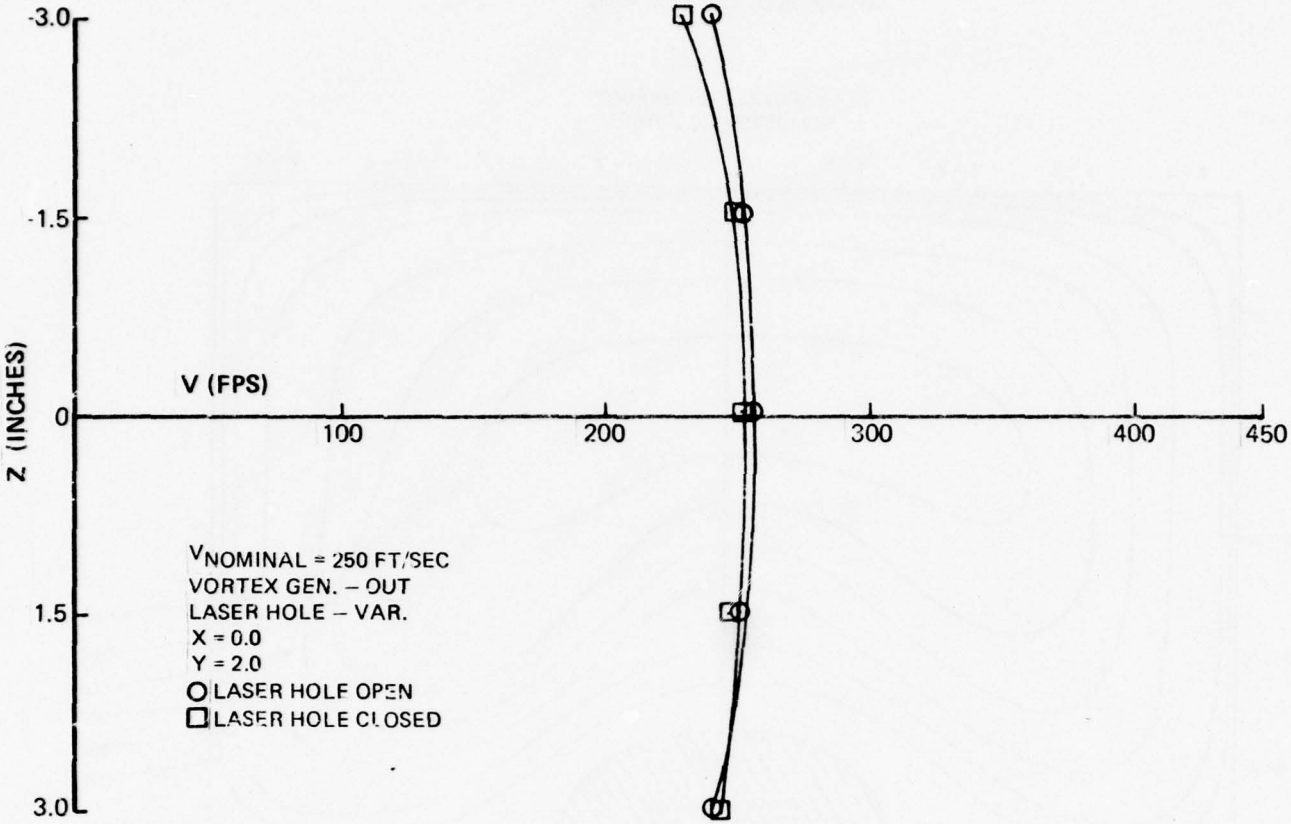

Figure IV-17. Velocity Calibration, Laser Flow Duct.

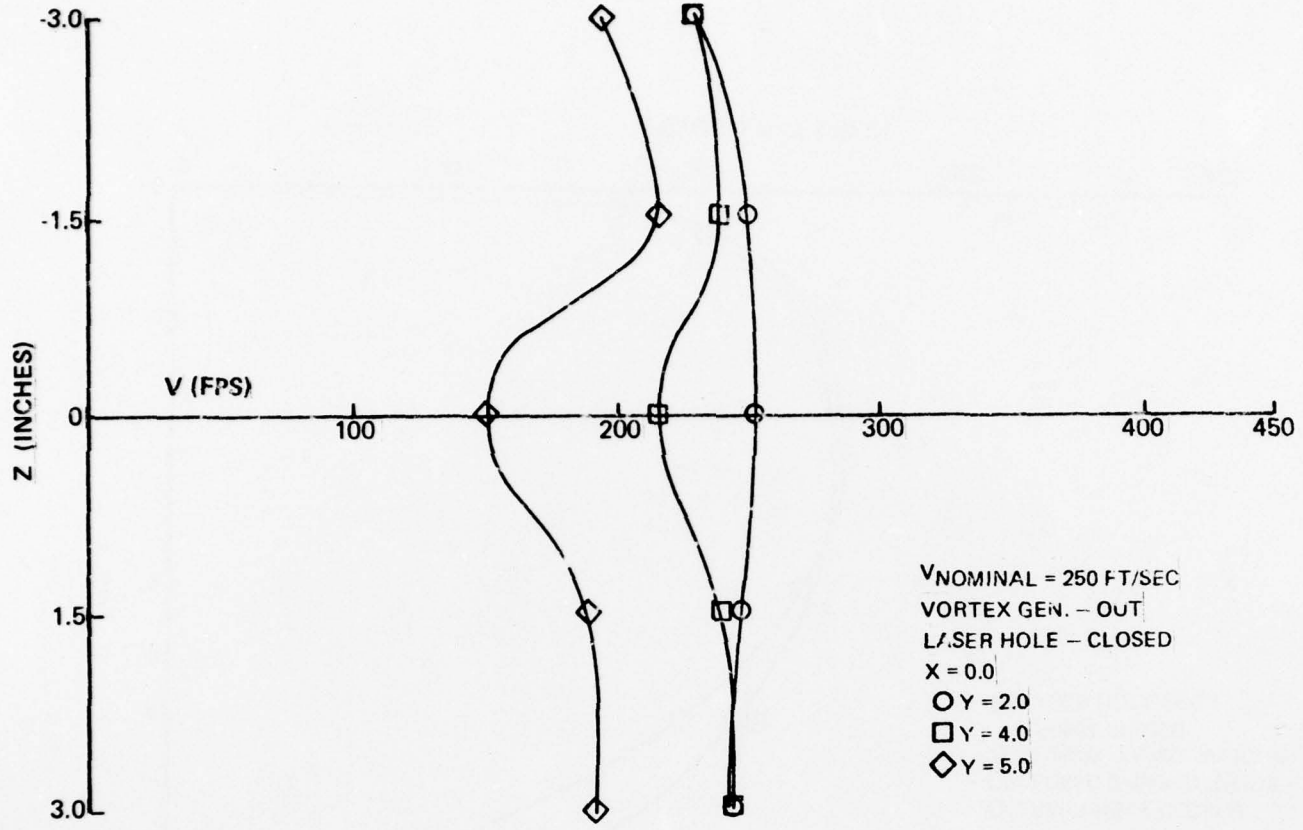

Figure IV-18. Velocity Calibration, Laser Flow Duct.

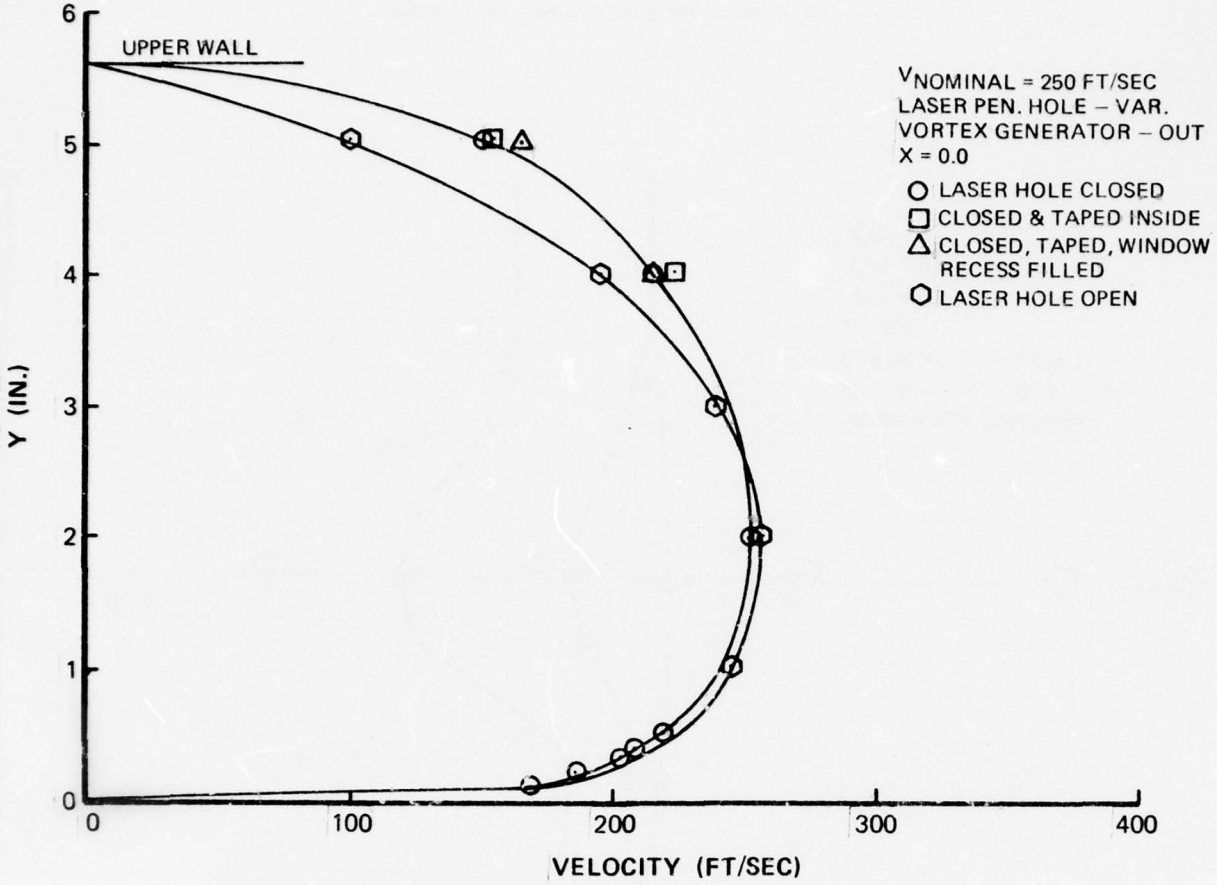

Figure IV-19. Velocity Calibration, Laser Flow Duct.

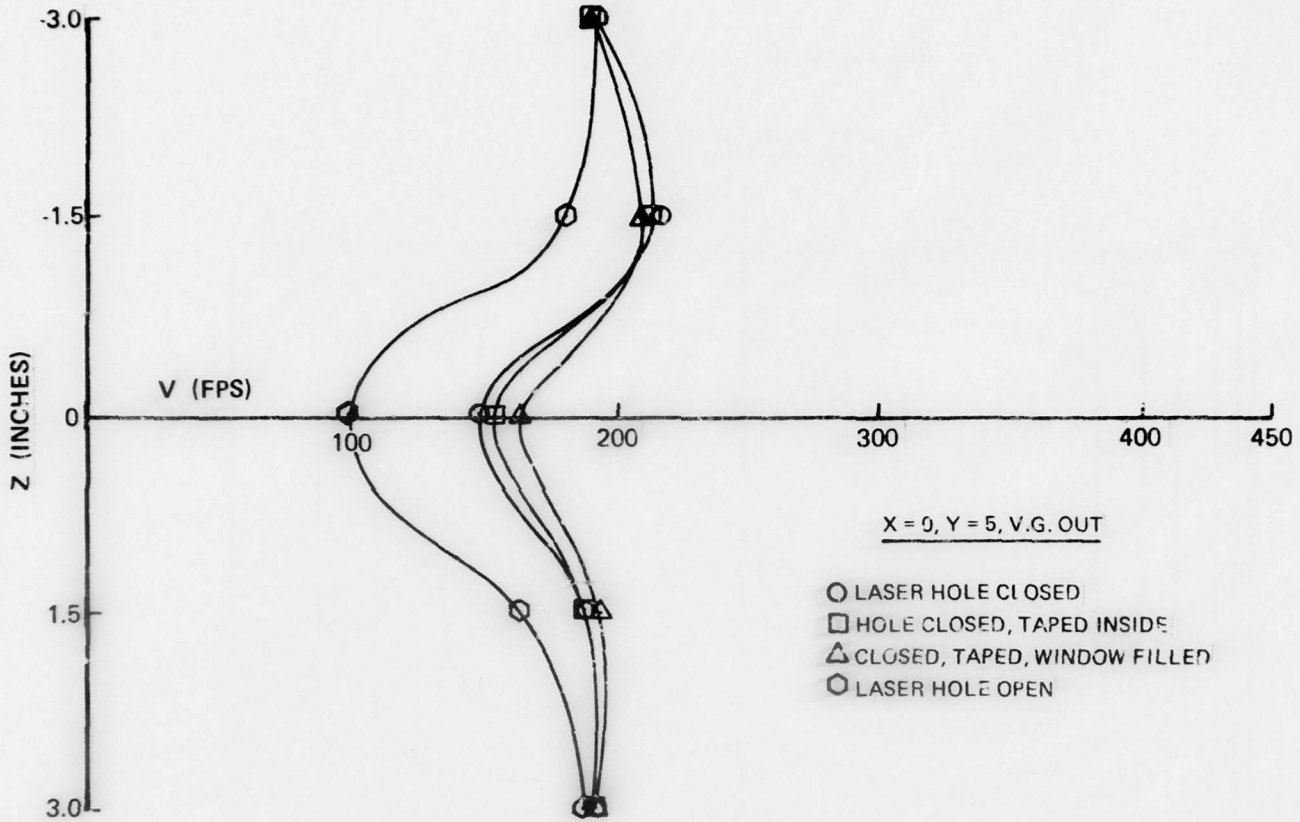

Figure IV-20. Velocity Calibration, Laser Flow Duct.

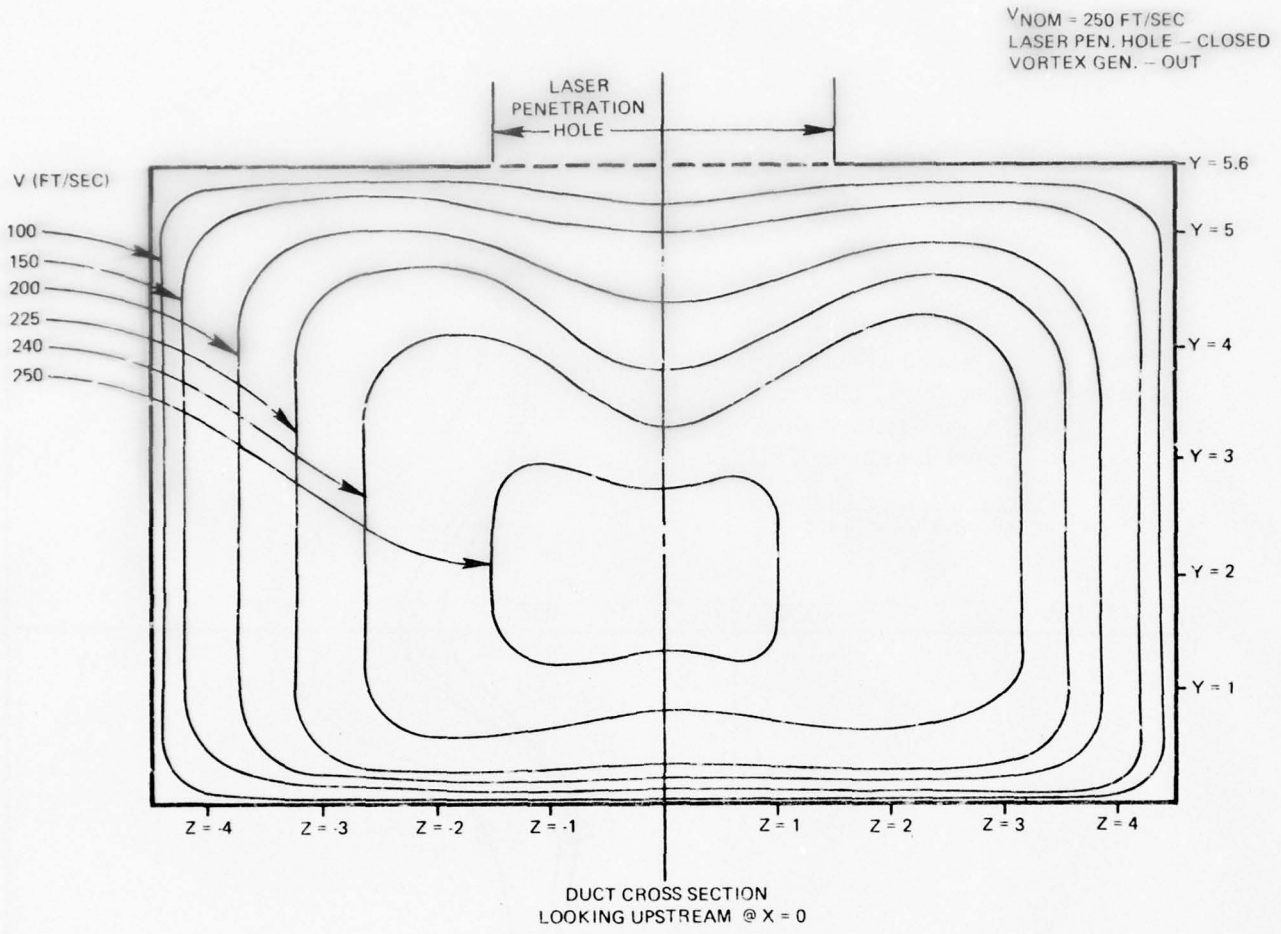

Figure IV-21. Velocity Contour Map.

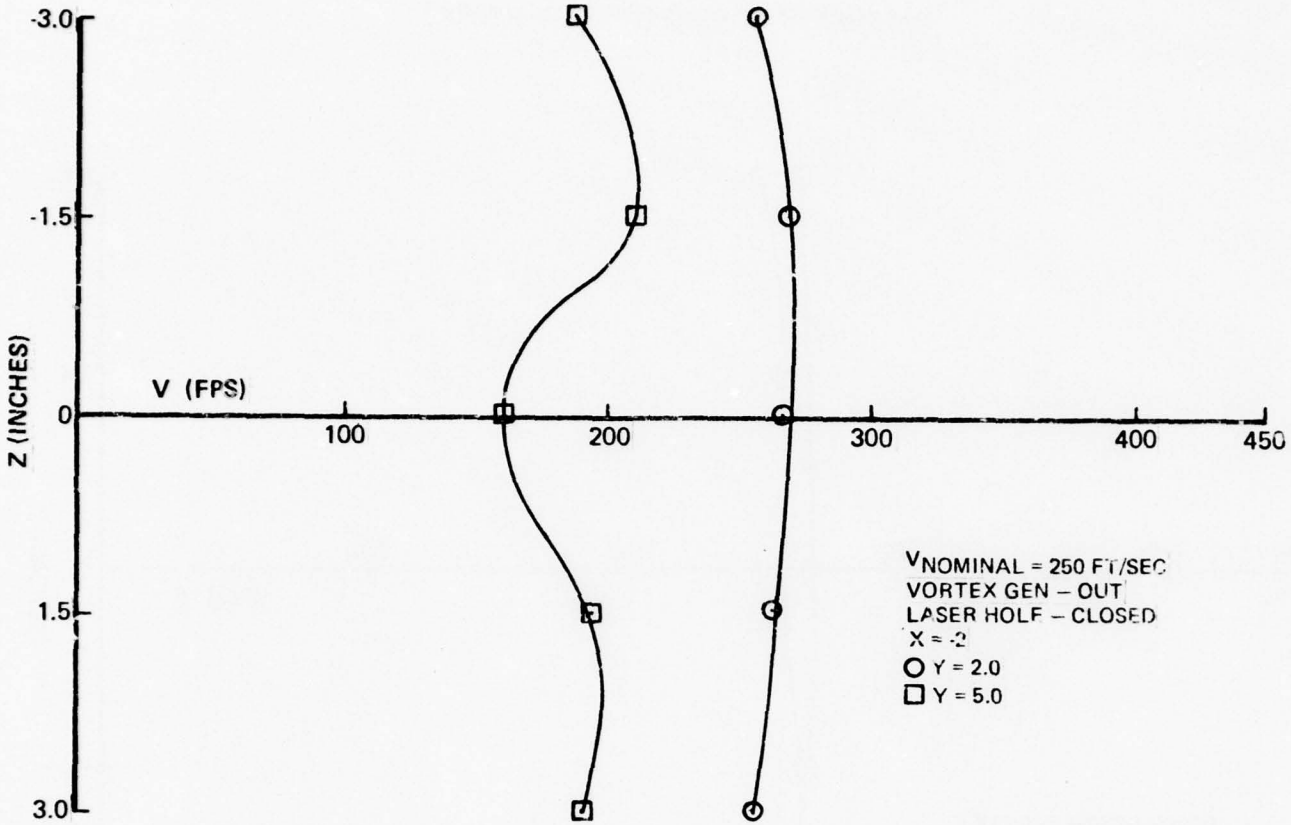

Figure IV-22. Velocity Calibration, Laser Flow Duct.

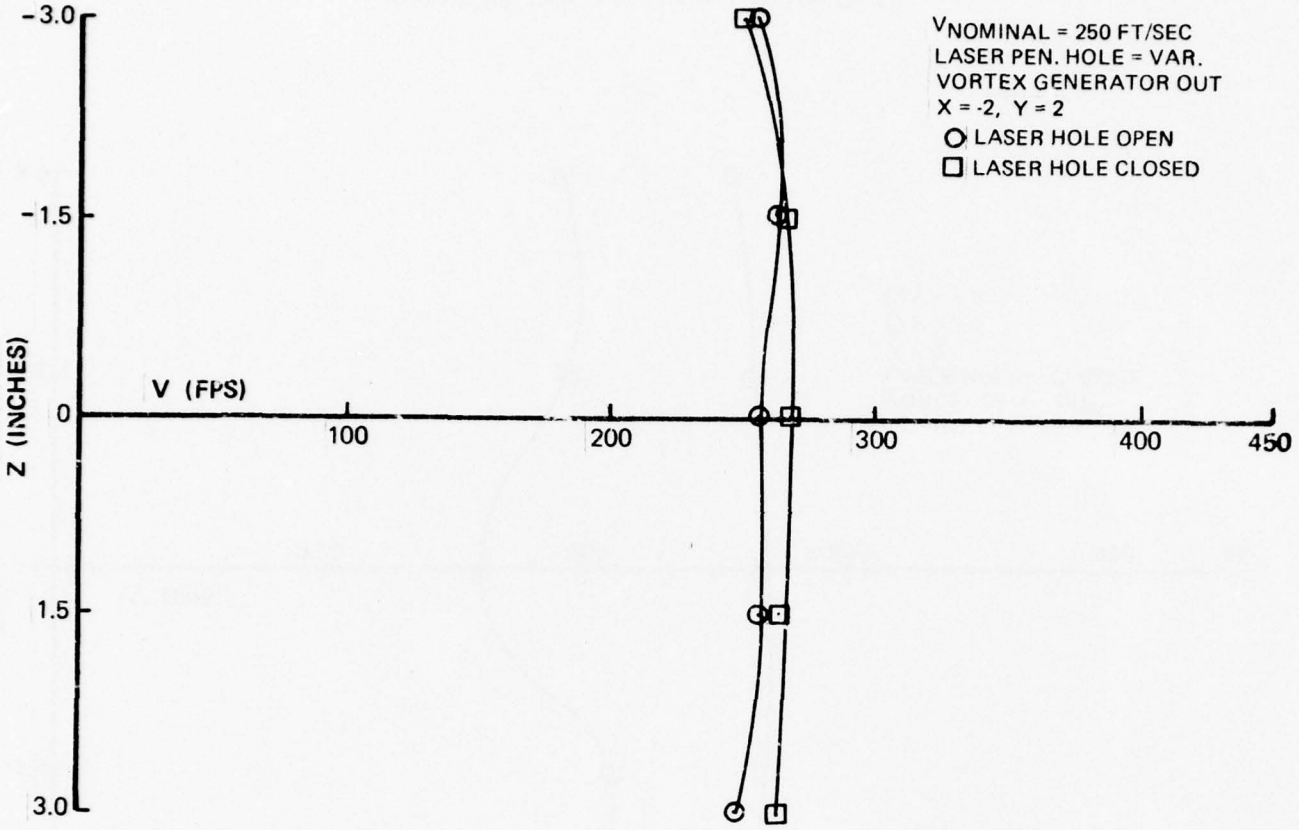

Figure IV-23. Velocity Calibration, Laser Flow Duct.

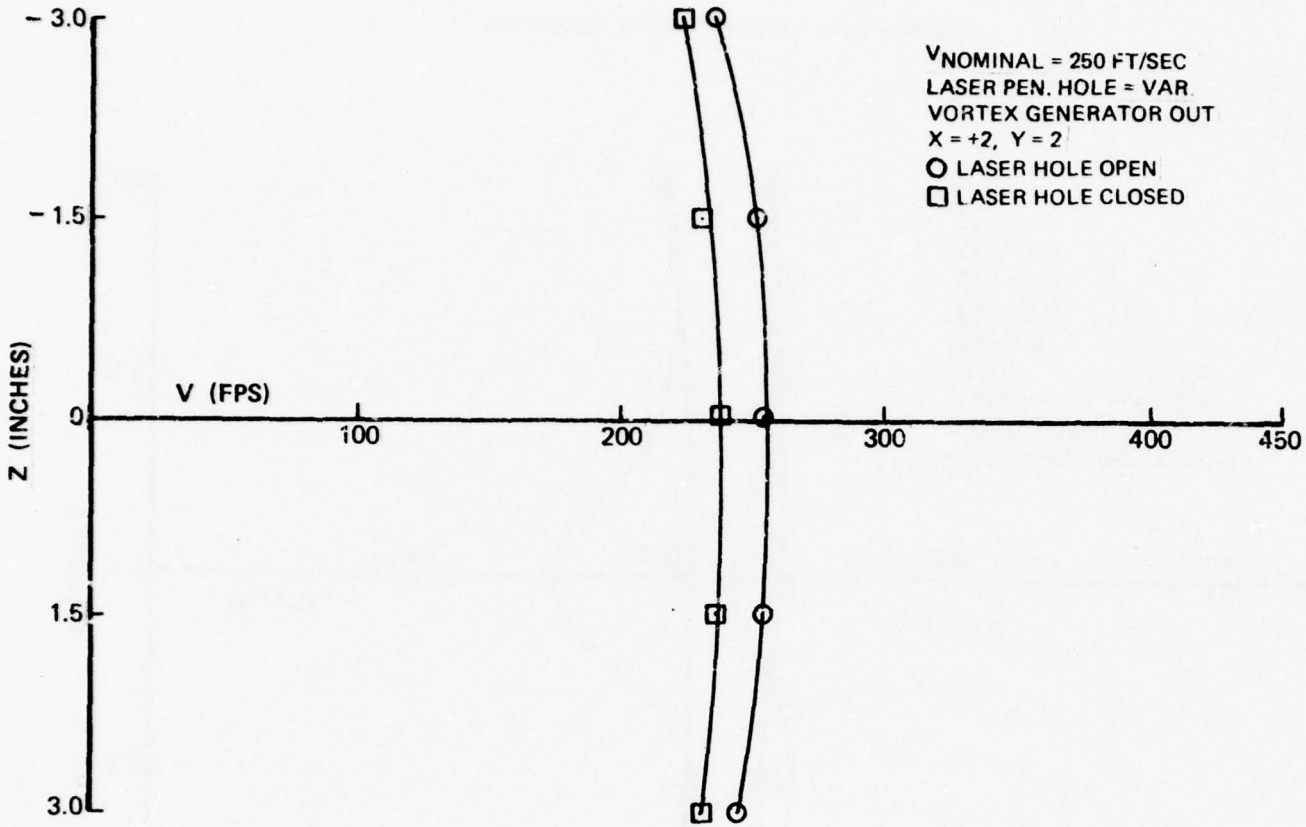

Figure IV-24. Velocity Calibration, Laser Flow Duct.

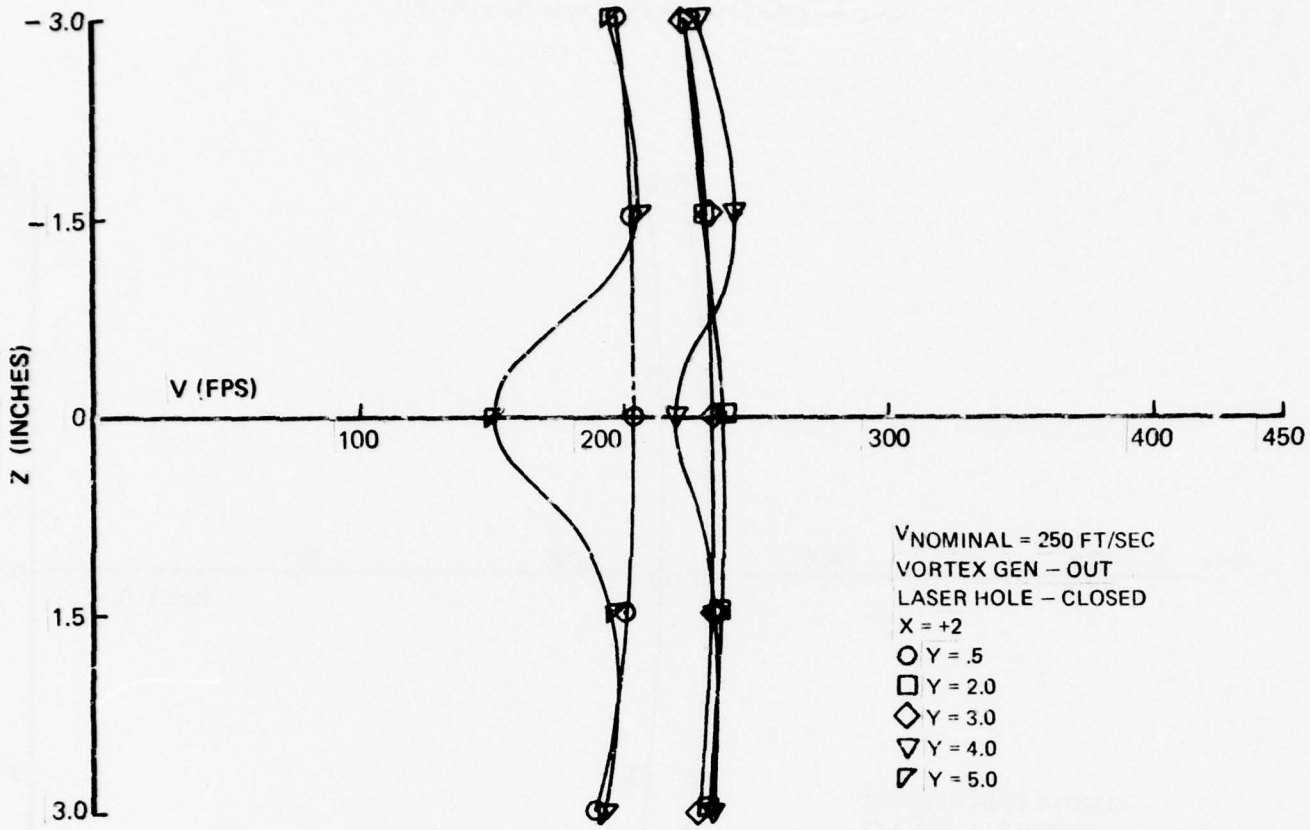

Figure IV-25. Velocity Calibration, Laser Flow Duct.

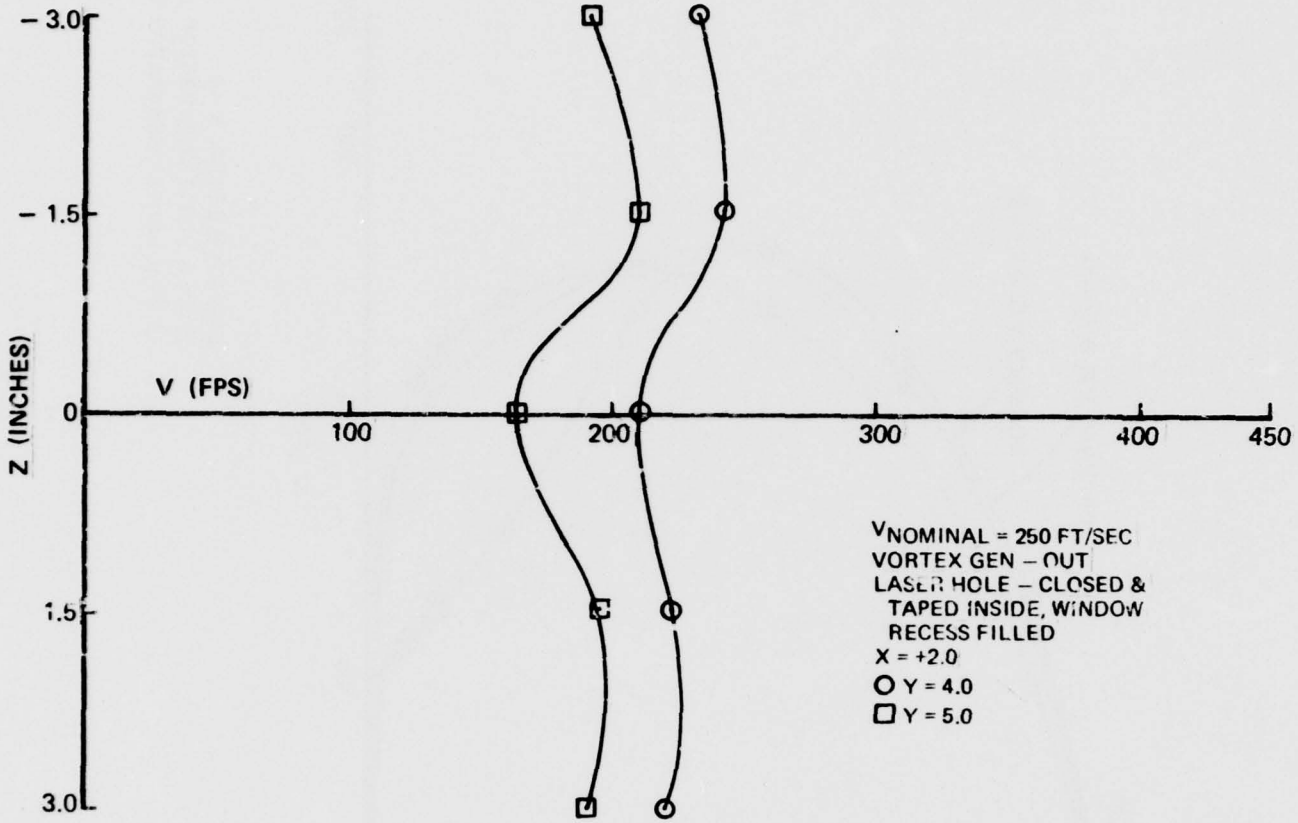

Figure IV-26. Velocity Calibration, Laser Flow Duct.

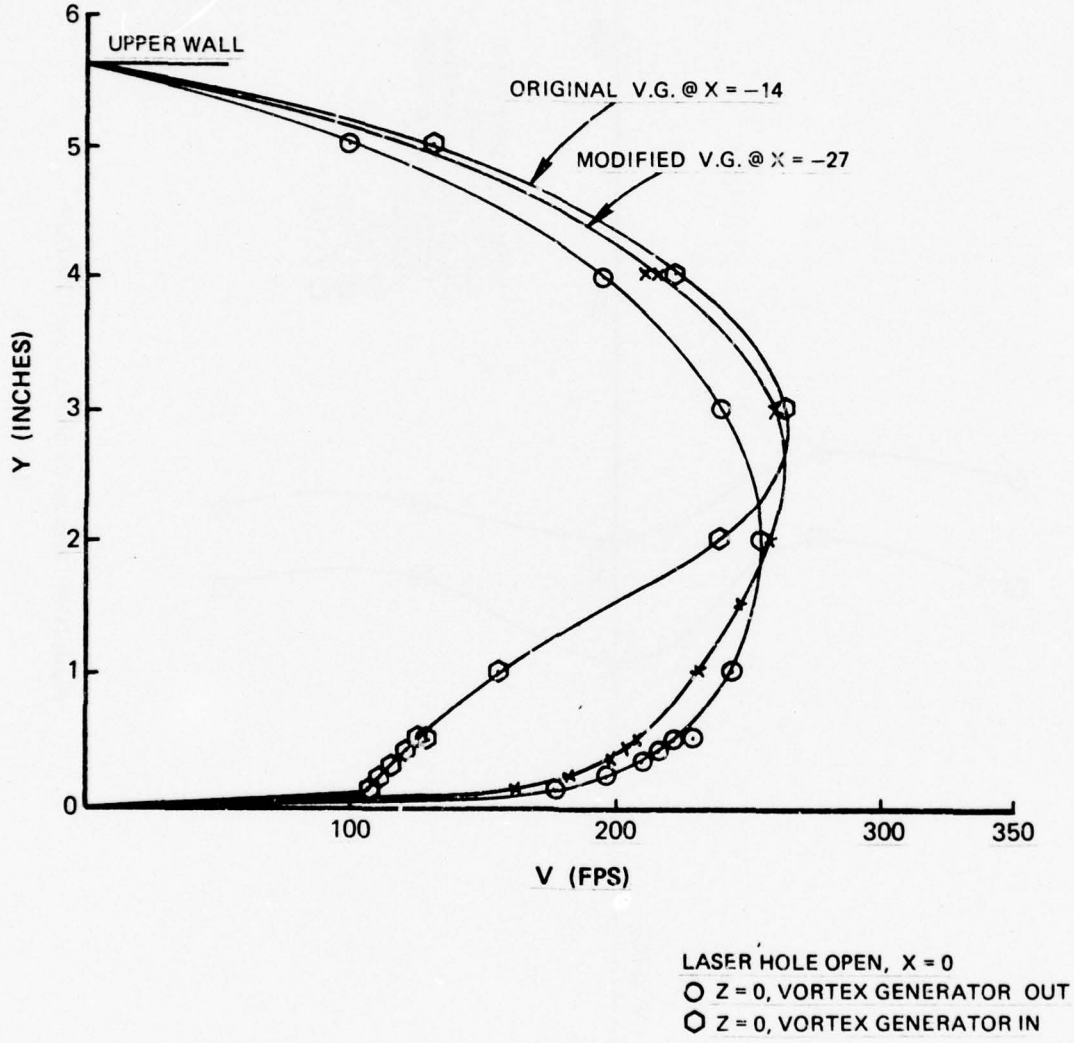

Figure IV-27. Velocity Profile Calibration.

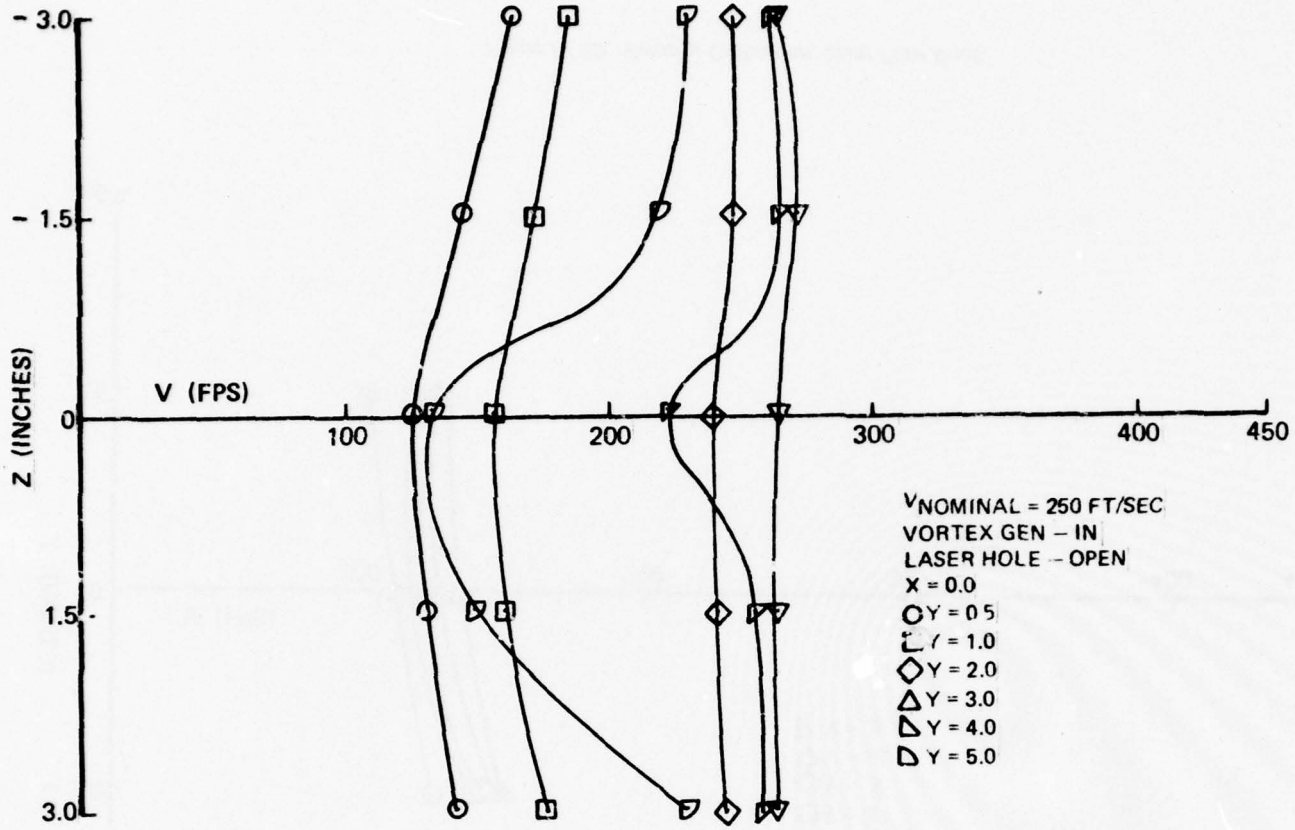

Figure IV-28. Velocity Calibration, Laser Flow Duct.

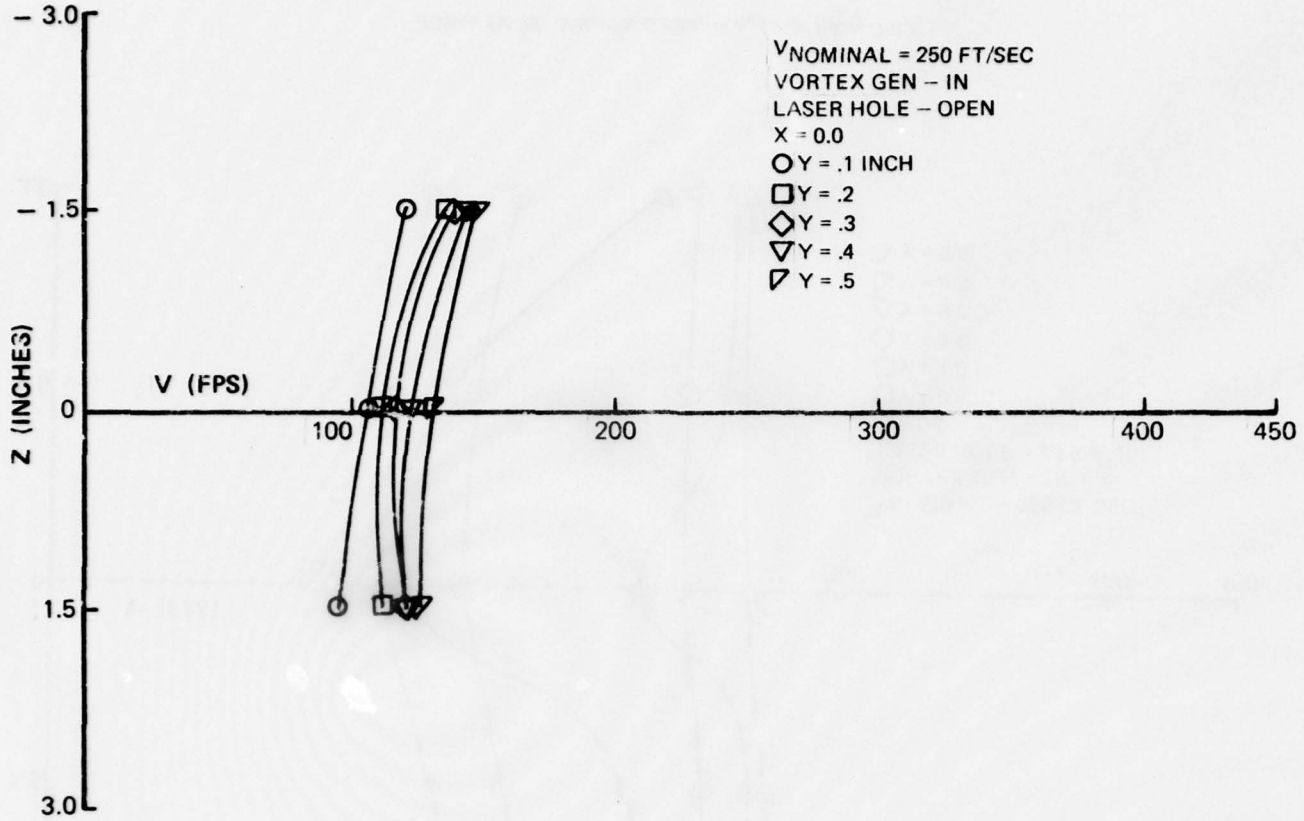

Figure IV-29. Velocity Calibration, Laser Flow Duct.

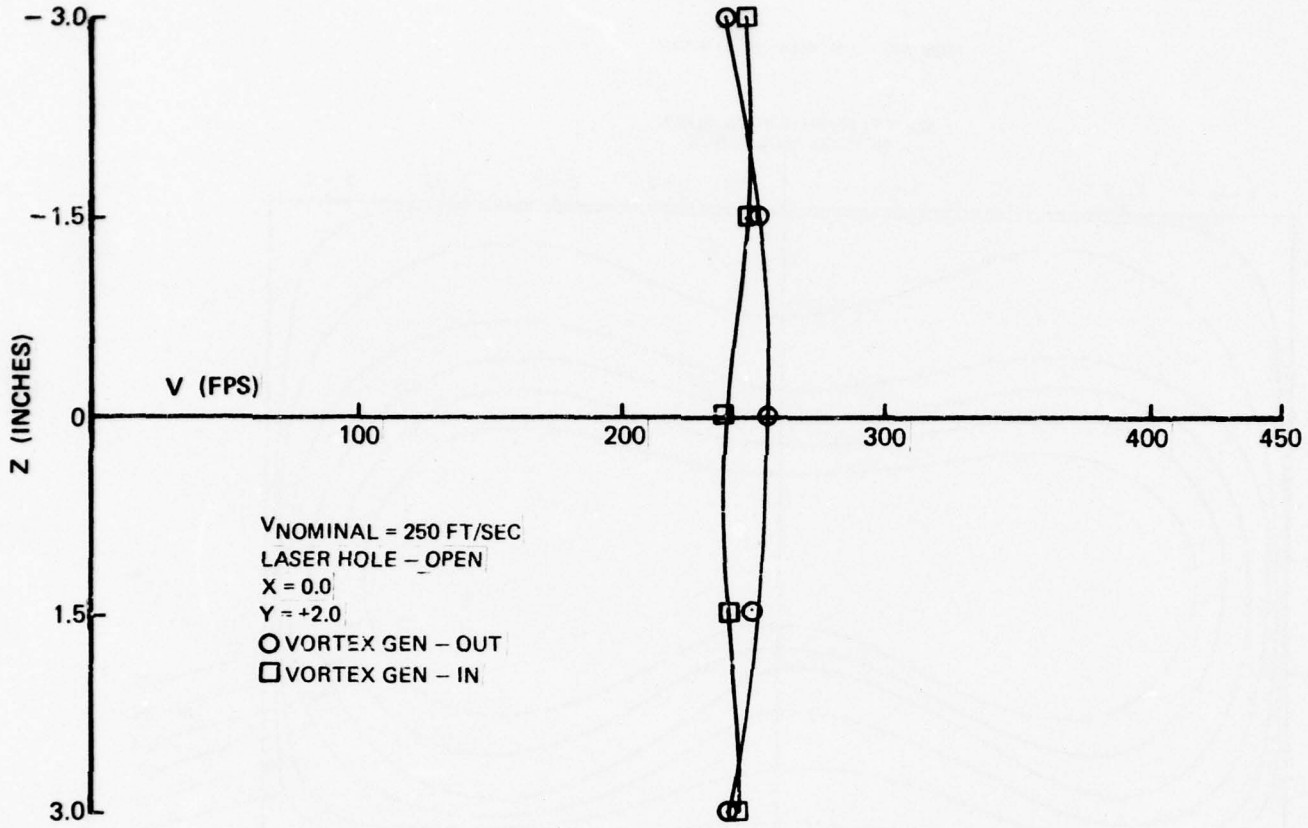

Figure IV-30. Velocity Calibration, Laser Flow Duct.

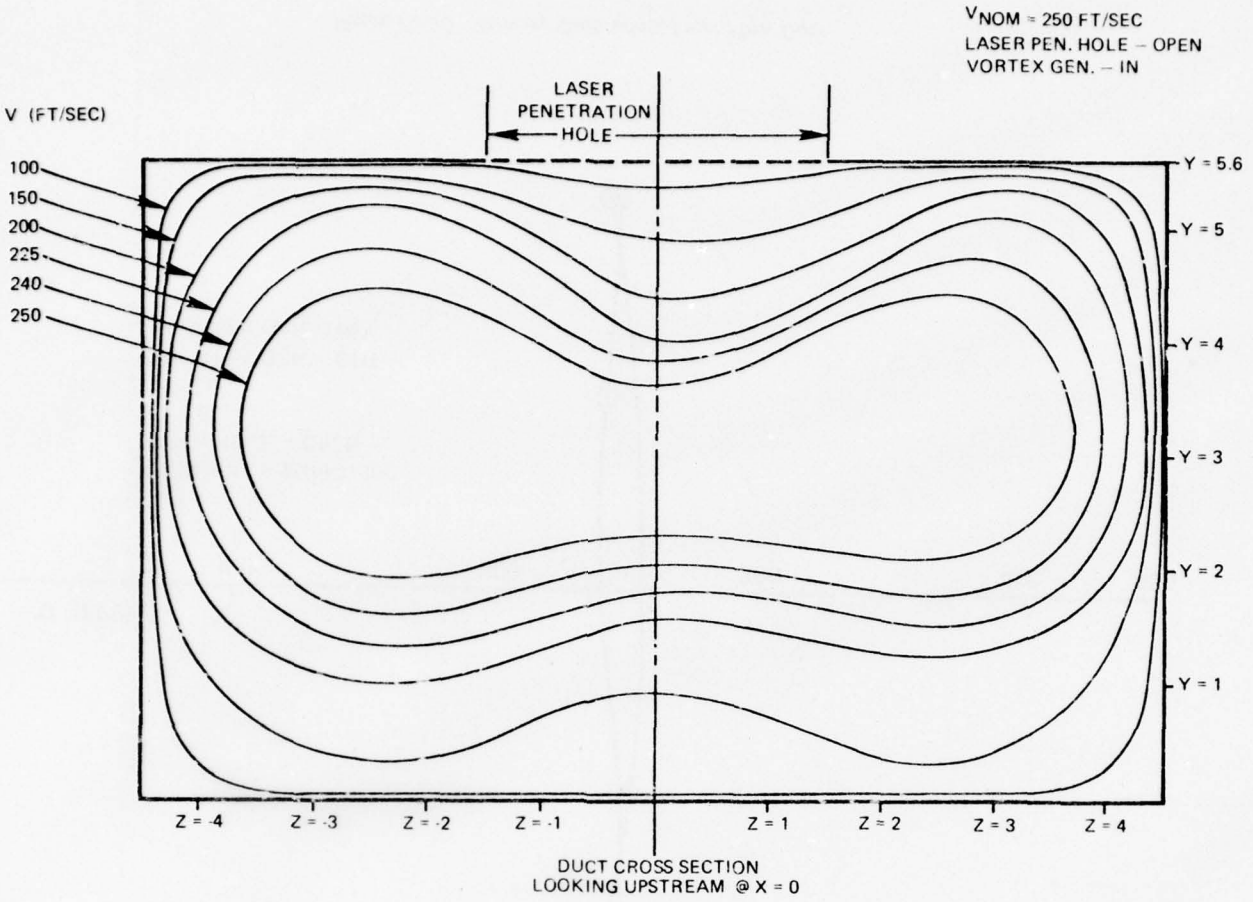

Figure IV-31. Velocity Contour Map.

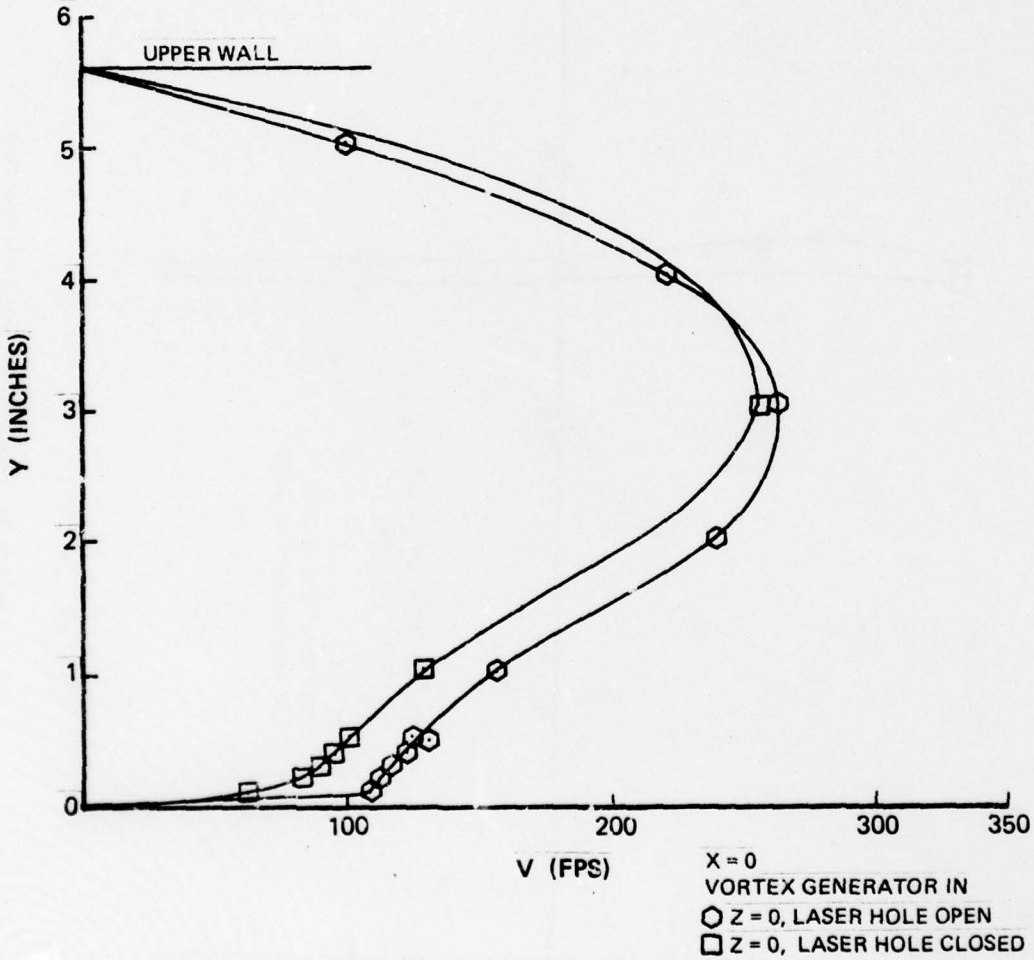

Figure IV-32. Velocity Profile Calibration.

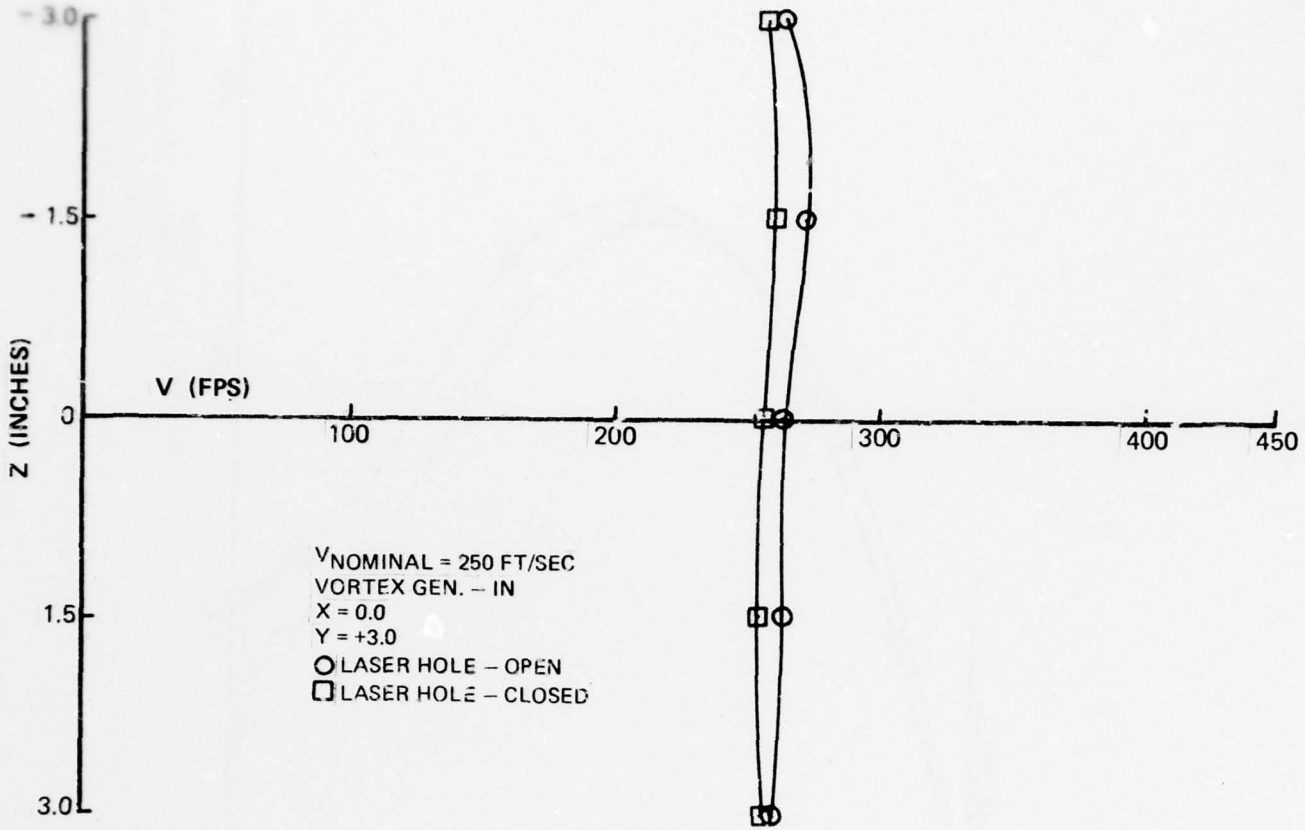

Figure IV-33. Velocity Calibration, Laser Flow Duct.

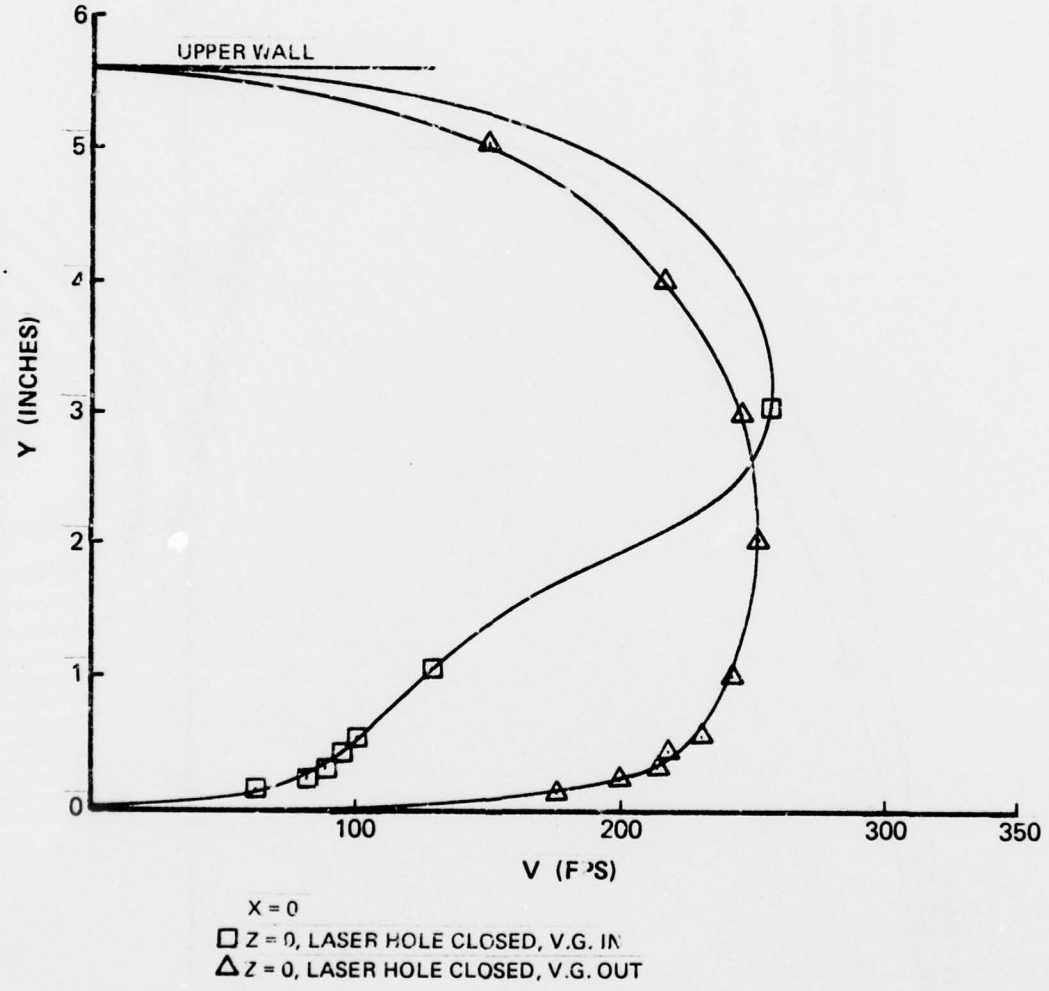

Figure IV-34. Velocity Profile Calibration.

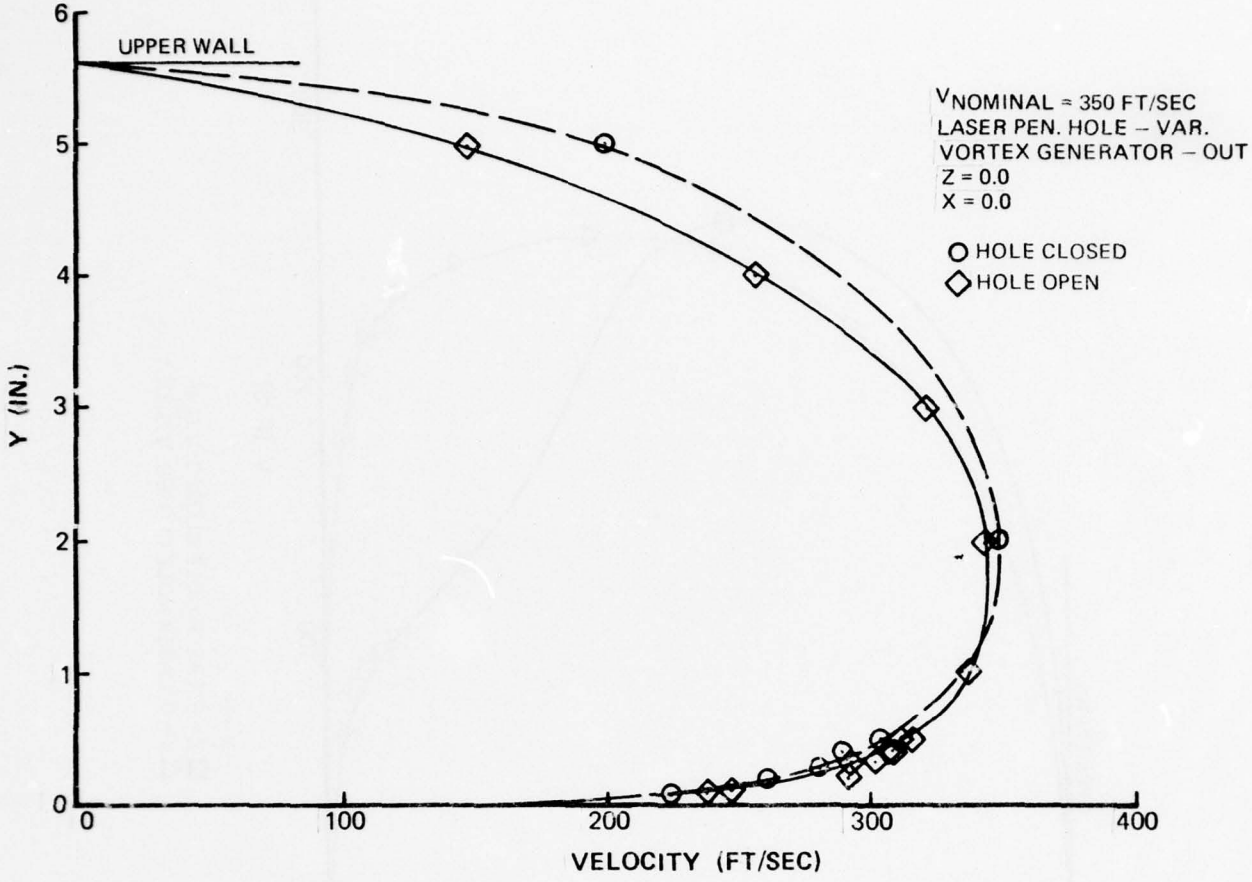

Figure IV-35. Velocity Calibration, Laser Flow Duct.

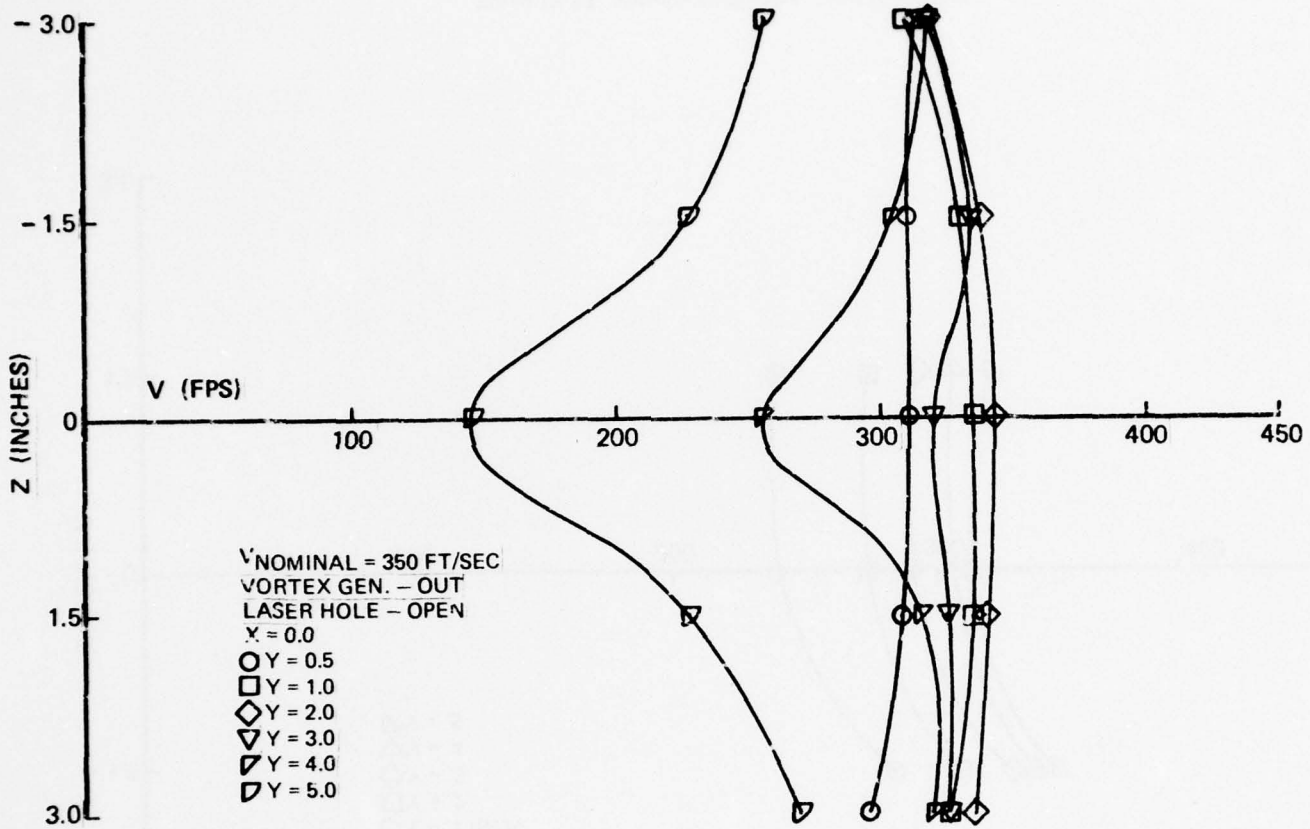

Figure IV-36. Velocity Calibration, Laser Flow Duct.

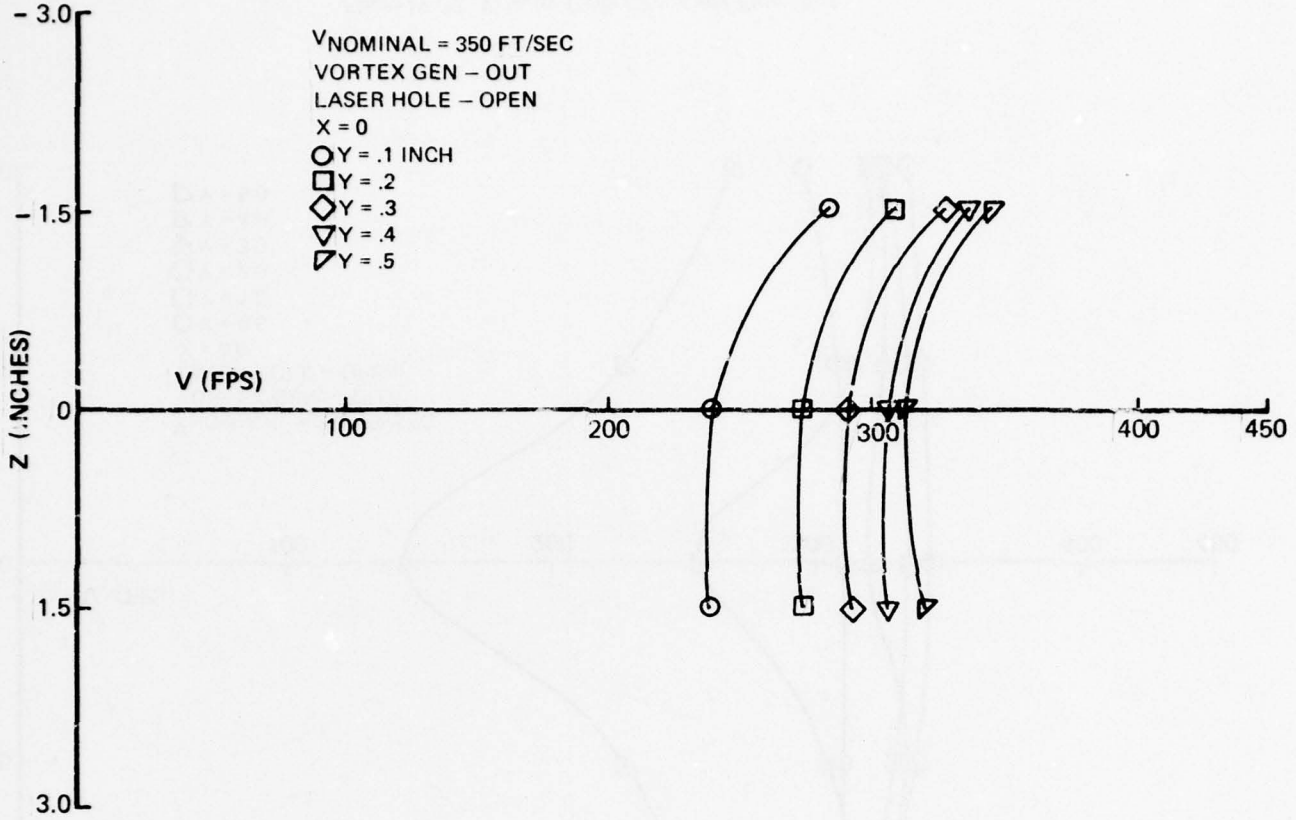

Figure IV-37. Velocity Calibration, Laser Flow Duct.

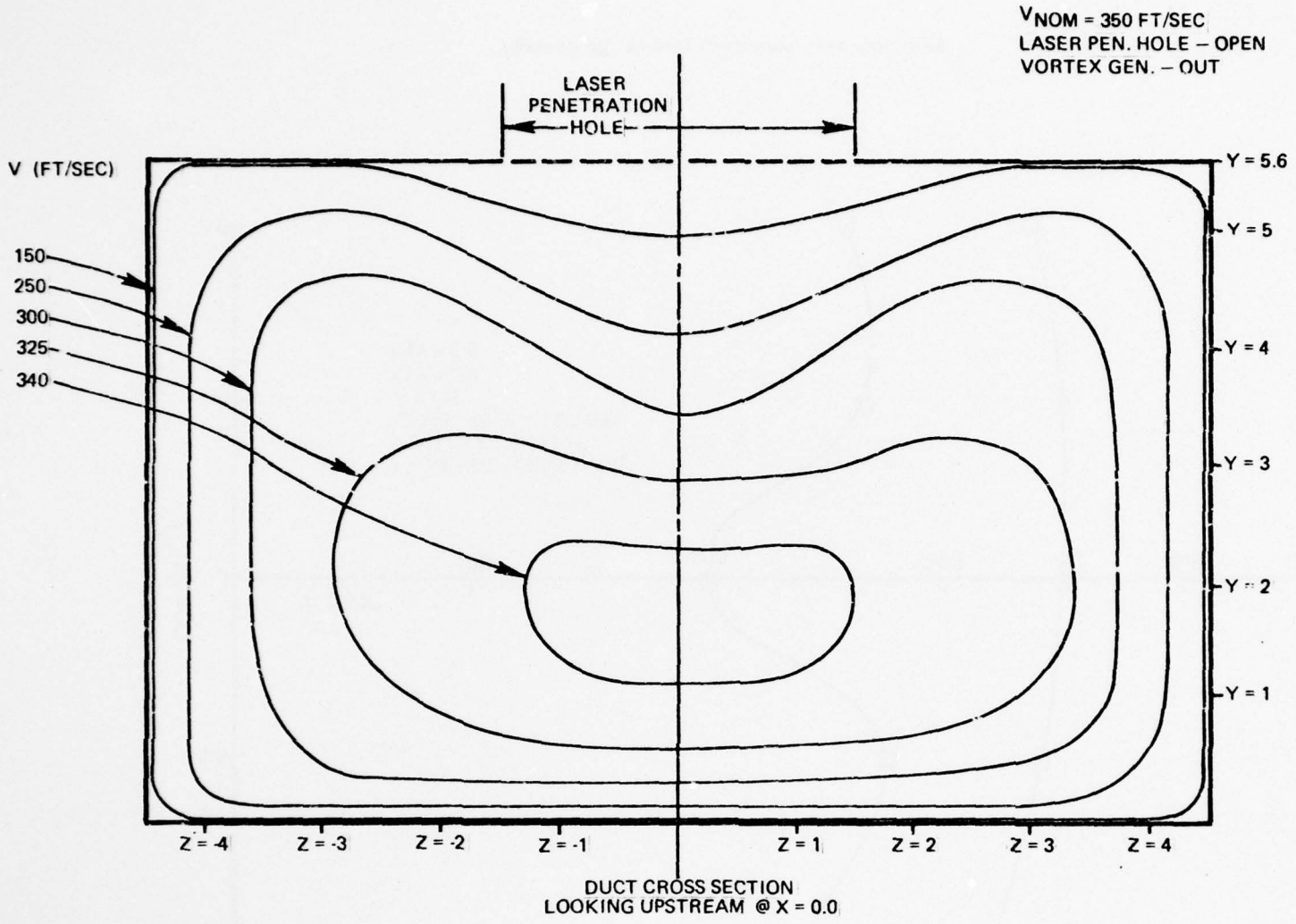

Figure IV-38. Velocity Contour Map.

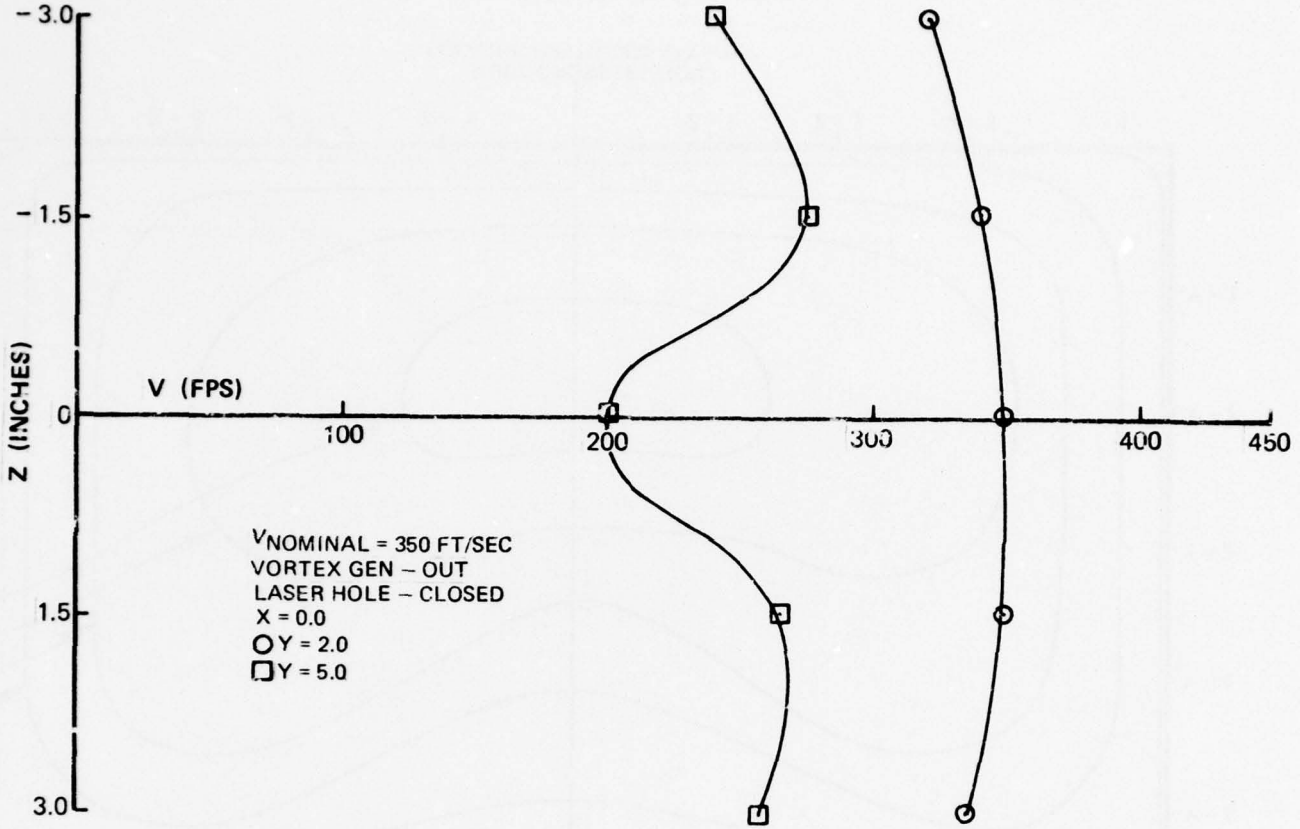

Figure IV-39. Velocity Calibration, Laser Flow Duct.

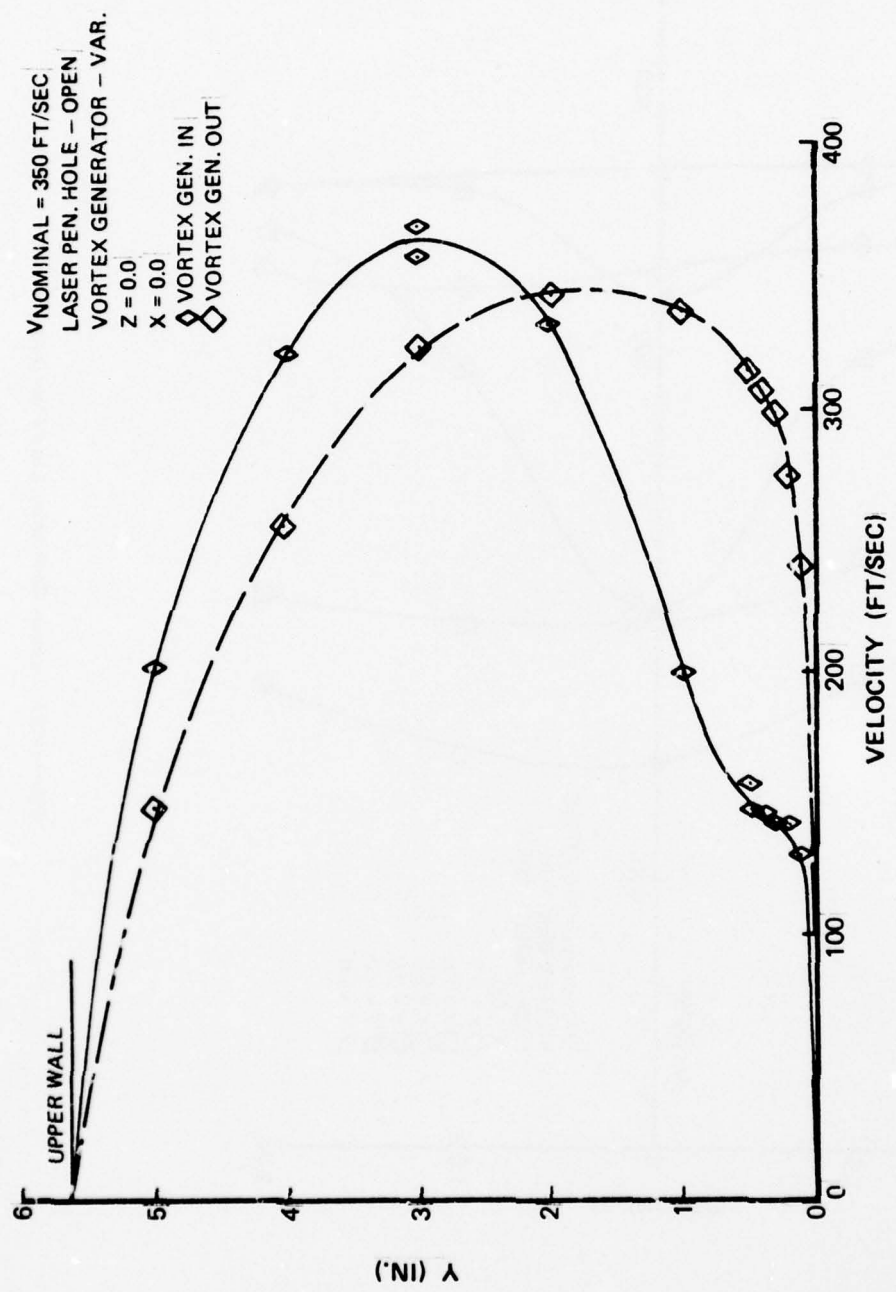

Figure IV-40. Velocity Calibration, Laser Flow Duct.

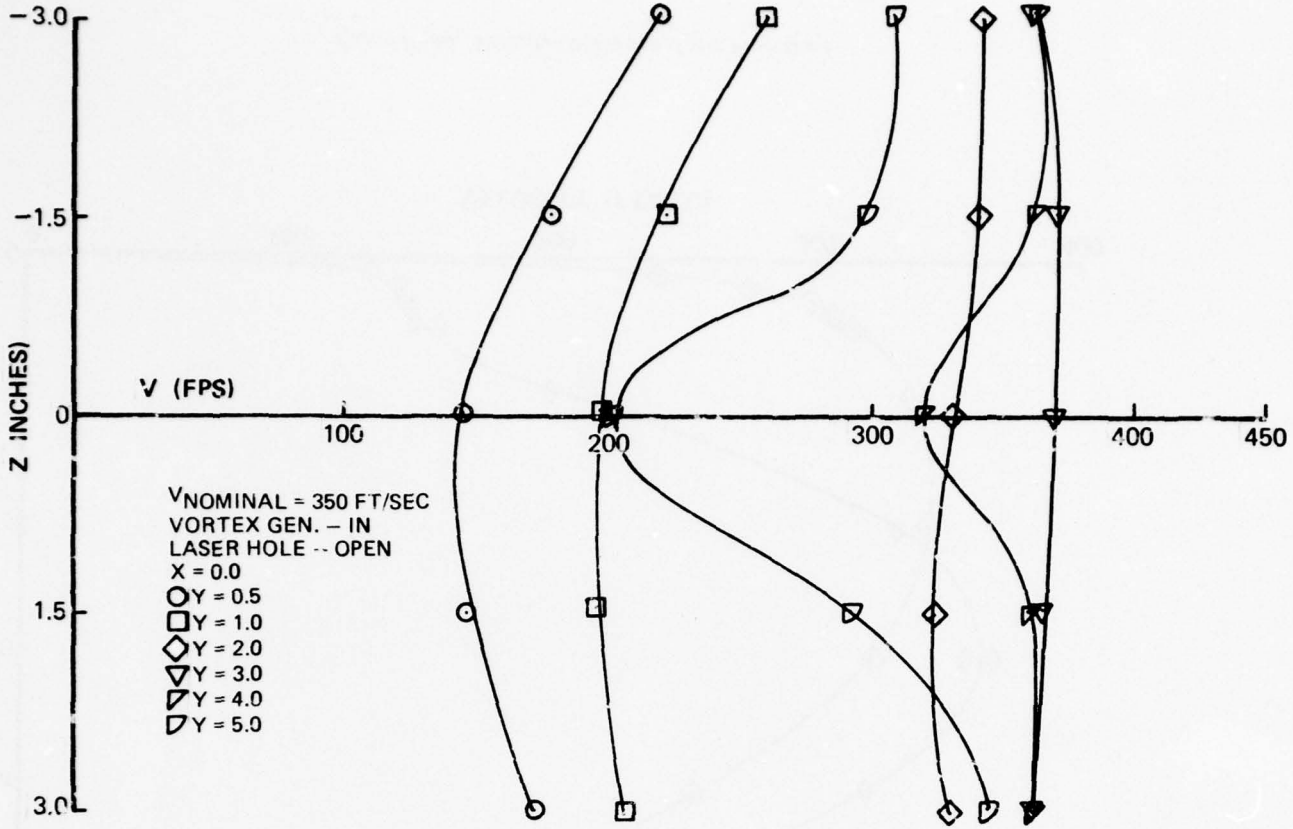

Figure IV-41. Velocity Calibration, Laser Flow Duct.

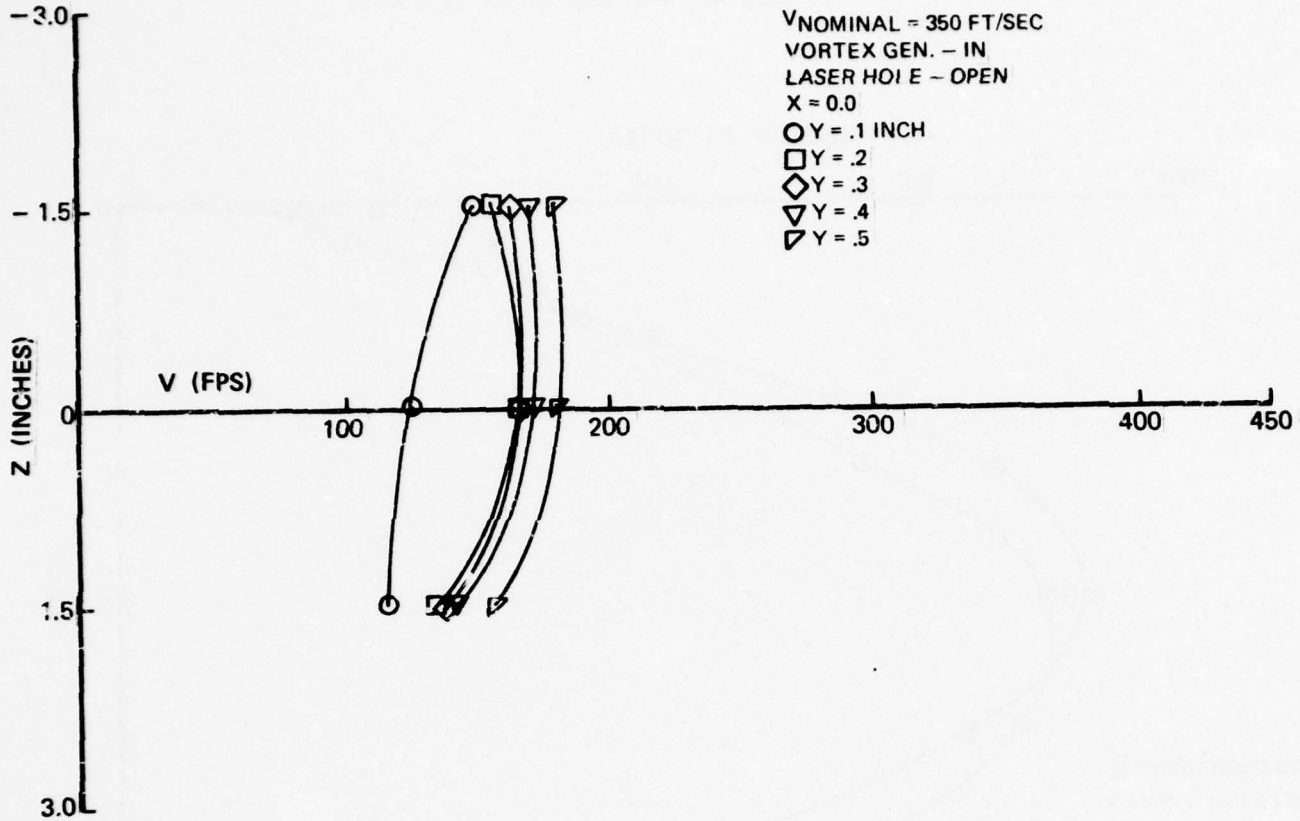

Figure IV-42. Velocity Calibration, Laser Flow Duct.

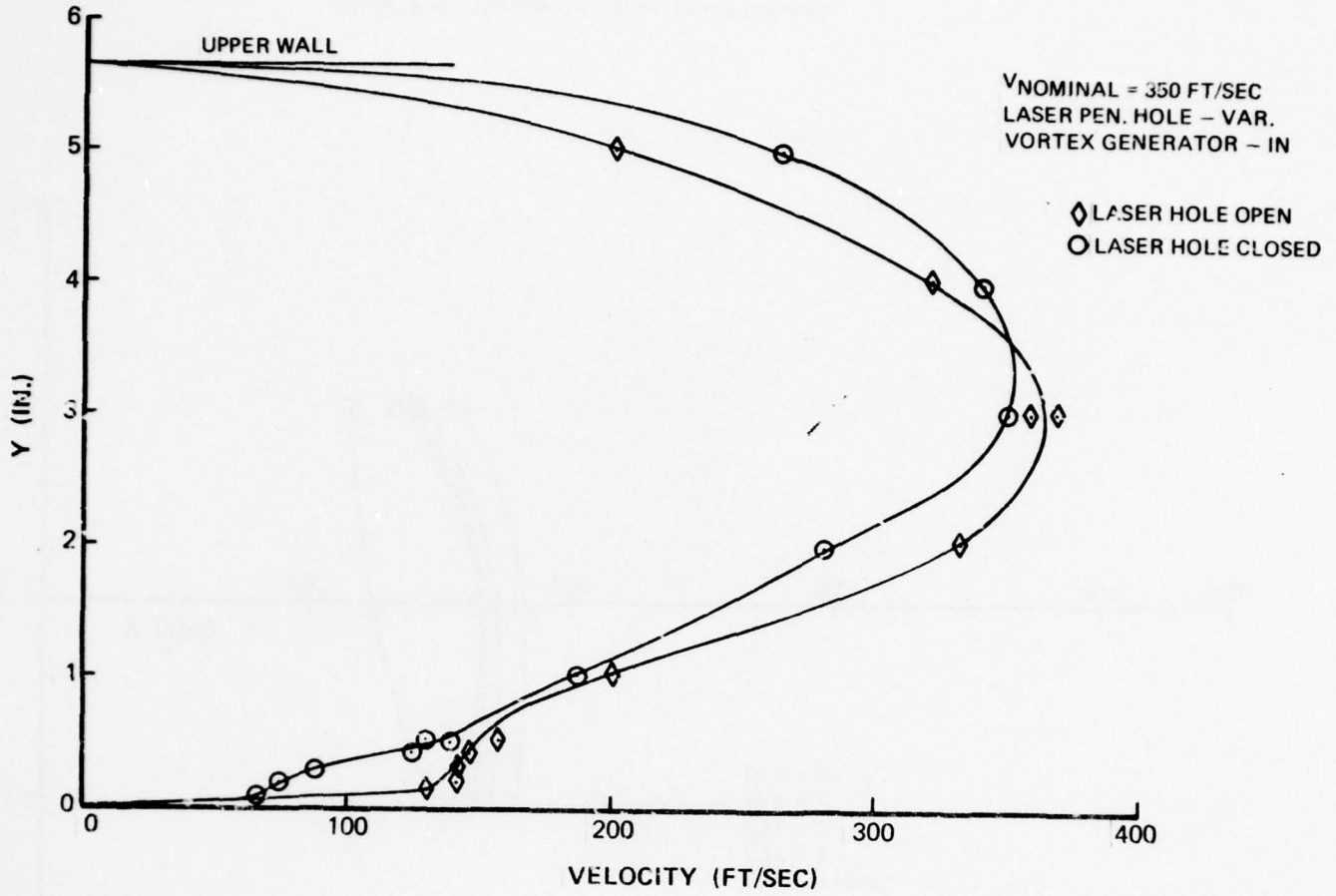

Figure IV-43. Velocity Calibration, Laser Flow Duct.

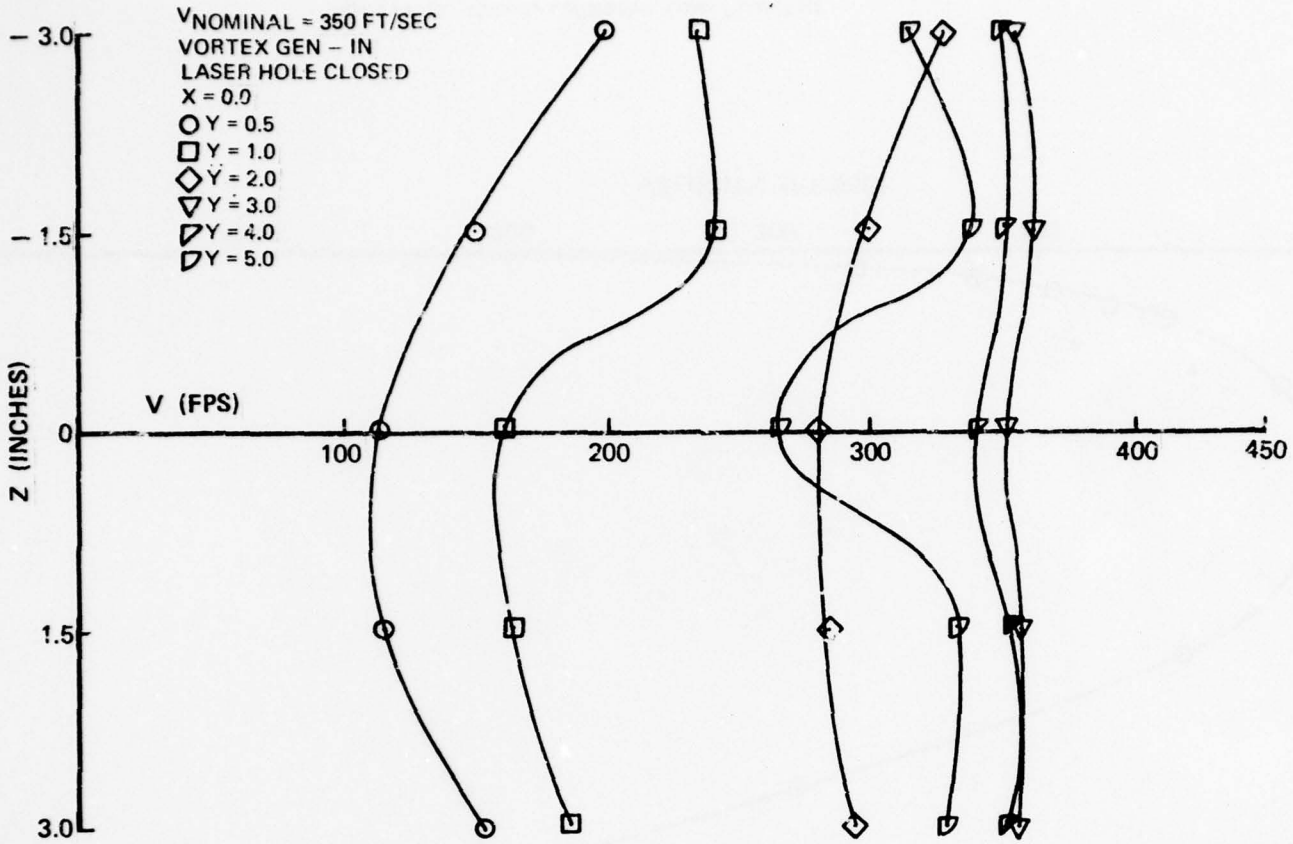

Figure IV-44. Velocity Calibration, Laser Flow Duct.

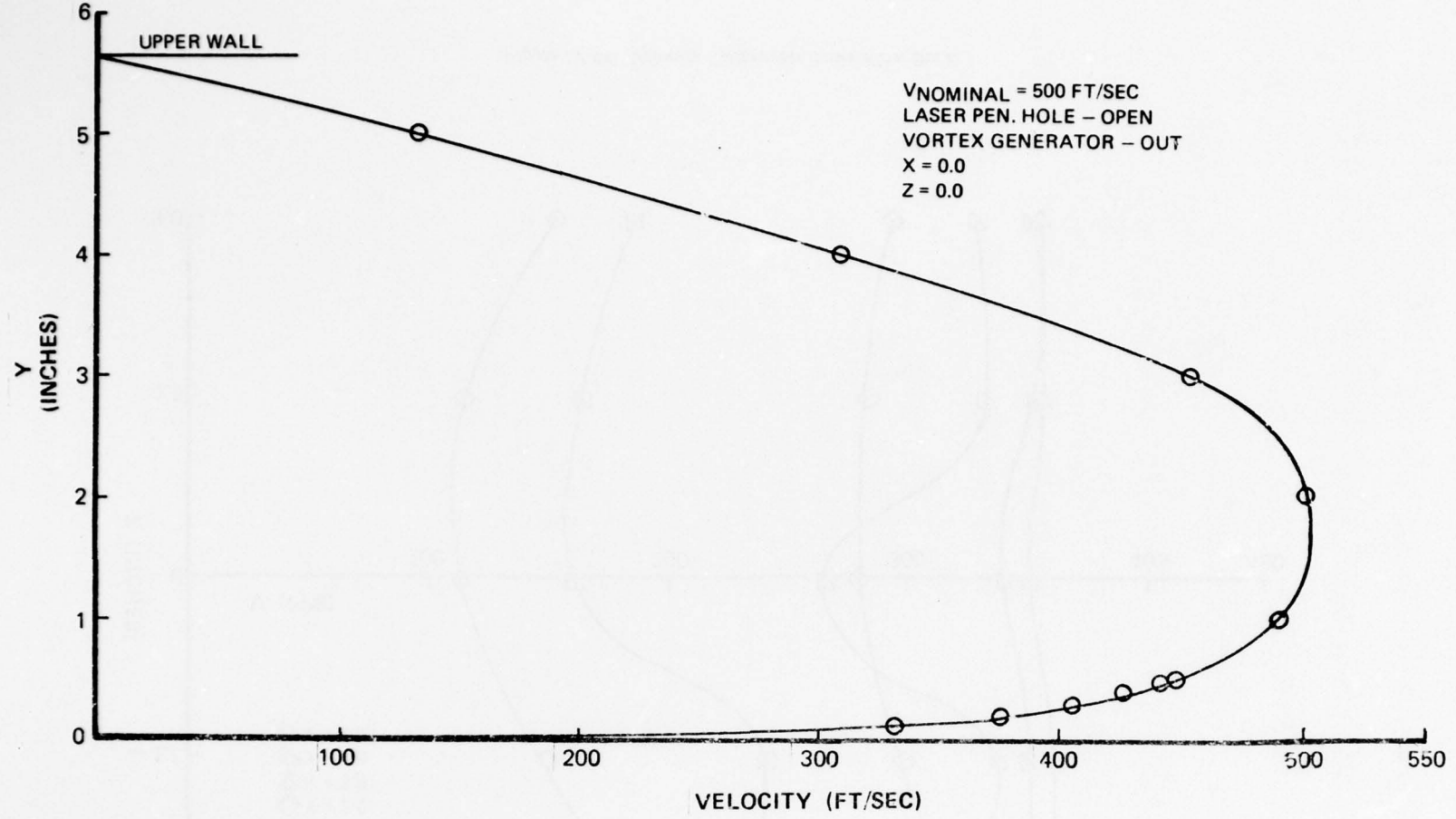

Figure IV-45. Velocity Calibration, Laser Flow Duct

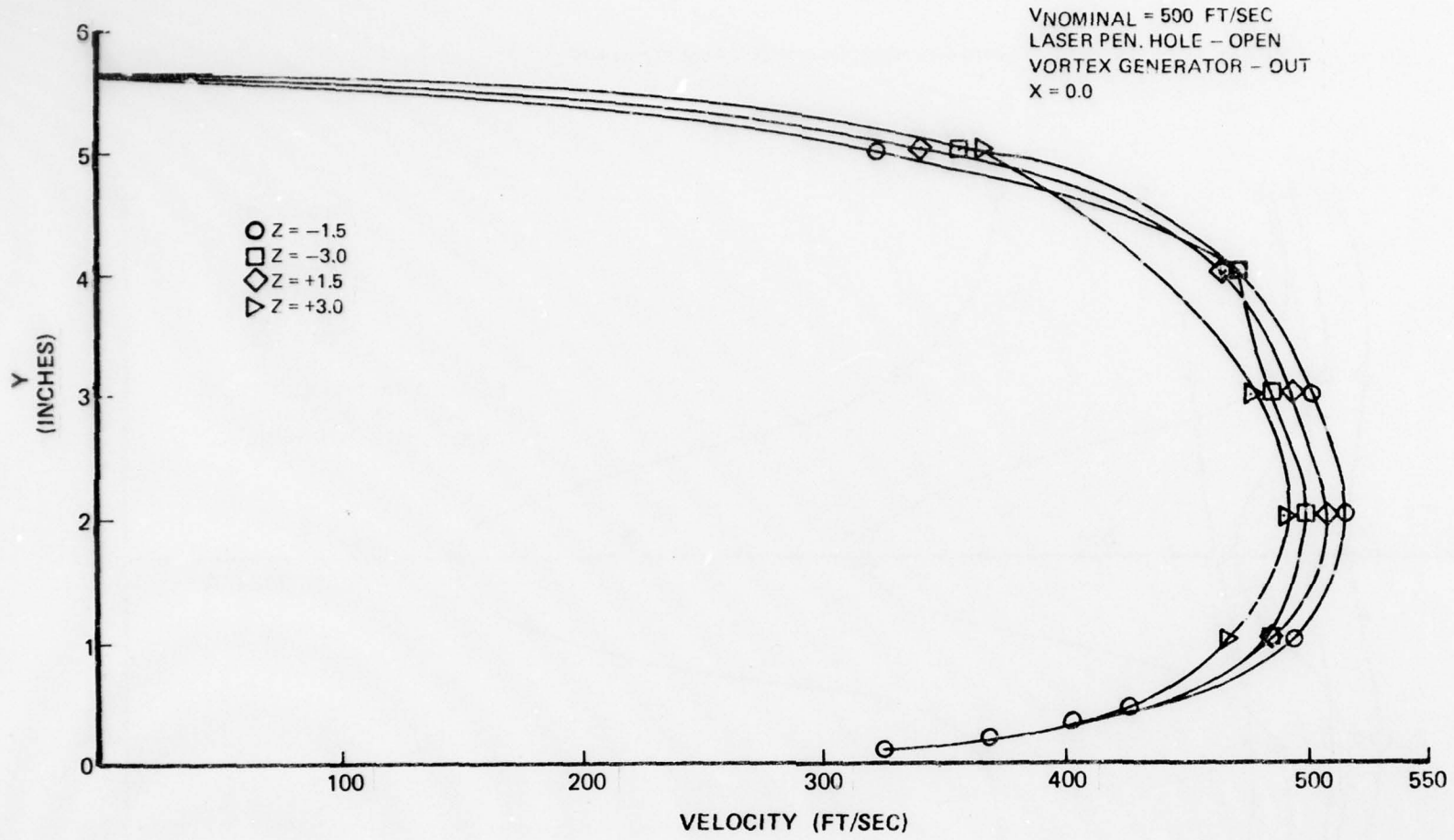

Figure IV-46. Velocity Calibration, Laser Flow Duct

AD-A042 187 SYSTEMS RESEARCH LABS INC DAYTON OHIO F/G 20/4
FLOW CALIBRATION OF THE LASER TEST SHELTER AIRFLOW DUCT.(U)
DEC 76 C N EASTLAKE, E E DITMER F33615-76-C-2095
UNCLASSIFIED AFAPL-TR-76-103 NL

2 OF 2
ADA042187

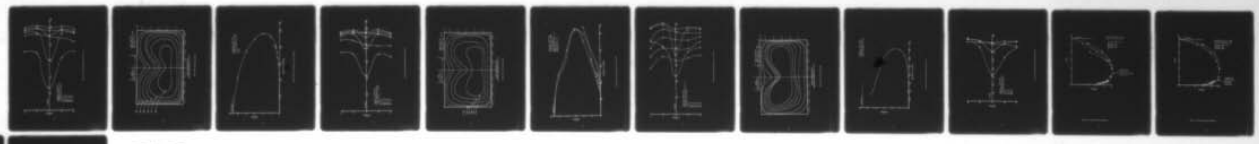

END

DATE
FILMED
8 - 77

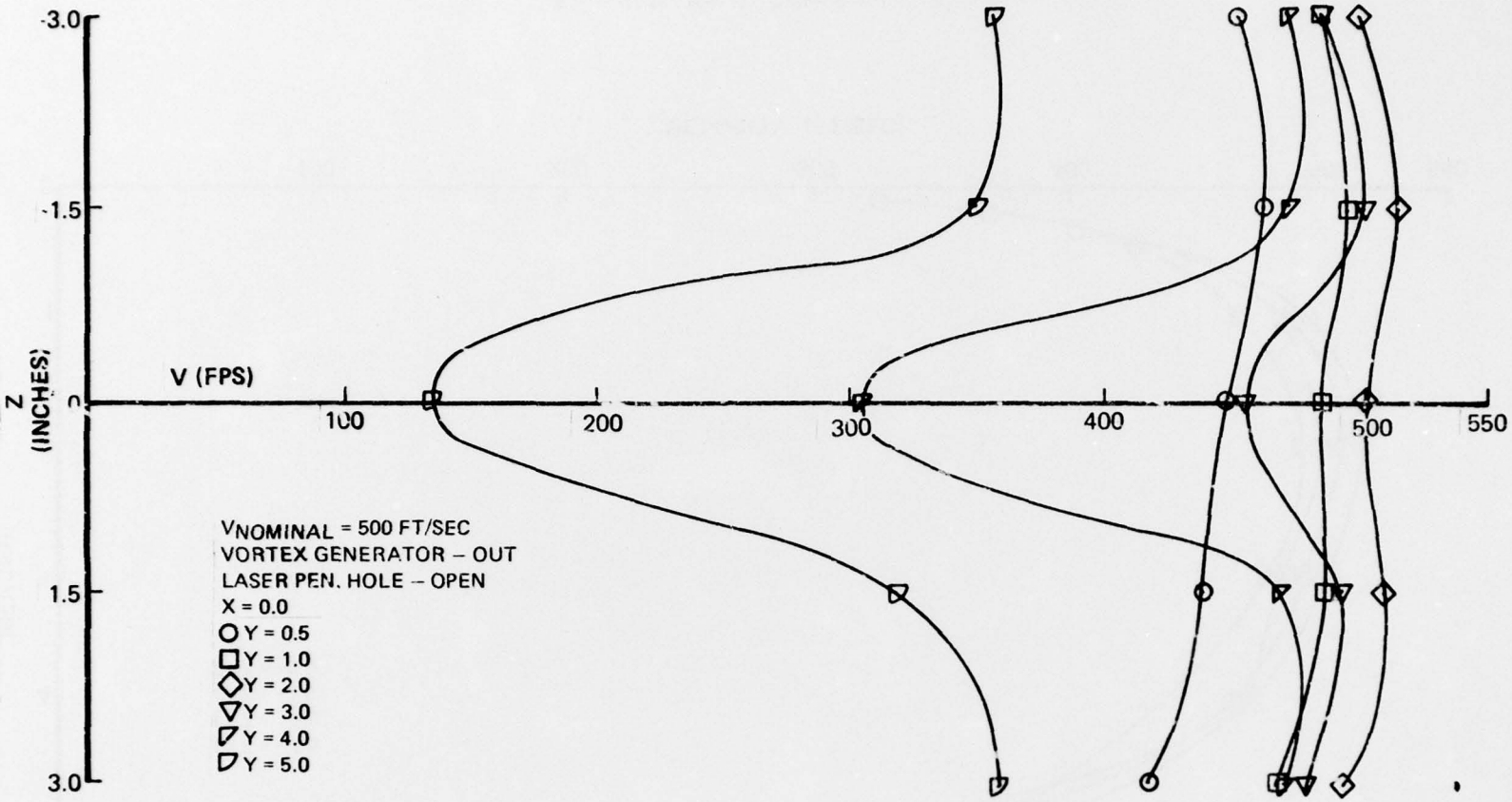

Figure IV-47. Velocity Calibration, Laser Flow Duct

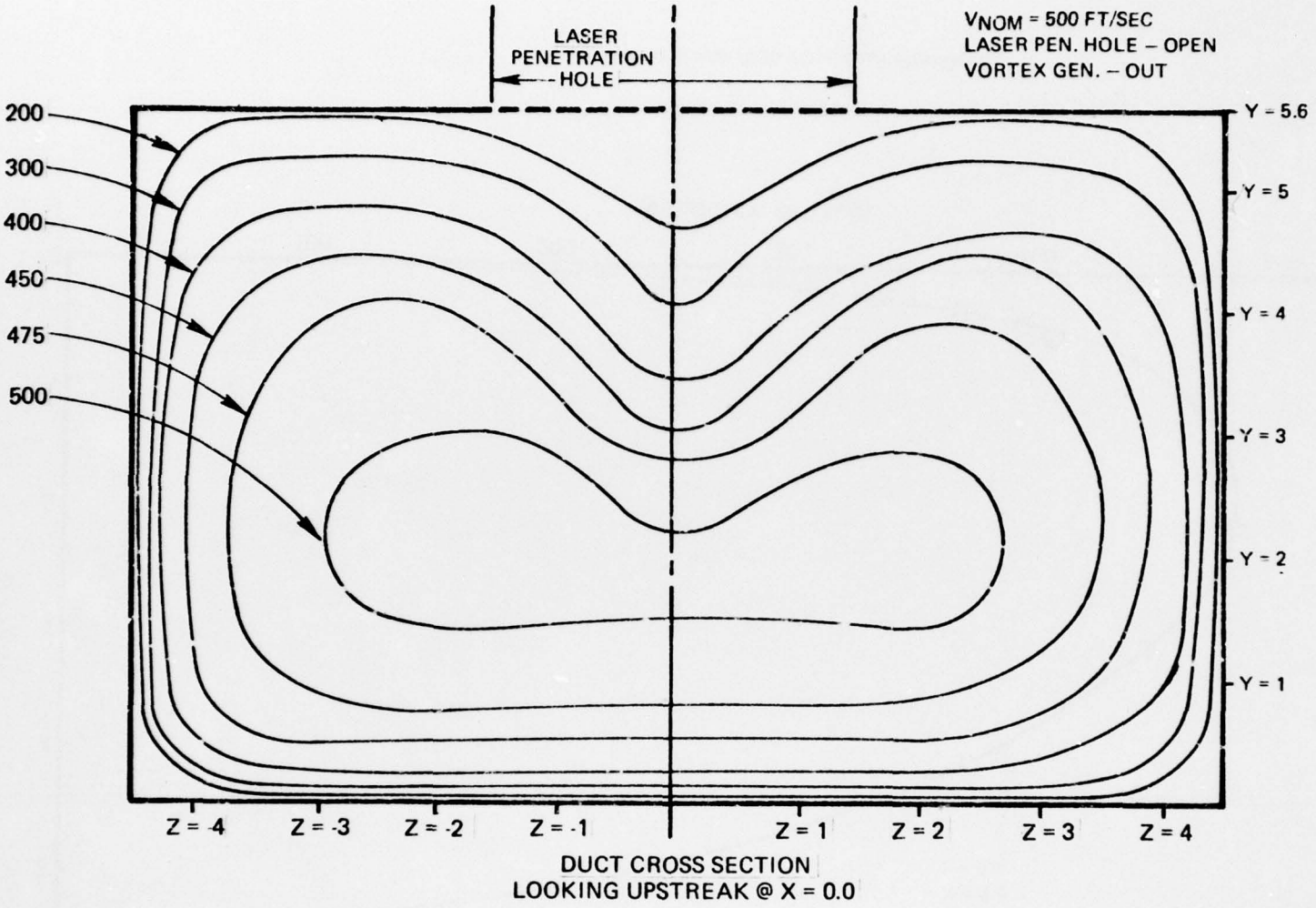

Figure IV-48. Velocity Contour Map

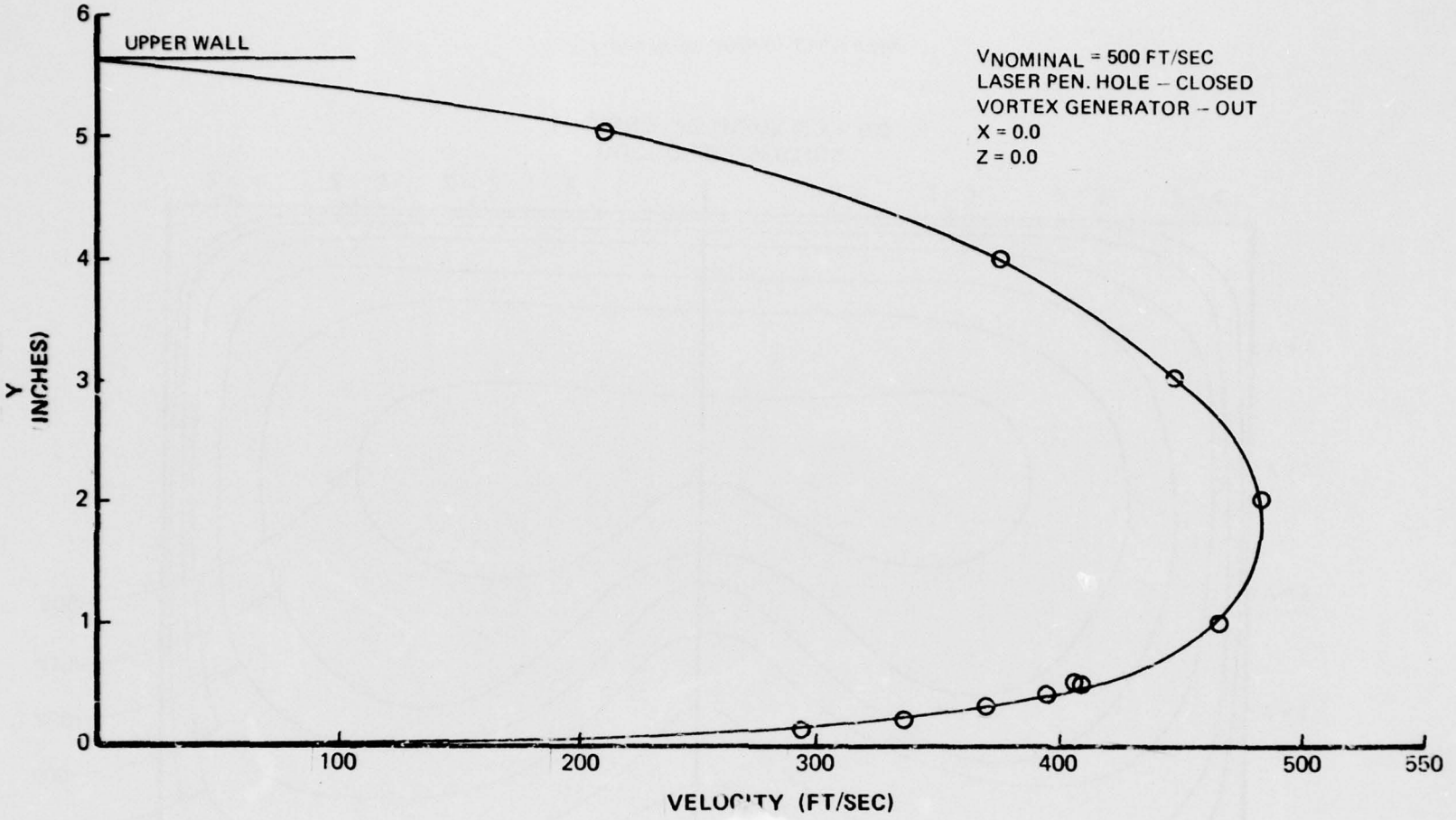

Figure IV-49. Velocity Calibration, Laser Flow Duct

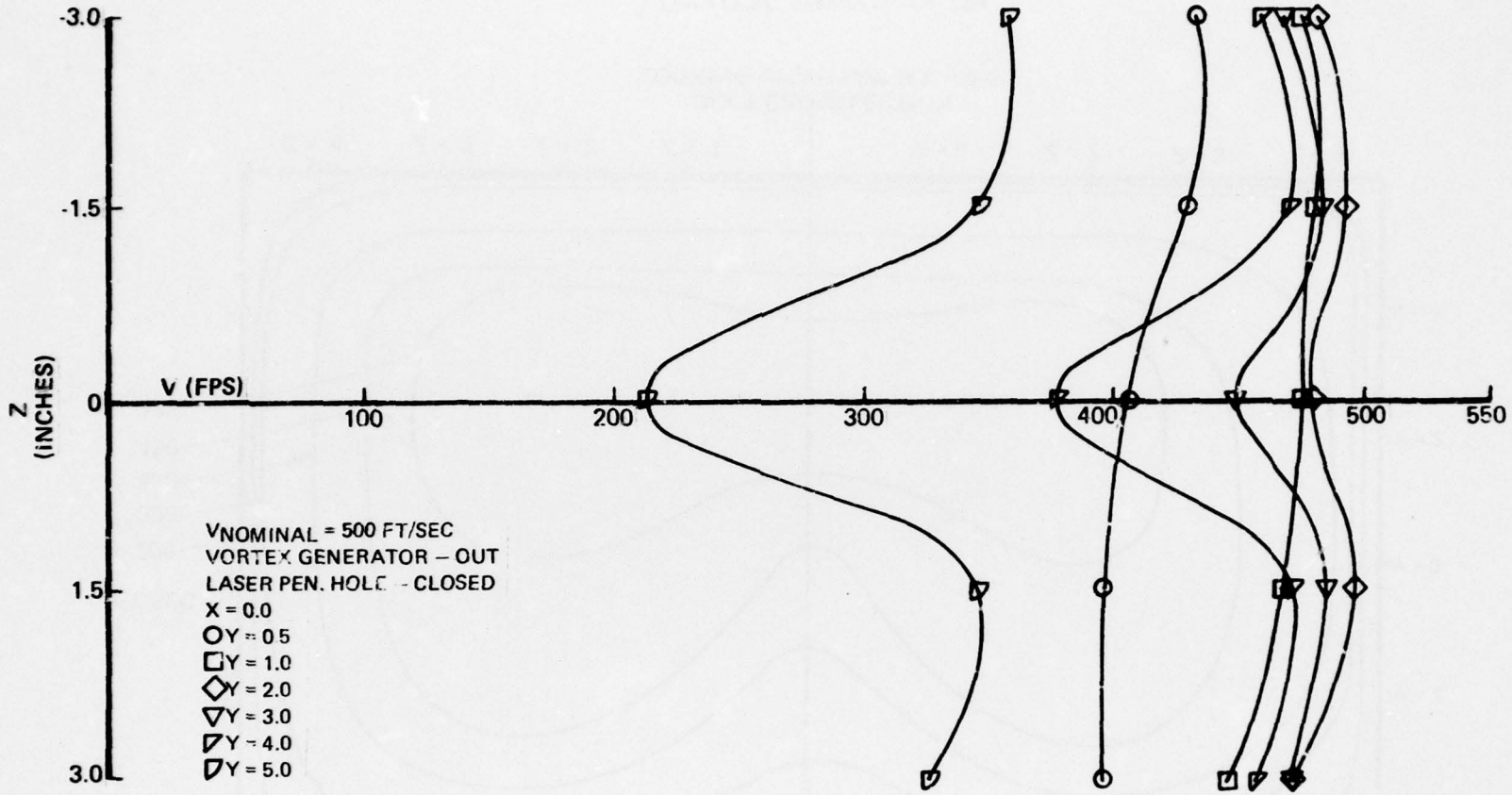

Figure IV-50. Velocity Calibration, Laser Flow Duct

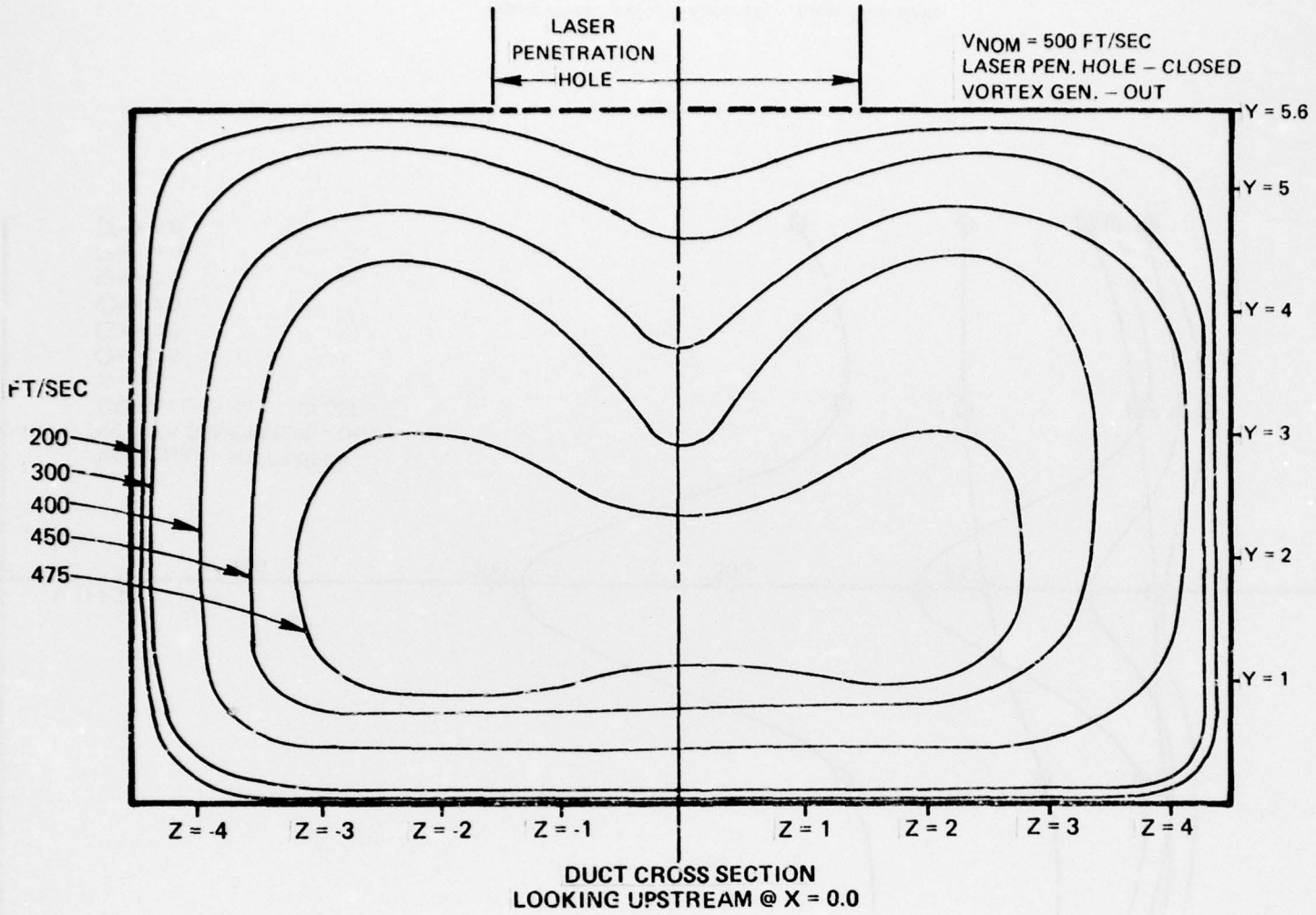

Figure IV-51. Velocity Contour Map

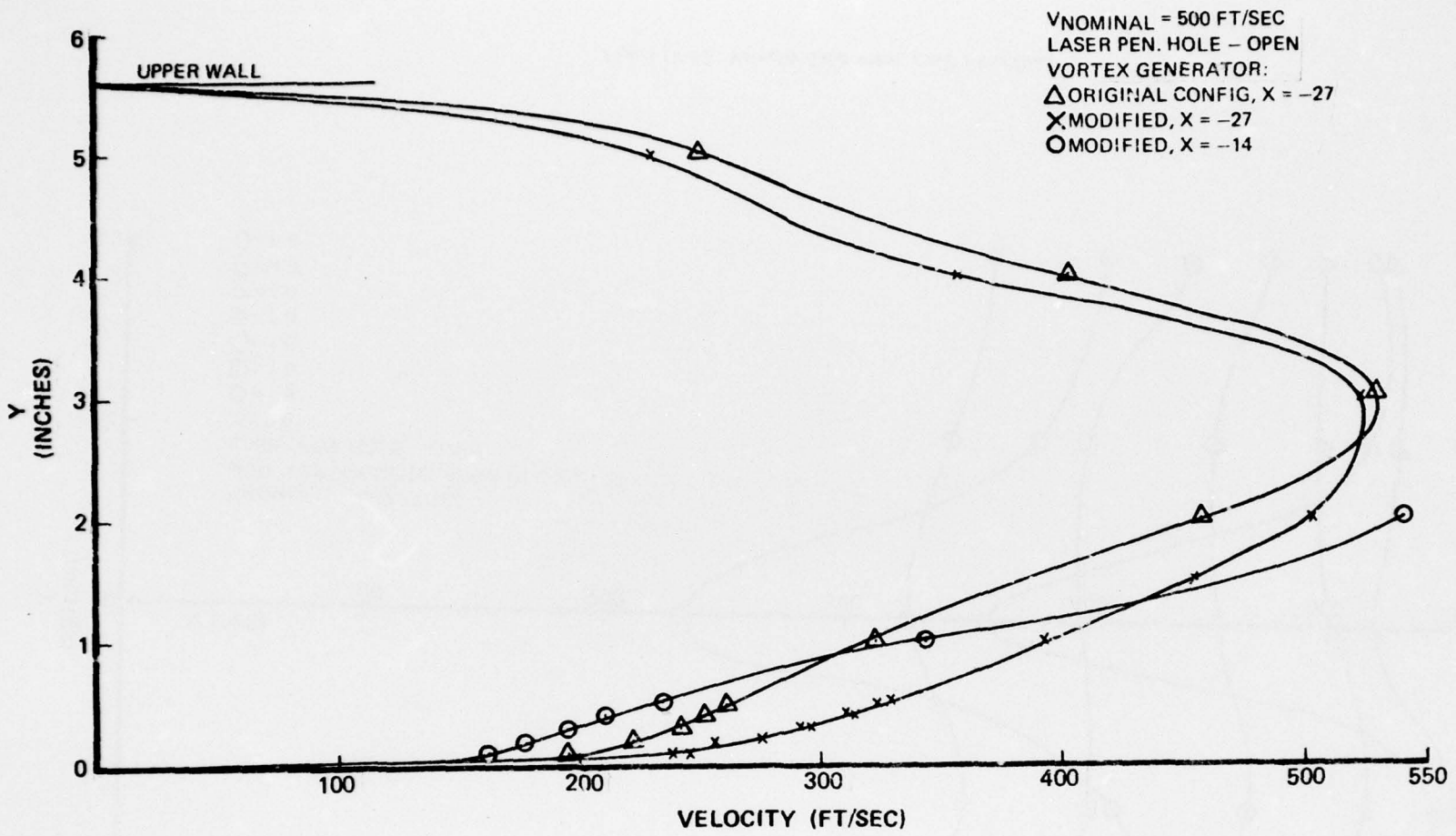

Figure IV-52. Velocity Calibration, Laser Flow Duct

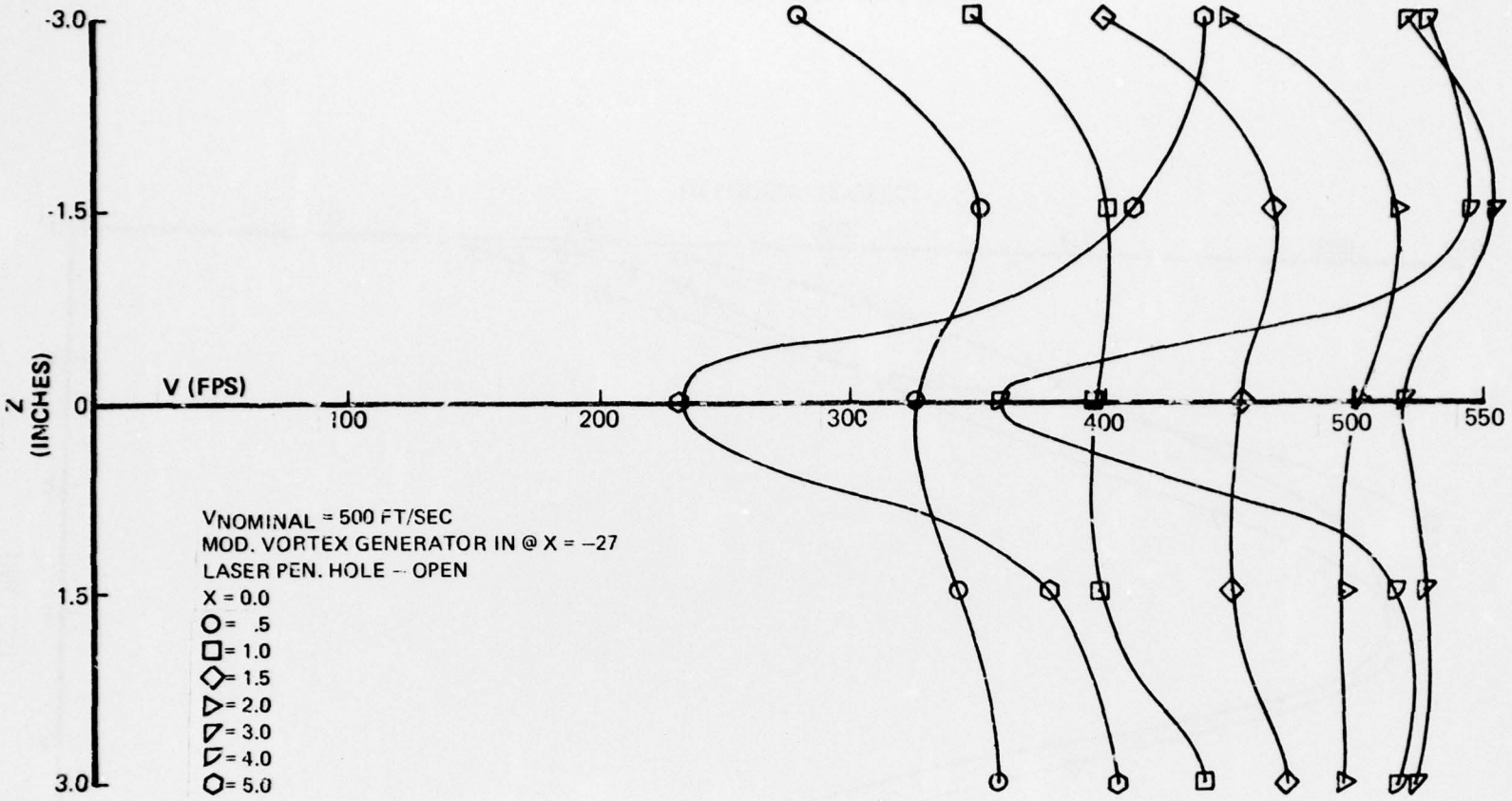

Figure IV-53. Velocity Calibration, Laser Flow Duct

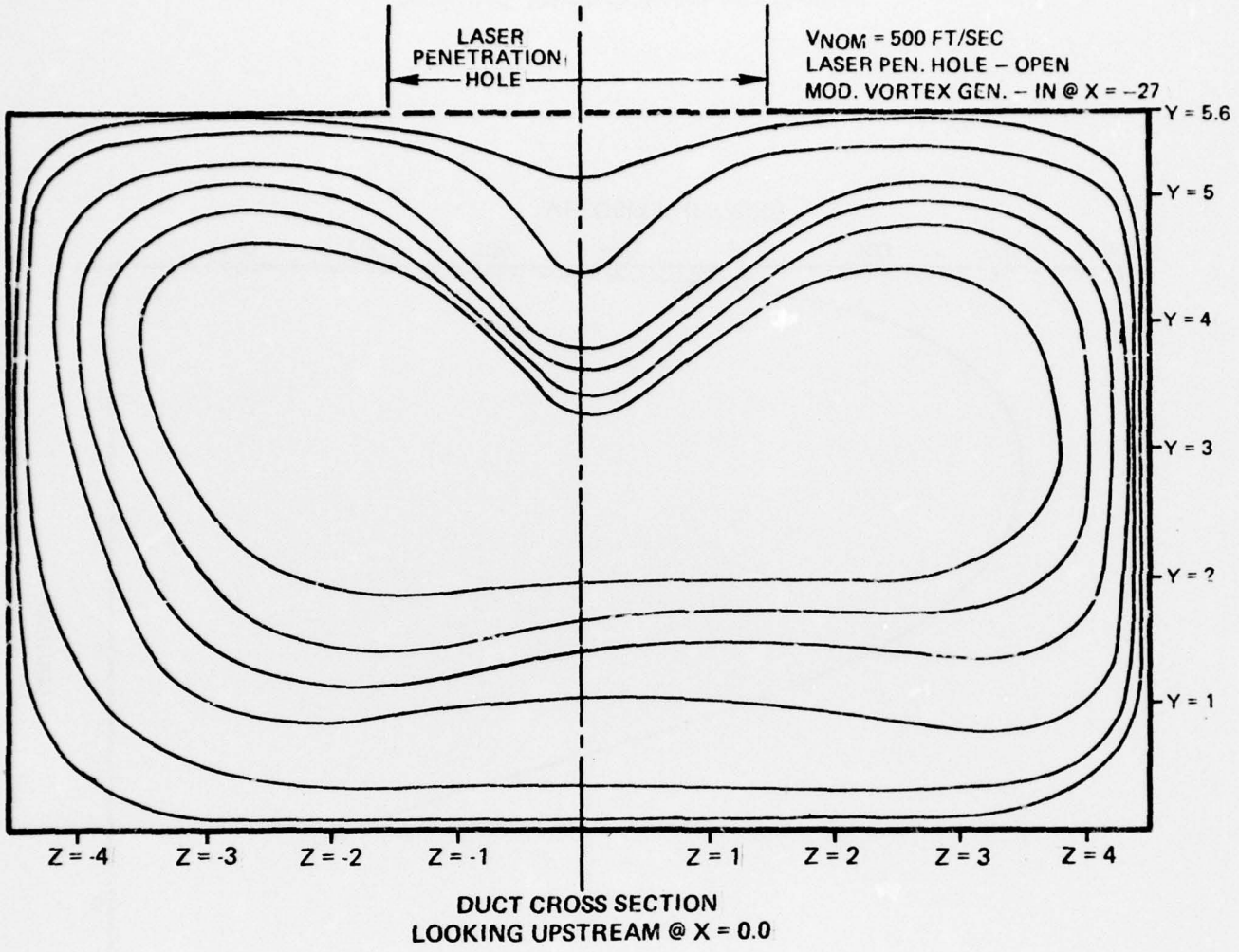

Figure IV-54. Velocity Contour Map

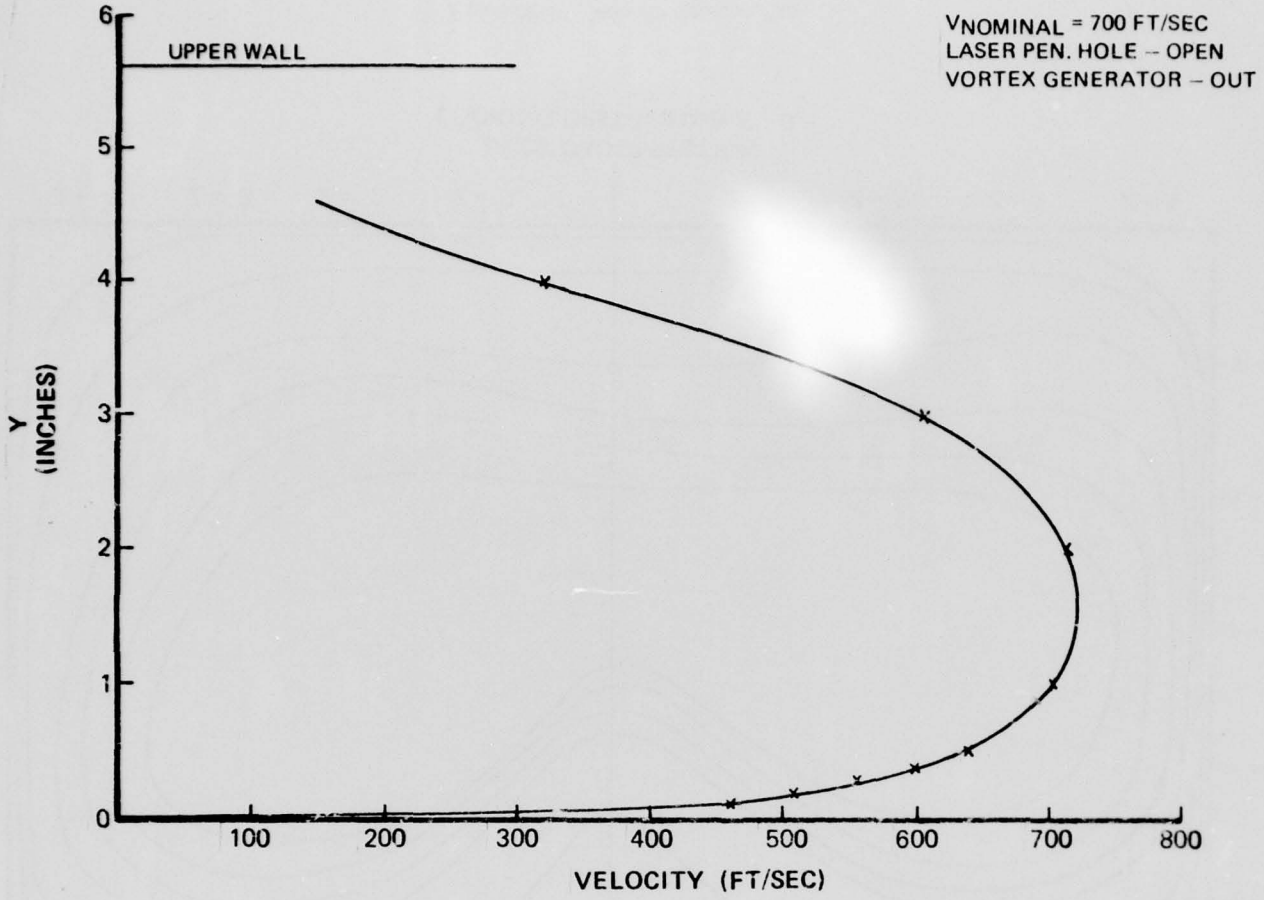

Figure IV-55. Velocity Calibration, Laser Flow Duct

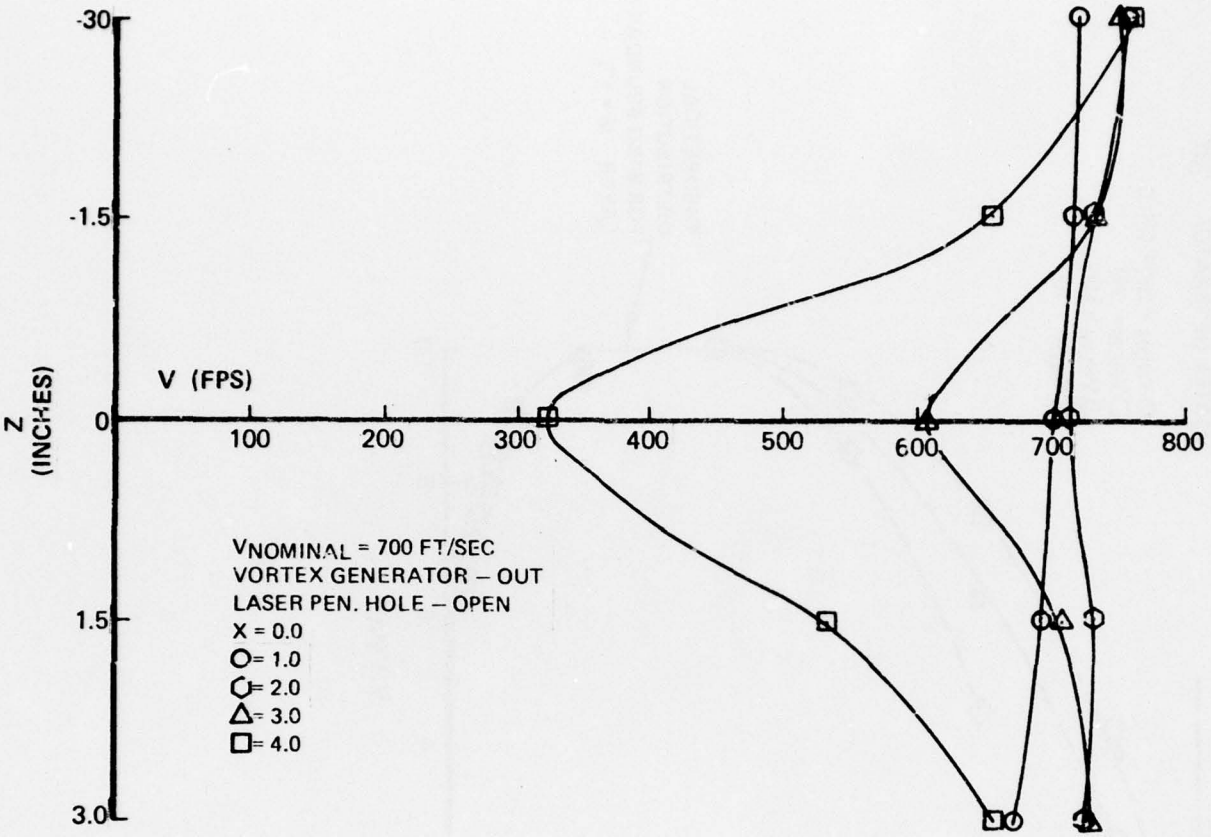

Figure IV-56. Velocity Calibration, Laser Flow Duct

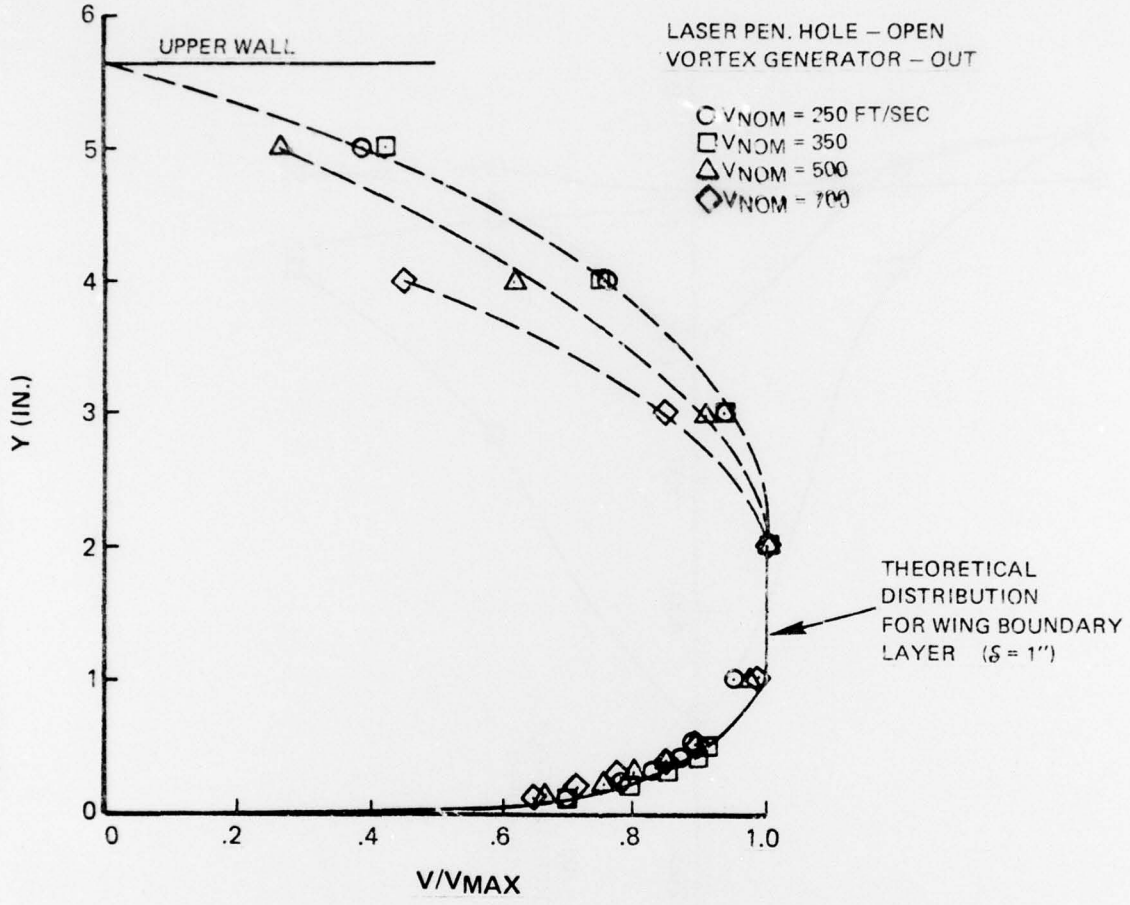

Figure V-1. Normalized Velocity Distribution

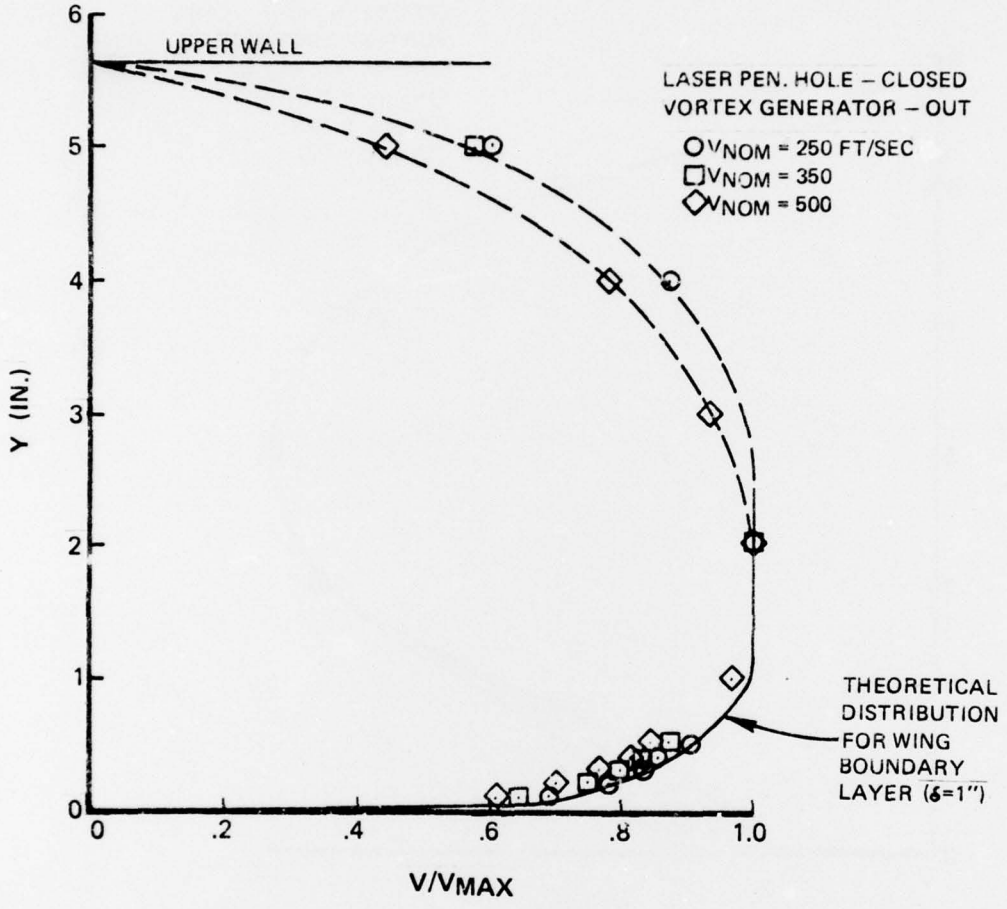

Figure V-2. Normalized Velocity Distribution

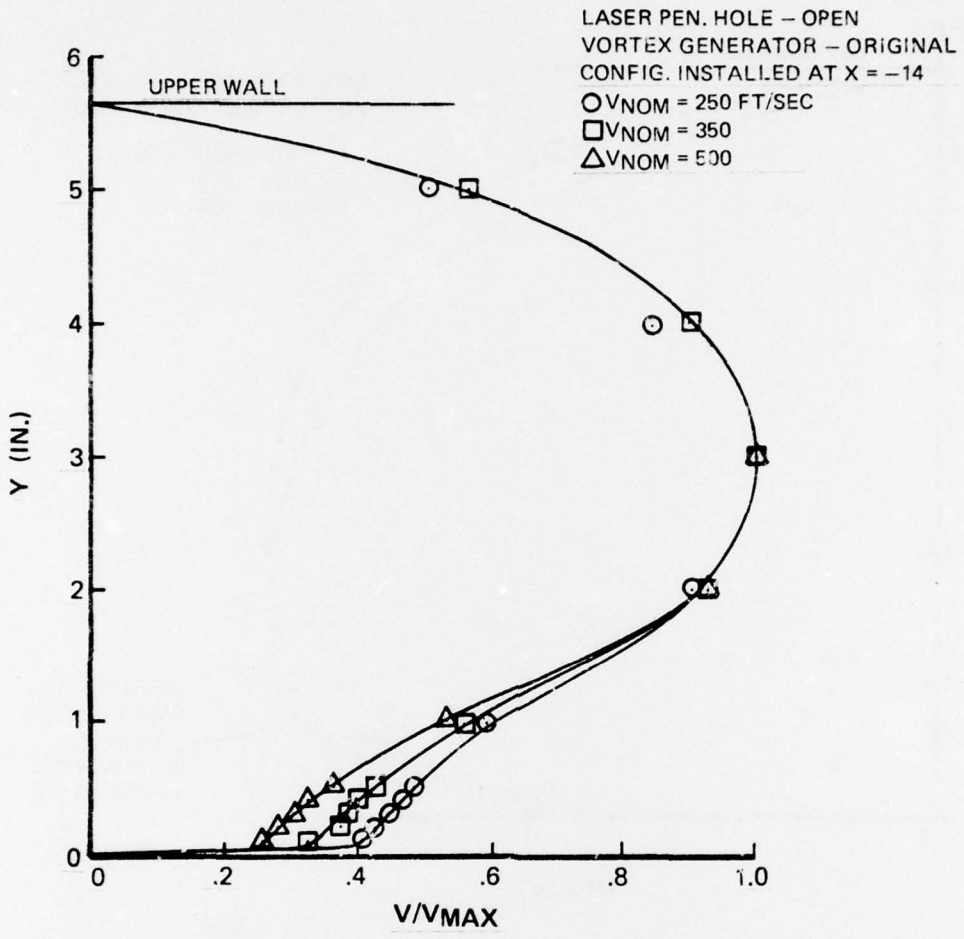

Figure V-3. Normalized Velocity Profiles.

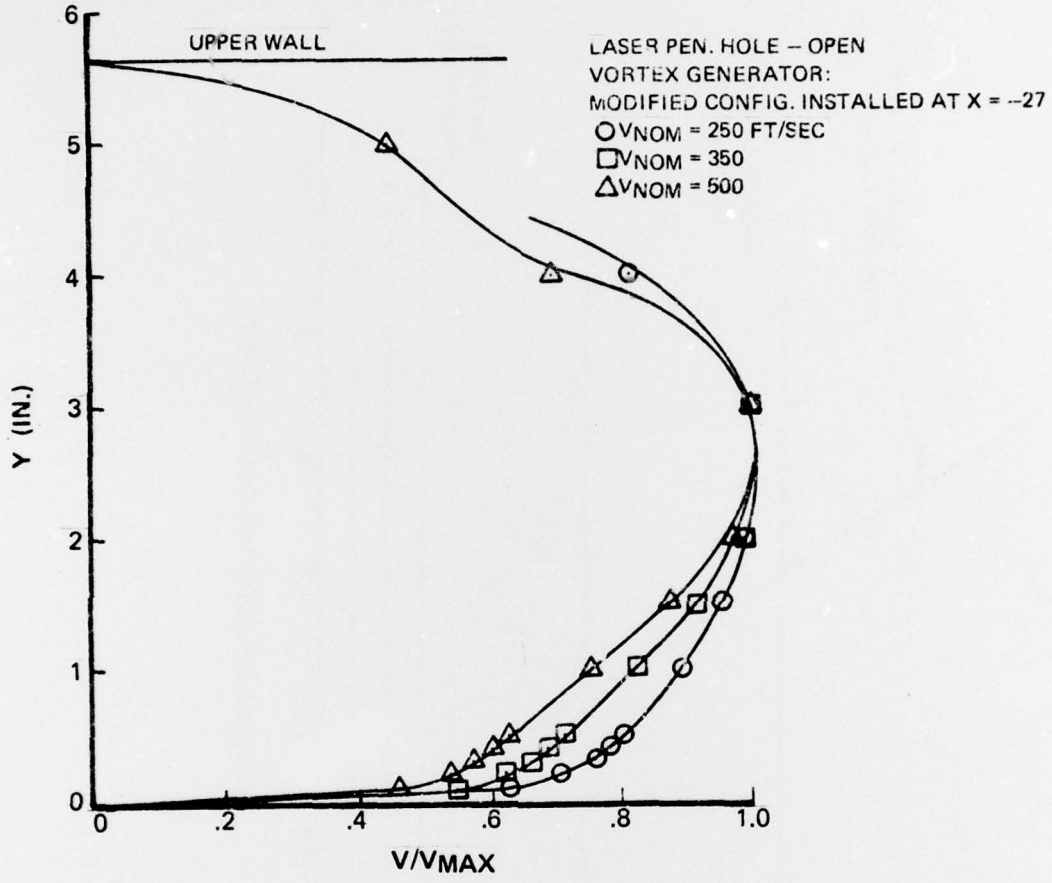

Figure V-4. Normalized Velocity Profiles

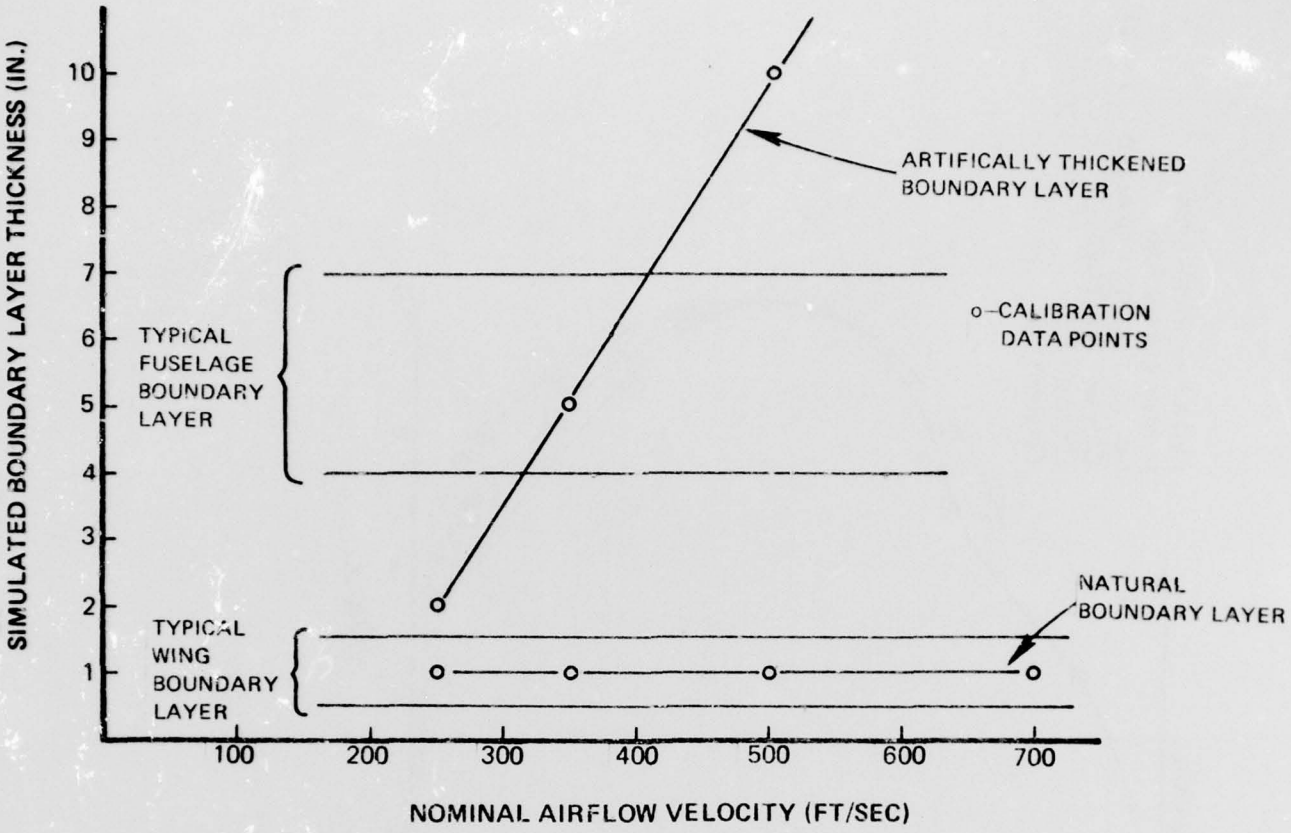

Figure V-5. Simulation of Flight Boundary Layer Conditions